PERFORMANCE ASSESSMENT OF RECONDITIONED FREIGHT RAIL BEARINGS USING EDDY CURRENT ARRAY FOR ENHANCED NONDESTRUCTIVE INSPECTION

A Thesis

by

EDUARDO MIRANDA

Submitted in Partial Fulfillment of the

Requirements for the Degree of

MASTER OF SCIENCE IN ENGINEERING

Major Subject: Mechanical Engineering

The University of Texas Rio Grande Valley
December 2025

PERFORMANCE ASSESSMENT OF RECONDITIONED FREIGHT RAIL BEARINGS USING EDDY CURRENT ARRAY FOR ENHANCED NONDESTRUCTIVE INSPECTION

A Thesis
by
EDUARDO MIRANDA

COMMITTEE MEMBERS

Dr. Constantine Tarawneh
Chair of Committee

Dr. Heinrich Foltz
Committee Member

Dr. Arturo Fuentes
Committee Member

December 2025

ABSTRACT

Miranda, Eduardo, Performance Assessment of Reconditioned Freight Rail Bearings Using Eddy Current Array for Enhanced Nondestructive Inspection. Master of Science in Engineering (MSE), December 2025, 112 pp., 29 tables, 89 figures, 32 references.

In North America, freight bearings removed from service must undergo a reconditioning process in accordance with Association of American Railroads recommended guidelines before reuse, with approximately 80% having been reconditioned at least once. This process includes bearing inspection, where repairable defects may be refurbished and returned to service with an extended performance range of 50,000 to 250,000 miles. Motivated by this extensive range in performance, researchers at the University Transportation Center for Railway Safety, in collaboration with MxV Rail, utilized a nondestructive evaluation method to enhance the reconditioning inspection process. An Eddy Current Array (ECA) was applied to bearing cup raceways to detect near-surface defects that may go unnoticed during the reconditioning process. Cups with and without ECA indications were tested under accelerated life conditions. The ECA results exhibit strong correlations between indications and spall development, enabling enhanced reliability of the inspection process and preventing compromised bearings from re-entering service.

DEDICATION

Me gustaria dedicar este tesis a mi familia. A mi madre, Alejandra Espinoza de Miranda, le agradezco por apoyarme durante todos mis años escolares, siempre cuidandome y empujandome a ser una mejor persona. A mi padre, Andres Miranda Barranco, le agradezco por formar al hombre que soy; sin importar cuantas veces chocamos cabezas, trabajar con usted dia tras dia me ayudo adquirir las habilidades y los conocimientos que necesito en la vida. A mis cinco hermanos mayores: Andrea, Kenia, Jazmin, Tamilla, y Andres Jr., gracias por todos los años de crecer juntos. Desde las peleas de hermanos hasta convertirnos en los adultos que somos hoy, no los cambiaria por nadie mas. A mi querida novia, Teresa Salazar-Flores, te agradezco enormemente por soportar mi actitud trabajadora y por acompañarme en este viaje escolar. Estuviste alli conmigo todos los dias, aun cuando no tenias que hacerlo, y te lo agradezco profundamente. Los amo muchisimo con todo mi corazon.

ACKNOWLEDGEMENTS

I would like to express my gratitude to all my companions and faculty from the UTRCS team. To Daniel, Adan, and Juan, your help in building all the bearings was immensely valuable for my research, and I am forever grateful to each of you. To Diego A., Diego L., Abel, Aaron, David, Roger, Lee, Joseph, Sergio, Alex, Jeff, Santana and everyone else, thank you for all the memories made here at the center. Persevering through the lows and highs together and sharing so many experiences are moments that I will carry throughout my life. Each of you has tremendous potential, and I know you all will be successful in your future endeavors, so let it ride. Shoutout to Joseph and Sergio for helping me revise my thesis defense and thesis. To the Salazar and REC (Steve, JAC, Israel, and Handro) family thank you all for your support outside of the center, many memories will be cherished. Also, to my girlfriend Teresa, thank you for putting up with me during my graduate years and always being there for me. Without you, this journey would have been far more difficult.

This research was made possible through a partnership with MxV Rail, who provided financial and logistical support for the project. The work was also financially supported by the University Transportation Center for Railway Safety through the USDOT UTC Program under Grant No. 69A3552348340.

I would like to extend my sincere gratitude to the engineers at MxV Rail, whose support greatly contributed to this research. I am thankful to Mr. Matt Wenger for giving me the opportunity to work on this project and for providing consistent guidance on testing the bearings throughout my master's journey. I am also thankful to Mr. Brian Lindeman for showing me how

to operate the Eddy Current Array (ECA) scanner and guiding me through that process. Also, I would like to thank Mr. Matt DeGeorge for generously taking time out of his day to pick me up from the hotel, bring me to the facility, and for giving me an MxV Rail shirt. Thank you all for your support and hospitality.

Lastly, to Dr. Constantine Tarawneh, thank you for taking me under your wing and giving me the opportunity to be a part of this center you have worked hard to build. None of this would have been possible without your guidance, wisdom, and mentorship. You have shaped me into a better version of myself, and I am forever grateful for everything you have done for me.

DISCLAIMER

The contents of this thesis reflect the views of the authors who are responsible for the facts and the accuracy of the information presented herein. This document is disseminated under the sponsorship of MxV Rail and the USDOT, in the interest of information exchange. MxV Rail and USDOT assume no liability for the contents or use thereof.

TABLE OF CONTENTS

Page

LIST OF TABLES

Page

LIST OF FIGURES

Page

CHAPTER I

BACKGROUND & INTRODUCTION

1.1 Introduction

The freight rail industry plays a vital role in supporting the North American economy by transporting large volumes of raw materials and finished products, effectively connecting industrial, agricultural, and commercial regions. The freight rail network is broadly acknowledged to be the "largest, safest, and most cost-efficient" transportation system by the Federal Railroad Association (FRA) [1]. Derailments pose a safety risk not only to the freight rail industry but also to surrounding communities. Critical railcar components, such as tapered roller bearings, are known to be among the primary contributors to mechanical failure, often resulting in derailments [2]. Prioritizing safety within the rail industry begins with proper inspection and maintenance of railcar components. Proper reconditioning of tapered roller bearings is essential for minimizing risk of derailments. Incorporating a post-reconditioning Nondestructive Evaluation (NDE) method, via Eddy Current Array (ECA), can further enhance reliability by identifying near-surface or subsurface defects that may be missed during standard reconditioning procedures.

1.2 Tapered Roller Bearings

Freight railcars consist of numerous components that work together to support and transport load efficiently. The suspension system, referred to as a bogie, includes a variety of dynamic elements such as axles, springs, dampers, wheels, and tapered roller bearings. Mounted on the outer portion of the suspension system, the tapered roller bearing supports both the weight

of the railcar and the additional load it carries during operation. The tapered roller bearing is composed of multiple subcomponents: rollers, cage, cones (inner rings), spacer ring, cup (outer ring), grease seal, and the wear ring as depicted in Figure 1.

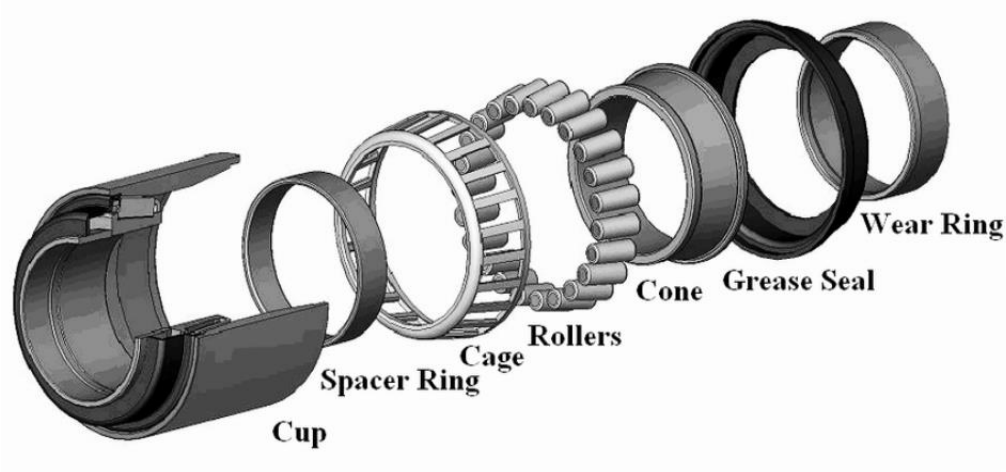

Figure 1: Subcomponents of a tapered roller bearing [3]

Among the subcomponents of a tapered roller bearing, there are elements that experience rolling contact; primarily among these are the two cone assemblies housed within the cup. Each cone holds 23 rollers, which are evenly spaced and secured by a cage to prevent misalignment during operation. A spacer ring is positioned between the two cone assemblies maintain proper spacing between them to prevent axial movement (end play) and to control internal clearance and preload. Grease seals enclose the cone assemblies and spacer ring on both ends of the cup, protecting the internal components and grease by preventing contaminants or debris from entering the bearing. Additionally, wear rings assist the grease seals by providing a contact surface that enhances the overall sealing of the bearing assembly. On the outboard side of the bearing, facing away from the railcar suspension, an end cap is installed to secure the press-fitted bearing onto the axle. This ensures that it remains firmly in place during operation as depicted in Figure 2.

Figure 2: Side view of a freight railcar bogie [4]

The Association of American Railroads (AAR) classifies bearings used in service based on their dimensional specifications and load-carrying capacities. The two primary bearing classes used in North America are class F and class K. Historically, class F bearings were the main population; however, their usage has declined in recent years. Class K bearings have since become the most commonly utilized in North America. Due to the reduced availability of new class F components, reconditioned class F bearings are now often paired with older, previously used parts [5]. This study focuses on evaluating the performance of reconditioned class F bearings.

Table 1 outlines the dimensions and load ratings of class F, K and other commonly used bearing classes. Notably, class F and K bearings share the same cup (outer ring) diameter, allowing them to support similar loads and use interchangeable cone (inner ring) assemblies.

Table 1. Dimensional specifications and load-carrying capacities of AAR bearing classes

Bearing Class	Cup Dimension Diameter × Width [inch]	Bearing Load [kN] / [kips]
E	6 × 11	117.0/26.3
F	6 ½ × 12	153.0/34.4
G	7 × 12	169.0/38.0
K	6 ½ × 9	153.0/34.4

The load from the railcar is distributed on the outer surface of the cup, which ideally remains stationary during operation. The top half of the bearing cup is defined to be the loaded zone. The cone assemblies freely rotate while the train is in motion, causing the cone and rollers to cycle in and out of the loaded zone as depicted in Figure 3. This cyclic loading reduces the overall stress and wear experienced by the cones and rollers. The stationary cup, however, endures the most radial stress and is very susceptible to spalling, as the raceways within the loaded zone undergo repeated surface and rolling contact fatigue (RCF) from the freely rotating cone assemblies. The rollers experience the least amount of stress as they are elements that revolve around the entire raceways of both the cup and cone.

These three components are the most pertinent for health monitoring.

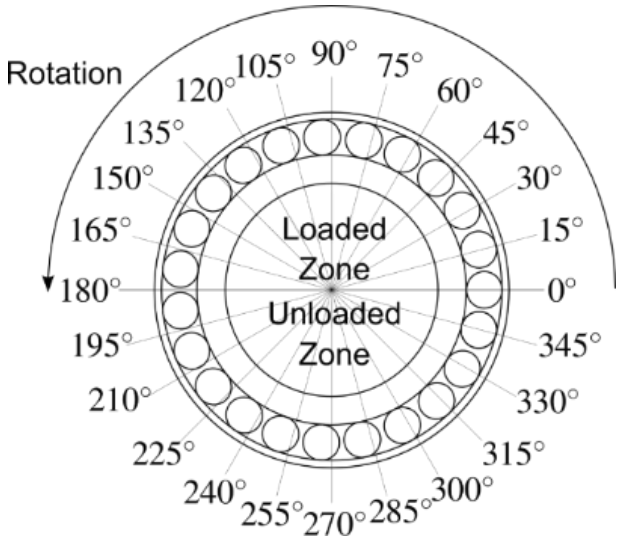

Figure 3: Schematic of bearing rotation relative to the loaded and unloaded zone

1.2.1 Types of Defects

When a spall begins to propagate on any component of a tapered roller bearing, it typically falls into one of the following three defect categories: localized, geometric, or distributed. A localized defect, as shown in Figure 4 (left), is the most common type. These typically appear as isolated damage, such as pitting, cracks, or spalls, concentrated in a specific area of the bearing surface. Geometric defects originate during the manufacturing process, where components fall outside specified dimensional tolerances. Examples include: cups with out-of-round raceways, out of tolerance cone concentricity referenced to a central point, and rollers with inconsistent diameters that would cause misalignment and abnormal stress distribution. Finally, distributed defects resemble localized defects that cover larger surface areas. Figure 4 (right) displays a spall distributed across the raceway of a cone, indicating more widespread fatigue and/or wear.

Figure 4: Example of a localized defect (left) and distributed defect (right) [6]

As mentioned previously, geometric defects occur due to errors during the manufacturing processes. Localized and distributed defects result from near-surface or subsurface inclusions that overtime will propagate and develop into spalls due to RCF.

1.3 Wayside Technologies

In North America, the AAR employs wayside detection technologies to identify defective bearings or other components within the railcar suspension system. These technologies serve as a preventative measure aimed at reducing the risk of freight train accidents. As trains pass through designated monitoring points, wayside systems collect and analyze data in real-time. This data is evaluated against established thresholds designed to detect anomalies or signs of failure, particularly in critical components such as a tapered roller bearing. If a bearing operates above the established threshold, it is flagged as defective, prompting an alert for the train conductor to stop the train [7]. The affected wheelset is then removed for detailed inspection, with components undergoing a reconditioning process before returning to service.

1.3.1 Hot Bearing Detectors (HBDs)

Hot Bearing Detectors (HBDs), shown in Figure 5, are wayside technology systems that employ infrared sensors to scan and measure the temperature profiles emitted from the bearing,

axle, and wheel as the railcar passes by the detector. Over 6,000 HBDs have been positioned in North America, typically spaced 15 to 22 miles apart, with wider spacing up to 40 miles in areas with lower traffic density [5]. HBDs operate based on predefined temperature thresholds either 94.4°C (170°F) above ambient or 52.8°C (95°F) above the operating temperature of the mate bearing on the same axle. When a bearing exceeds these thresholds, an alert is triggered to notify the train conductor of the potential issue. Recent advancements in the algorithm have allowed for more sophisticated comparisons, including the bearing temperature relative to the average temperature of bearings on the same side of the railcar. If a bearing is operating at a higher temperature than the average bearing temperature, it is classified as “warm trending” [8]. Bearings exhibiting warm trending behavior are flagged and subsequently removed from service for disassembly and detailed inspection.

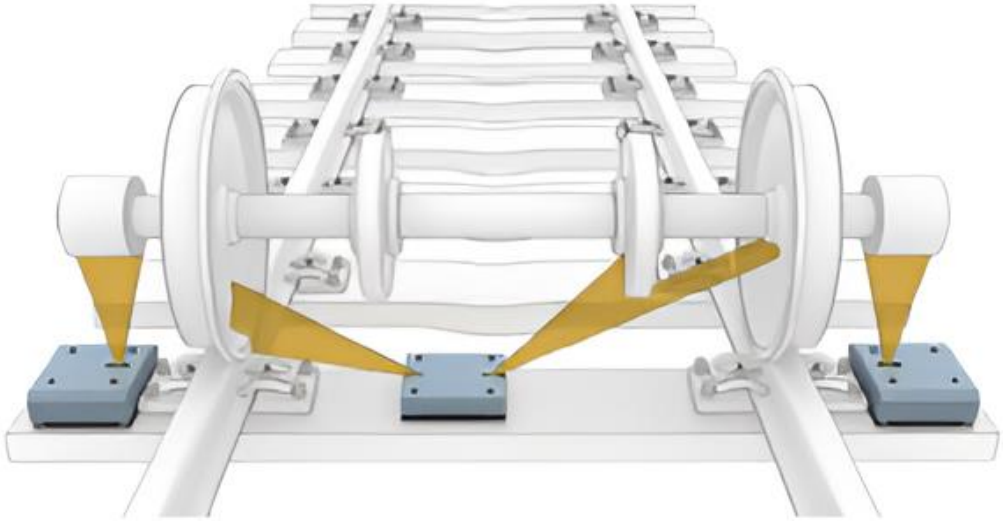

Figure 5: Schematic of a Hot Bearing Detector (HBD) [9]

As previously discussed, HBDs rely solely on temperature measurements to monitor bearing health. However, temperature alone is insufficient to proactively distinguish between healthy and defective bearings. Many flagged bearings are inspected and found to be non-verified, meaning no discernible defect was present. Furthermore, some bearing failures, such as

seizures, can develop rapidly within three minutes [10]. This timeframe could potentially be too short for HBDs due to the wide spacing between installations, even though thousands of HBDs have been installed. Studies have shown that there is a weak correlation between elevated temperature and bearing health trending, indicating that temperature monitoring alone is inadequate for proactively assessing the health of a bearing [11]. As a result, HBDs provide only a reactive response; a bearing is flagged only after it becomes severely defective and passes the detector, by which point a critical event, such as a derailment, may already be unavoidable.

1.3.2 Trackside Acoustic Detection System (TADS™)

Trackside Acoustic Detection Systems (TADS™), displayed in Figure 6, represent another type of wayside technology currently used in the rail industry. These systems utilize acoustic sensing to detect potential internal bearing defects. Unlike HBDs, which rely on temperature changes, TADS™ systems employ high sensitivity microphones to capture and analyze the acoustic signatures emitted by bearings in motion. This enables early detections of internal defects before they escalate to the point of overheating or failure. Despite their diagnostic advantages, the deployment of TADS™ remains limited, with approximately 19 systems installed across North America [5]. As a result, bearings in active service have a low probability of passing by a TADS™ site, limiting the overall effectiveness of the system in routine defect detection [11].

Figure 6: Trackside Acoustic Detection System (TADS™) site [5]

1.3.3 RailBAM (Rail Bearing Acoustic Monitor) [7]

The RailBAM (Rail Bearing Acoustic Monitor) is a wayside condition monitoring system that monitors the acoustic signature of each bearing that passes through at full speed. It can provide fully accurate and reliable data, being able to identify defects in bearings and provide the train operator with the severity of the defects. These systems were developed by Track Intelligence (now known as Track IQ) and were then acquired by Wabtec in 2015. As of March 2017, 20 RailBAMs have been installed across the US and approximately 190 installed worldwide. It can detect early signs of defects, having a reliability exceeding 95%. Despite the RailBAM system being able to detect defect signatures (cup, cone, roller and wheel) in early stages, there is only a limited amount of installed units across the US. This presents similar issues as the TADS™ where bearings have a low probability of passing by during their service life.

1.4 Importance of Reconditioning Practices

When a wheelset is removed from service, the bearings mounted on the axle are also extracted and sent out for reconditioning, even in cases where the removal was prompted by a

defect in the wheel rather than the bearing itself. Bearings removed in this fashion are categorized under *Why Made Code 11*, an AAR practice for removing bearings from service. This practice was introduced into the U.S. rail industry in the early 1980s to help improve the reliability and readiness of bearings [12]. This practice ensures that all bearings returned to service are free of defects and follow safety standards. The reconditioning process involves a comprehensive inspection of all bearing components to identify potential defects. Once identified, the defect is then classified based on the severity of the defect and the level of repair required to restore the component. An in-depth review of this reconditioning process is detailed in CHAPTER II.

1.4.1 Reconditioning Benefits and Performance Gains

The reconditioning process offers substantial cost-efficiency benefits by restoring rather than replacing bearing components. This approach not only reduces overall expenditures but also extends the service life of existing components and eliminates delays associated with procuring new parts to be delivered [13]. Additionally, reconditioning enables quicker turnaround times and reduces dependency on newly manufactured components, thereby minimizing system downtime and ensuring that railcars return to service more rapidly. For the rail industry, minimizing operational delays is critical, as continuous service delivery is central to business performance. Beyond economic advantages, the inspection phase of reconditioning provides valuable insight into component fatigue and potential failure modes, which enhances the predictive capabilities of maintenance. This detailed approach allows for more efficient scheduling of repairs and contributes to long-term reliability. Furthermore, it reinforces safety and quality assurance, ensuring that all components are restored to recommended dimensional specifications and safety guidelines specified by the AAR [14].

1.5 Nondestructive Evaluation (NDE)

Nondestructive Evaluation (NDE) refers to techniques employed across scientific and industrial applications to identify flaws, discontinuities, or variations in physical properties of materials without compromising the integrity or functionality of the original part. The application of NDE methods may vary depending on the design specifications and intended performance criteria of the final product [15]. These methods could play a vital role in ensuring operational safety by validating manufacturing quality and adherence to maintenance standards within the rail industry if integrated at certified reconditioning facilities.

1.5.1 Ultrasonic Testing (UT)

Ultrasonic Testing (UT) is an NDE method that utilizes high-frequency sound waves to detect internal flaws within materials. This method can detect cracks, voids, and delamination in metals, composites, and welds. Sound waves are introduced into the material and reflected by the microstructure of the material, with the resulting attenuation and reflection patterns analyzed to locate flaws [15]. UT utilizes various wave propagation modes including longitudinal (L-mode), shear (T-mode), surface (Rayleigh), and plate (Lamb) waves, each suited to a different purpose such as types of materials or types of defects [16]. Longitudinal waves are more utilized for thickness measurements while shear is more for perpendicular oriented flaws. This technique enables accurate size and location of flaws within the test material. It is capable of penetrating thick materials to detect inclusions or discontinuities. Gel or water is commonly utilized as a medium to transmit the sound waves from the transducer into the surface as the wave speed is known.

1.5.2 Radiographic Testing (RT)

Radiographic Testing (RT) is an NDE method that introduces X-rays or gamma rays into the test material to examine the internal structure. When radiation penetrates the test material, it is partially absorbed based on the density and thickness of the material, and an image density reveals the presence of internal flaws. Variations of the image density display the presence of internal flaws such as porosity, voids, inclusions, shrinkage, and delamination [17]. RT is extensively applied in inspecting welds, castings, and composite materials due to its effectiveness in detecting volumetric defects and its suitability for assessing complex geometries. Despite its advantages, RT has some notable limitations, including the health and safety risks associated with radiation exposure, requiring strict regulatory compliance and specialized operator training. RT has limited effectiveness in detecting surface-level defects, making it less suitable for certain applications. The method is costly and time-intensive, particularly with film processing and interpretation.

1.5.3 Acoustic Emission (AE)

Acoustic Emission (AE) is a technique that listens to transient elastic waves (stress waves) generated by sudden energy releases from localized sources within a material under stress. These emissions are caused by events such as crack growth, plastic deformation, corrosion, or fiber breakage. The use of AE signals can provide insight on the onset of discontinuity of the material, making it suitable for analyzing structural integrity, assessing weld quality and detecting flaws [18]. Unlike other NDE technologies, AE does not need to supply the energy into the material, instead it utilizes the energy that is released from the material itself. For this reason, AE is mostly utilized in structures that are in operation rather than idle. However, its application is only limited to identifying the amount of damage a material has within, not

specifying where the defects are located. Another limitation is that the signals from the AE source are affected by the noise of the environment, potentially biasing results.

1.5.4 Eddy Current Testing (ECT)

Eddy Current Testing (ECT) is an electromagnetism-based NDE method that detects defects characterized by physical, structural, and metallurgical conditions in electrically conductive metals [15]. High frequency alternating current (AC) flows through a probe coil and into the test material. The current is affected by factors such as conductivity, permeability, thickness, inclusions, and geometry. Subsurface or near-surface defects affect these induced currents and are detected through changes in the impedance of the coil. ECT is limited to conductive materials, has restricted depth penetration, and requires skilled interpretation. However, ECT is extensively applied in many industry fields such as aerospace, power generation, and manufacturing due to its ability to identify cracks, inclusions, and tooling marks, whilst providing rapid results. This can be utilized for the inspection of rail components such as wheels, axles, and tapered roller bearings. This research focuses on the implementation of ECT on reconditioned tapered roller bearings and will be discussed further in subsequent chapters.

1.6 Motivation

Previous research on utilizing nondestructive evaluation (NDE) methods on rolling stock bearings dove into the microstructure of the bearing steel and parameters that would alter them. A thesis conducted by Trevor Adelung at the University of Nebraska-Lincoln (UNL) utilized ultrasonic inspection to quantify the effective case depth (ECD) for cones (inner rings) [19]. This study served to establish a baseline for the focal regions to be inspected on the freight tapered roller bearing components. Another study that utilized NDE methods was a study conducted by Kobayashi et al., estimating the remaining useful life (RUL) of a bearing via eddy current testing

(ECT) [20]. This was then compared to a known effective method in estimating the RUL of the roller bearing, using X-ray diffraction (XRD). The research conducted for this study focuses on utilizing eddy current to inspect reconditioned bearings. A thesis conducted by Veronica Hernandez at the University of Texas Rio Grande Vally (UTRGV) assessed the performance of reconditioned bearings [3]. Specifically, this research emphasized how proximity between the stress-relief holes influences the initiation and propagation of spalls and leads to shorter extended service life.

The research presented here focused on exploring another potential factor that could contribute to shorter extended service life of select reconditioned bearings, which is subsurface defects. Current inspection methods are visual and rely on the expertise of the individual performing the repairs. Subsurface defects or small microcracks, that are not easily discernible, may exist in the repaired regions, which can initiate and propagate spalls due to rolling contact fatigue (RCF). The presence of these undetectable defects likely explains why some reconditioned bearings run for <50,000 mi whilst others that are defect-free are able to run for up to 250,000 mi or more. This study evaluates the effectiveness of the use of an Eddy Current Array (ECA) scanner to detect near-surface defects, if any, in reconditioned bearings that would compromise their service life. The ultimate goal would be the potential integration of this method with current reconditioning practices to ensure that bearings that re-enter revenue service are not susceptible to early failure.

The remainder of this thesis is organized as follows. Chapter II introduces the process of reconditioning bearings and the principles of eddy current. Chapter III details the laboratory setups and methodologies utilized to collect the data used for this study. Chapter IV presents the findings from the ECA scanner, differentiating between bearings that indicated a subsurface

defect beforehand and bearings that did not. Also presented in this chapter were the results for select dynamic experiments to validate the efficacy of the ECA scanner. Conclusions and recommendations for improvements to the scanning procedure are discussed in Chapter V.

CHAPTER II

RECONDITIONING PROCESS AND EDDY CURRENT ARRAY

2.1 Reconditioning Process

Bearings are usually pulled out of service before reaching the end of their service life, either due to wheels or other components being defective within the suspension of the railcar. As mentioned previously, bearings pulled from service under these conditions fall under *Why Made Code 11* [14]. These bearings are then brought to an AAR-approved facility for reconditioning. The reconditioning process requires complete disassembly of the bearing, followed by thorough cleaning, detailed inspection, and repair if needed. If every component is within tolerance, the bearing is then reassembled and deemed suitable for return to service. Notably, the reconditioning process includes the repair of defects such as spalls, shown in Figure 7 (left). Targeted restoration techniques are applied to bring the component back within tolerance, as depicted in Figure 7 (right). It is estimated that over 80% of the population of tapered roller bearings used in North American freight rail service are reconditioned and have a life expectancy ranging from 50,000 to 250,000 miles of service before exhibiting signs of failure [5].

Figure 7: A propagated spall and its subsequent repair (circled) on a bearing raceway (left) and method of repair (right) [5]

2.1.1 Levels of Reconditioning

To provide a framework for bearing restoration, Schaeffler Technologies categorizes reconditioning into four levels, as illustrated in Figure 8. Level I involves disassembly, cleaning, and inspection of the bearing assembly. If there are minor scratches or rough surfaces present, the reconditioning process continues to Level II, where those components are then polished. Defects that outlast the polishing process undergo a full grinding procedure, with unrepairable components being replaced as needed (Level III). Level IV is the last level of reconditioning in which the inner and outer rings are assessed and replaced with brand new healthy components if needed. All levels make sure that any refurbishments done on components are verified to meet AAR tolerances before returning to service.

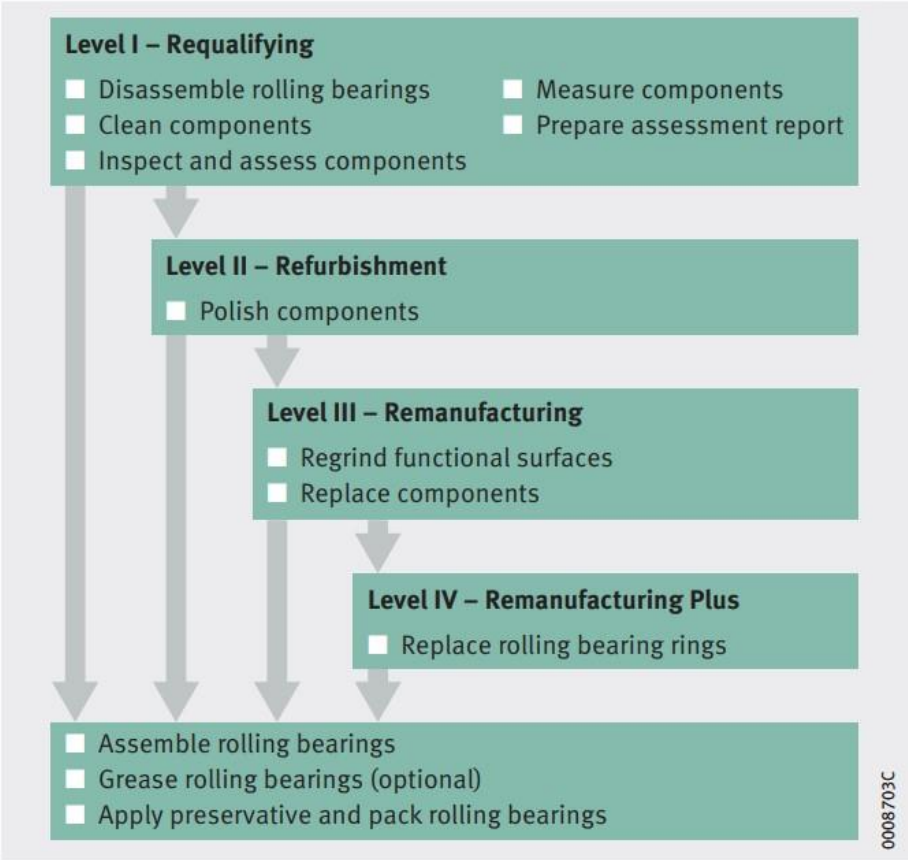

Figure 8: Levels of reconditioning [21]

This standardized framework is a foundational basis that all certified facilities follow within the rail industry. This framework ensures consistency in quality assurance. To ensure structural integrity and operational reliability of reconditioned bearings, the AAR enforces strict criteria that prohibit the return of bearings that exhibit any of the following conditions: cracks or spalls present on rollers, cups (outer rings) or cones (inner rings) with unrepaired spalls, repaired spalls that exceed allowable dimensions, two or more repaired spalls within a 2 inch circumferential area, less than 3/16 inch of separation between any two repaired spalls, and/or a total of six repaired spalls present on a single raceway [22]. Its implementation has yielded substantial economic benefits, with cost reductions ranging from 50 to 80% depending on the class of bearing [23].

The raceways of the components that have spalls or cracks must be refurbished to meet proper tolerances. Recommended material removal via grinding is permitted up to 75 μm (0.003 in) per surface, or up to 300 μm (0.012 in) for outer diameters that are greater than 400 mm (0.016 in) [24]. Portable grinders with fine abrasive wheels less than 5/16 inch in diameter are used to perform surface level spall repairs. Small stress relief holes are made across the surface of the cup (outer ring) raceways. The damaged material is smoothed out with the same intent of preventing stress concentrations. Prior research suggests that the proximity of stress relief holes may contribute to the propagation of spalls on raceway surfaces. Also, the removal of material can alter the geometric profile which would cause roller misalignment to occur more often and possibly localize stresses that can lead to axle failure [3]. Each component must be permanently scribed to indicate reconditioning post repair. The cup (outer ring) is marked on the spacer ring region, as depicted in Figure 9. Cones (inner rings) are marked on the face of the large-diameter end. The markings must include the month, year, and the reconditioning facility identification code. After full repair and refurbishment, the bearing components are fully assembled under clean conditions and prepared for use in rail revenue service.

Figure 9: Scribe marks applied to the bearing cup (outer ring) post reconditioning

To summarize, the reconditioning process plays a vital role in the rail industry by restoring used bearings to a condition comparable to brand-new bearings, reducing costs for customers and minimizing material waste. The integrity of the repairs performed during reconditioning is critical to ensure safety and reliability. To enhance the reconditioning process, MxV Rail has been exploring options beyond traditional physical inspection for verifying if components are truly suitable for re-entry into service. One such method is the use of a flexible Eddy Current Array (ECA), which is a nondestructive evaluation (NDE) technology that inspects otherwise undetectable subsurface anomalies. MxV Rail has specifically focused on scanning bearing cup (outer ring) raceways as they are the subcomponent most exposed to rolling contact fatigue [25].

2.2 Eddy Current Array (ECA)

The Eddy Current Array (ECA) inspection method is a nondestructive evaluation (NDE) technology that uses electromagnetic induction to detect surface or subsurface defects in electrically conductive materials, such as steel alloys. The ECA system presents a unique advantage when inspecting reconditioned bearings compared to conventional methods by enabling the early detection of microstructural defects such as cracks, voids, and other discontinuities. This system can further strengthen the framework of the reconditioning process.

More than 80% of in-service bearings in North America are reconditioned, with extended service lives ranging anywhere from 50,000 miles to 250,000 miles. The variation in extended life is likely explained by the presence of subsurface inclusions that go unnoticed in the reconditioning procedure. Given such prevalence in the industry, there is a need for implementation of an enhanced inspection system capable of detecting these subsurface defects that may be generated during the reconditioning process or through the bearing's service life. The process of reconditioning requires grinding, stress-relief drilling, and removal of material which alters the structure of alloys at a micro level and potentially initiates fatigue damage. This also affects the electromagnetic properties of the steel alloy, which makes it possible for eddy currents to be used to detect these discontinuities. Therefore, the application of ECA would further reassure that reconditioned bearings meet the dimensional and structural integrity requirements set forth by the AAR whilst also accounting for near-surface defects that are not visually discernible.

2.2.1 Principles of Eddy Current: Electromagnetic Induction Theory

Eddy current inspection is governed by the principles of electromagnetic induction, where alternating current through a coil is introduced into an electrically conductive material, as

illustrated in Figure 10. A time-varying electromagnetic field, also referred to as the secondary magnetic field, is generated from the flow of alternating current, also known as the primary alternating magnetic field. The eddy currents circulate in a parallel direction to the surface but flow perpendicular to the magnetic field [26]. The frequency output from the induced currents is equal to the frequency of the excitation source, which allows for precision and control of the penetration depth into the material.

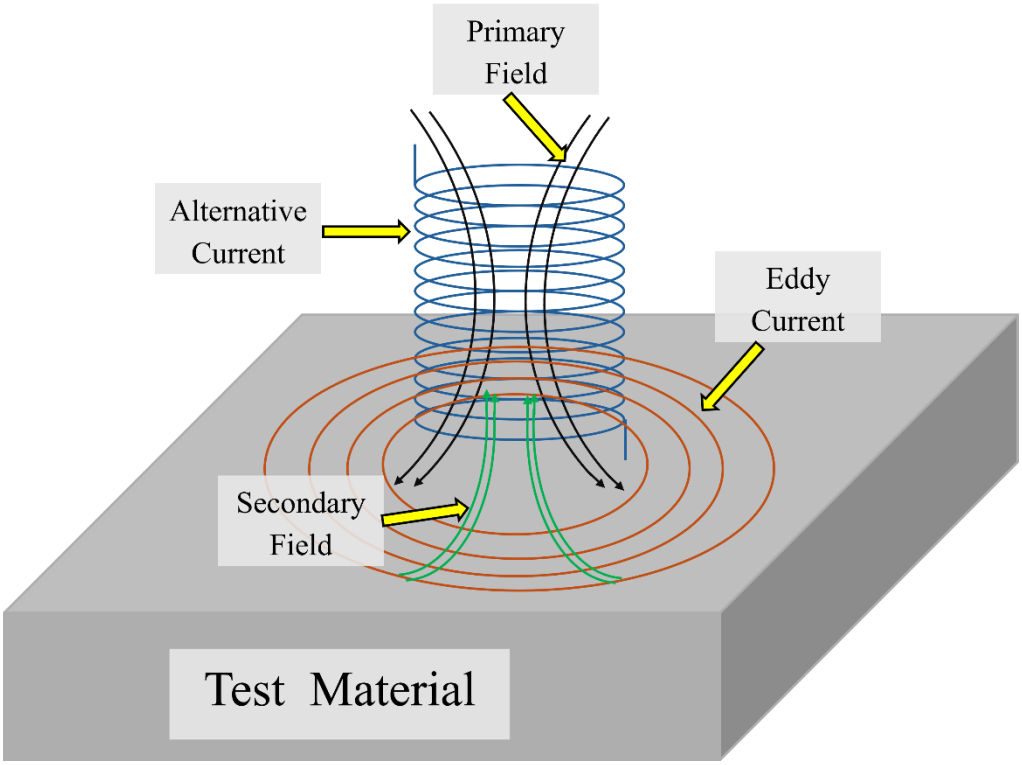

Figure 10: Principles of eddy current [26]

The secondary magnetic field opposes the primary magnetic field, making it suitable for detecting discontinuities on the material, as described by Lenz's law. From the secondary field, the amplitude and distribution are dependent on the electrical conductivity, permeability, and geometric continuities of the material. If the surface is defect free, the eddy currents induced form consistent uniform loops in the secondary field but if a defect is present then the currents

would be disrupted, thus distorting the secondary field. This would then alter the impedance of the coil.

The changes in the magnetic field are detected by changes in the original coil impedance, which enables the detection of discontinuities on the material. This behavior is explained by Faraday's law of electromagnetic induction, where the magnitude of the change in magnetic flux is directly proportional to both the rate of change in the magnetic field and electrical conductivity of the material as demonstrated in Eq. (1) [27]. Where ε is the electromotive force and Φ_B is the magnetic induction flux density.

$$\varepsilon = -\frac{d\Phi_B}{dt} \tag{1}$$

Eddy currents are highly dependent on the frequency of the alternating current that is being applied to the material. The frequency used determines the focal region of eddy current scans, with higher frequencies detecting defects in near or subsurface regions, and lower frequencies allowing for more penetration depth. The eddy current density decreases with depth as the magnetic field induces circulating currents at the surface. This phenomenon is governed by three principal factors: frequency, electrical conductivity, and permeability of the material. The depth of penetration, or skin depth, is defined as the depth where the current density decreases to 36% of the surface value [28].

Decreasing the frequency output by the coil increases the depth of penetration and allows for the detection of subsurface defects. However, this action also reduces the magnitude of surface current density, which decreases the sensitivity to near-surface defects. Therefore, the frequency must be optimized to balance the depth of penetration and detectability of defects based on material properties and other inspection requirements.

2.2.2 Variables Affecting Eddy Current

Key factors to consider when utilizing eddy currents for nondestructive evaluation include: frequency, electrical conductivity, permeability, surface conditions, lift off, and temperature. The permeability of a material heavily influences the behavior of ferromagnetic materials, such as steel, by altering the eddy current density at or near the surface. When the primary field is applied, the permeability of the ferromagnetic material enhances the secondary field, resulting in much higher eddy current density at the surface. As a result, the intensity of the field decreases with depth, reducing the effectiveness in penetration of the eddy currents, resembling a shielding effect preventing the eddy currents from propagating into deeper regions within the cross section, as depicted in Figure 11 [29].

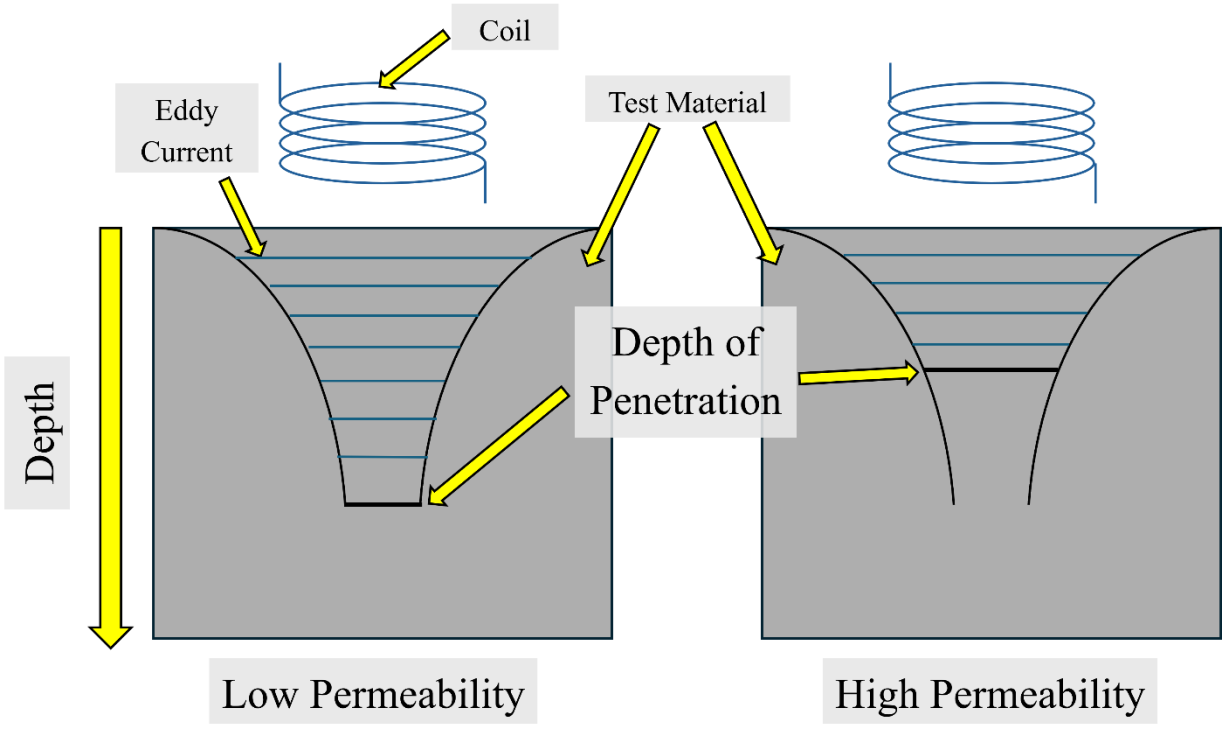

Figure 11: Effects of permeability on eddy current induced into a material [29]

The surface conditions refer to the geometric properties of the material, such as smoothness and roughness, that affect the distribution of eddy current through the material.

Surface conditions such as dimples or stress-relief holes disrupt the flow of eddy currents and can be interpreted as false indications. The roughness of the material can distort the magnetic field by introducing sharp or rigid transitions within the surface. Any sort of coating or signs of corrosion can alter the response of eddy currents which would reduce the sensitivity. These conditions all highlight the need for surface preparation to output precise and accurate results.

Finally, lift off is defined as the distance or separation of the probe to the surface of the test material. As lift off increases, the strength of the induced eddy currents decreases.

CHAPTER III

EXPERIMENTAL SETUP AND METHODOLOGY

To validate the effectiveness of the eddy current array (ECA) method, the scanned reconditioned bearings were run under simulated rail service conditions on the University Transportation Center for Railway Safety (UTCRS) dynamic bearing test rigs housed at the University of Texas Rio Grande Valley (UTRGV). The performance and health of the reconditioned tapered roller bearings in operation was assessed via vibration and thermal monitoring techniques that are explained later in this chapter. The ECA scanner was utilized to scan the bearing cup (outer ring) raceways and indicate regions with subsurface inclusions, if any.

For this study, two batches of reconditioned bearings were tested and evaluated: a defective batch with at least one ECA indication found on any of the cup raceways, and a healthy batch with no ECA indications on any of the bearing cup raceways.

The first batch consisted of eight class F bearings that were chosen by engineers from MxV Rail in consultation with a bearing reconditioning facility. These bearings were all removed from service due to *Why Made Code 11*, meaning that the bearings were not responsible for the removal of that wheelset. These eight bearings were first sent to MxV Rail to be inspected and scanned using their ECA scanner. These eight bearings all indicated that at least one subsurface defect was present on a raceway of the cup (outer ring). This batch was then shipped to UTRGV for accelerated service life testing as explained earlier. The second batch also consisted of eight class F bearings that were chosen by engineers from MxV Rail in

consultation with a bearing reconditioning facility. These eight bearings went through the same scanning procedure but were labeled “non-indicated,” meaning no defect was detected by the ECA on any of the cup raceways. The second batch of bearings was also sent to UTRGV to undergo accelerated service life testing.

3.1 Eddy Current Array (ECA) Scanner

The ECA system (EVi Uniwest), displayed in Figure 12, was used to scan reconditioned bearing cup raceways in this study. A total of sixteen reconditioned bearings were visually inspected and subjected to identical ECA scanning procedures. From the batch of sixteen bearings, eight were labeled as “indicated”, meaning that a defect was detected by the ECA scanner, while the other eight were labeled as “non-indicated”, meaning no defect was detected. During the scanning procedure, the ECA roller probe was positioned on the raceway surface while the bearing cup was rotated. The 0° position was established using a traceable reference point (i.e. the serial number). From this reference point, the scan covered 180°, corresponding to half of the bearing cup raceway. Accordingly, two profile scans were acquired for each bearing cup raceway: one spanning from 0°–180° and the other spanning from 180°–360°. All profile scans were conducted at a frequency of 1 MHz. This frequency was used to find the focal zone on the surfaces, having a depth of penetration of 1 mm (0.04 in). When a discontinuity or defect was present, the ECA roller probe transmitted a signal to the scanner, which generated a red region on the C-scan output. A C-scan is a 2-D map of the eddy current responses across an area from multiple A-scans, whereas an A-scan is the individual signal trace from a singular coil. Any recorded indication of the C-scan output was treated as a potential defect.

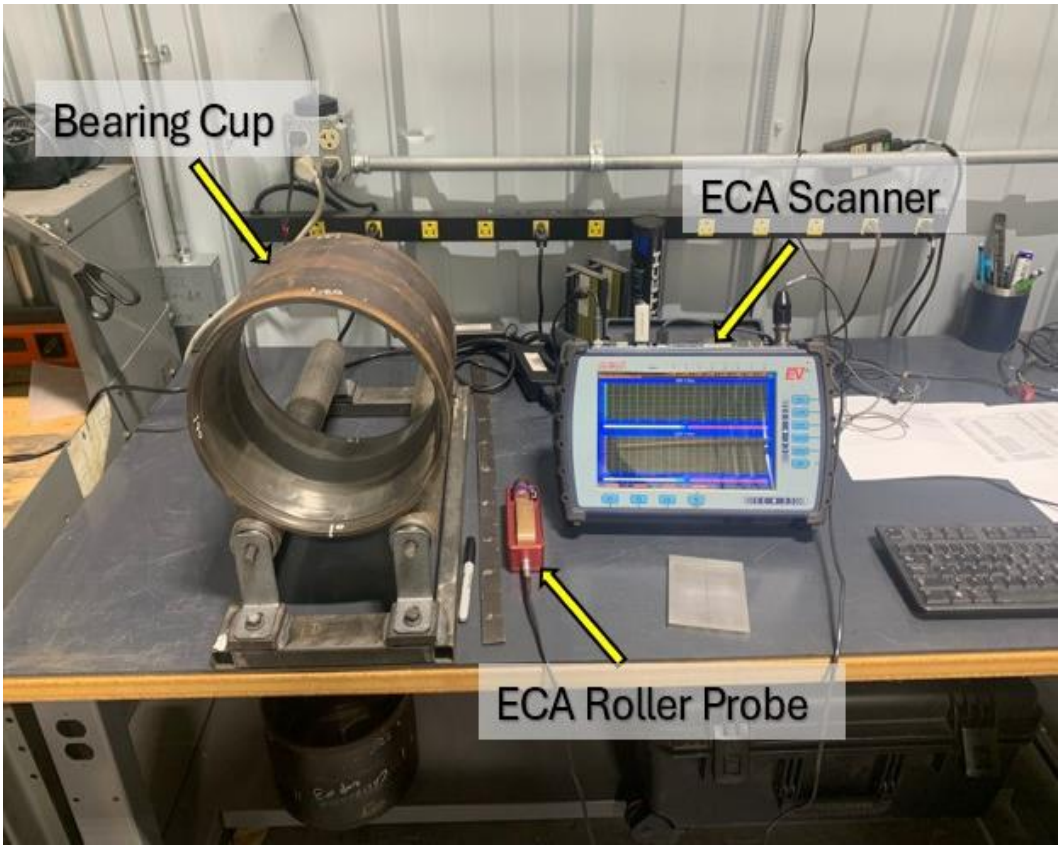

Figure 12: Flexible ECA scanner setup

The working principle of the ECA probe on a bearing cup surface is depicted in Figure 13. This graphic illustrates how a crack can disrupt the flow of eddy currents that are induced into the material [20]. When testing, the probe induces many circulating eddy currents within the bearing cup raceway. These eddy currents are influenced by discontinuities or variations in material properties. Such variations alter the probe coil impedance, which is measured as voltage signals on an impedance plane. A bridge circuit is utilized to precisely capture these impedance changes.

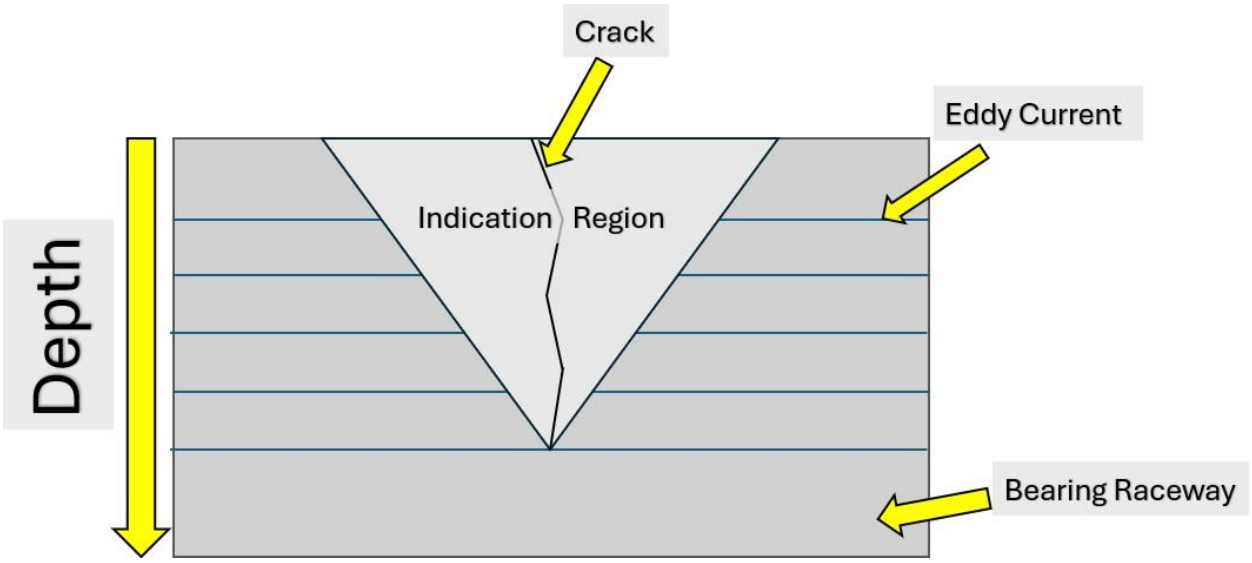

Figure 13: Eddy current disruption due to crack on material surface [20]

In some cases, bearing cup raceways contained intentionally manufactured repair dimples. These repair dimples also alter the impedance of the coil and as such were detected by the ECA probe. To ensure that there was no fatigue cracking or any defect on the dimple itself, a secondary probe, a pencil probe, was utilized, depicted in Figure 14, which outputs an A-scan. This inspection allowed for differentiation between defects and false responses associated with variations in permeability, conductivity, or other non-defect-related factors.

Figure 14: Pencil probe [30]

3.2 Bearing Assembly

The experiments that were conducted for this study only included class F bearings since the majority of class F bearings used in the rail industry are reconditioned. These class F bearings are fabricated from AISI 8620 steel and contain hardened tapered rollers. Class F bearings have a height of 12 in (30.48 cm) and a diameter of 6.5 in (16.51 cm). They require a large spacer in the middle of the two cone assemblies that measure around 1.45 to 1.55 in (3.68 to 3.94 cm). Furthermore, a lubricant is needed to help reduce friction between the rolling elements. Grease is applied within the cone assemblies and the spacer ring region to ensure that there is minimal wear or fatigue between the contact points of the rolling elements and the raceway surfaces.

3.2.1 Grease Application

Each bearing was lubricated and assembled to specifications set by the AAR. A table detailing the specific quantities of grease used per cone assembly is shown below in Table 2.

Since class F bearings are larger and have more room in the spacer ring region (center), grease must also be applied here.

Table 2. Grease quantities for class F bearings

Bearing Class	Cone Assembly		Center		Total	
	[mL]/[oz]	Squirts	[mL]/[oz]	Squirts	[mL]/[oz]	Squirts
F	192.2 / 6.5	8/Slot + 18	266.2 / 9	279	650.6 / 22	682

The grease seals prevent the grease from leaking out and stop outside contaminants from entering the bearing. Once a bearing is fully sealed, it is then weighed to ensure that an appropriate amount of grease was applied. It should be noted that the weight of a class F bearing may differ depending on the material of the cage used in the cone assembly. For this study, polyamide (polymer-based) cages were used, resulting in an average weight of approximately 79 lb (35.8 kg). If steel cages had been used, the weight would be approximately 82 lb (37.2 kg).

3.2.2 Component Tolerances and Dimensions

Bearing components, such as the cone assemblies, spacer ring, seal, wear ring and cup, are inspected for any defects or improper tolerances before use. Aside from the selected reconditioned cups, all other components are selected from a library of known healthy components. Roller spacing is measured using a feeler gauge, following AAR-suggested tolerances between the roller and cage of no greater than 0.060 in (1.524 mm) [22]. If the spacing is greater than the suggested tolerance, the assembly is deemed unfit for service.

Subsequent to roller spacing measurement, cage lift and cage shake are measured. These processes begin with the mounting of a cone assembly onto a chuck fixture, as depicted in Figure 15. The cage lift is measured by placing a dial indicator on the top surface of the cage and observing how much the cage shifts vertically around the circumference of the cage. Following

this, the cage shake is conducted by placing the dial indicator on the side of the cage before applying lateral force to one side of the cone and measuring the lateral movement. It should be noted that these measurements are taken when the cone assembly does not contain grease. These measurements assess the cage motion to ensure that the rollers were properly aligned, and the cage maintained stable motion during service.

Figure 15: Cage lift (left) and cage shake (right) measurements for cone assembly

Furthermore, lateral measurements of the bearings were taken before it was sealed for service. Using a dial indicator, the minimum and maximum lateral measurements were taken for each bearing. The desired range of 0.023 to 0.028 in (0.0584 to 0.0711 cm) was achieved by using an appropriate size of spacer ring.

Prior to pressing the bearings onto a test axle, the dimensions of the cone and axle were measured to ensure conformity with the guidelines provided by the AAR. The inside diameters of the cones were taken by using a three-point internal micrometer, displayed in Figure 16 (left) to confirm that the measurements were within the tolerance of 6.1860 to 6.1880 in (15.7124 to

15.7175 cm). A similar process was done to the test axles used for the experiments. An external micrometer was utilized to measure the outside diameter at designated surface areas on the axle displayed in Figure 16 (right). Four measurements per cone assembly were recorded for the eight cone assemblies that are to be pressed onto the test axle. The tolerance for the axle according to AAR guidelines is a range of 6.1905 to 6.1915 in (15.7239 to 15.7264 cm).

Figure 16: Three-point internal micrometer (left) and outside micrometer (right)

3.3 Chamber Four-Bearing Tester (C4BT) and Four-Bearing Tester (4BT)

The UTCRS dynamic four-bearing testers were utilized to carry out the accelerated service life testing for this study. These dynamic testers were designed to run bearings under simulated rail service operating conditions. Images depicting these testers are shown in Figure 17. The only difference between the C4BT and 4BT is that the C4BT is housed in an

environmental chamber that allows for precise control of ambient conditions, ranging from -40°C to 60°C (-40°F to 140°F).

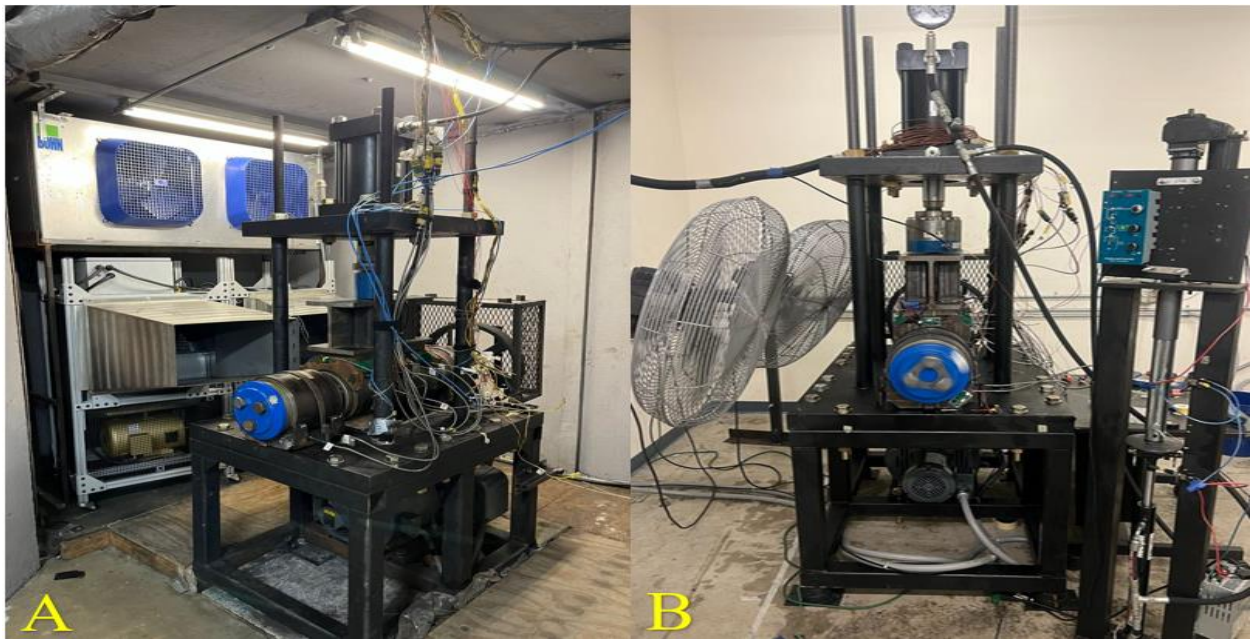

Figure 17: (A) Chamber Four Bearing Tester (C4BT), (B) Four-Bearing Tester (4BT)

To begin the testing procedure, four bearings were mounted on a custom test axle using a 300-ton hydraulic press. Two of the bearings would serve as the focus of the experiment, the reconditioned bearings in this case, and the other two would act as controls for comparison. These bearings would then be mounted on the C4BT or 4BT with two adapters under the two outer bearings (control bearings) and two adapters on top of the two middle bearings (test bearings) in a simply supported beam fashion, as pictured in Figure 17.

A hydraulic cylinder was used to apply load through an I-beam, ensuring uniform distribution across the two test bearings (i.e., middle two bearings). Each test rig is equipped with a hydraulic cylinder capable of applying up to 150% of the full load capacity for the respective bearing class, as suggested by the AAR and summarized in

Table 1. A custom-designed load controller system maintains consistent loading for the entirety of the service life test. A loading condition of 17% (5,850 lbs or 26 kN per bearing) simulates an empty railcar, and 100% (34,400 lbs or 153 kN per bearing) simulates a fully loaded railcar.

A 22kW (30 hp) variable speed electric motor controlled by a variable frequency drive (VFD) drives the test axle-bearing assembly via a pulley-belt system. Through this system, speeds up to 85 mph are achievable. For this study, the operating speeds ranged from 25 mph (40 km/h) to an accelerated service life speed of 85 mph (137 km/h) to reach a mileage goal of 120,000 miles (193,121 km). It should be noted that experiments were stopped before the mileage goal was achieved if a spall propagated. At the 60,000-mile mark of each test, a complete teardown inspection was conducted. The bearings were cooled by convective airflow provided by two industrial fans that simulated air speeds of about 6.7 m/s (15 mph) over the test bearings.

3.4 Tester Instrumentation

The two middle bearings (test bearings) were outfitted with specialized bearing adapters. These bearing adapters were custom-machined to accommodate two K-type bayonet thermocouples and a MEMS-based 100g accelerometer. The K-type bayonet thermocouples were positioned at the center of each cup raceway. Additionally, a standard K-type thermocouple was secured with a set screw on top of the adapter to measure the temperature of the adapter, as can be seen in Figure 18 (A). The 100g accelerometers were positioned at the Top-Dead-Center (TDC) location, as illustrated in Figure 18. Two additional thermocouples were placed to monitor the ambient temperature. One was installed on the fan side and the other on the non-fan side of the test rig.

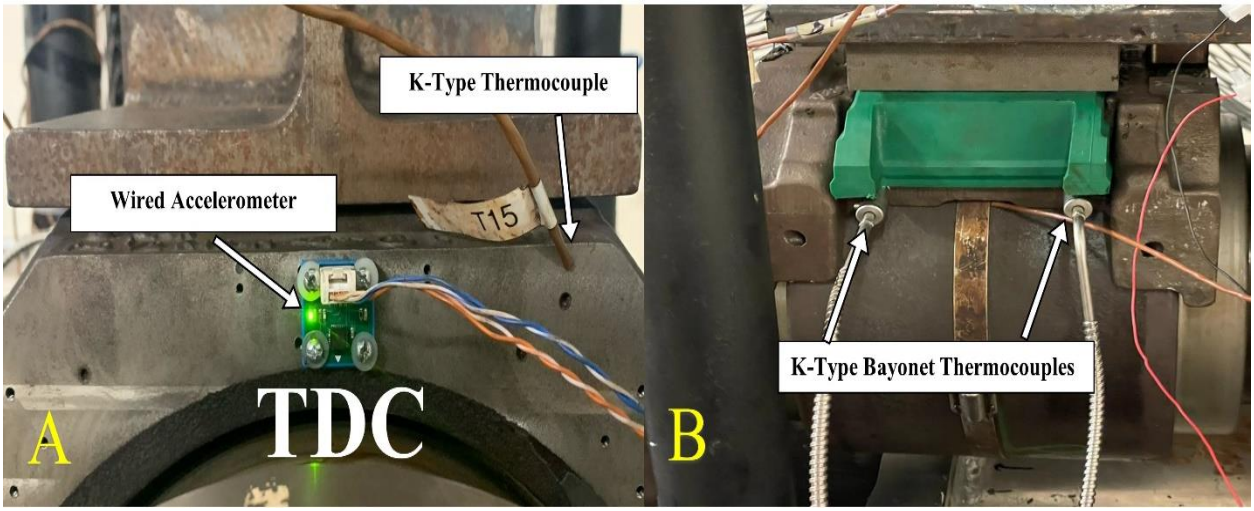

Figure 18: Modified 4BT adapters showing: (A) TDC location and outboard facing instrumentation, (B) side mounted temperature sensors

The data was recorded using a National Instruments (NI) NIcDAQ-9174 data acquisition system (DAQ), which was controlled through LabVIEW™ software. Temperature data from the K-type thermocouples was sampled every twenty seconds at a rate of 100 Hz for half a second using an NI 9213 card. Vibration data was captured every ten minutes at a rate of 5,120 Hz for sixteen seconds using a combination of NI 9234 and NI 9239 cards. Angular speed and motor power data from the VFD were recorded every twenty seconds at a rate of 100 Hz for half a second using an NI-9205 card. The collected data was analyzed using MATLAB™ to create detailed profiles for each bearing. The temperature profile was generated by averaging the readings from the two K-type bayonet thermocouples, providing a comprehensive temperature average across the entire span. The accelerometer located at the Top Dead Center (TDC) location was used to characterize the vibration profiles.

This study utilizes a field-tested algorithm for detecting defects in tapered roller bearings developed by researchers at the UTCRS [2]. This algorithm was designed to identify whether a bearing is defective, the defective component, and to estimate the size of the defect based

on empirical results at the corresponding operating conditions. The three-level analysis of the algorithm begins with a comparison of the acceleration (G_{RMS}) levels of the test bearing to those indicative of a spall. The second level of the analysis then classifies the defective component (cup, cone, or roller defect) by analyzing Power Spectral Density (PSD) plots. The final level estimates the size based on empirical data, as illustrated in the flowchart in Figure 19.

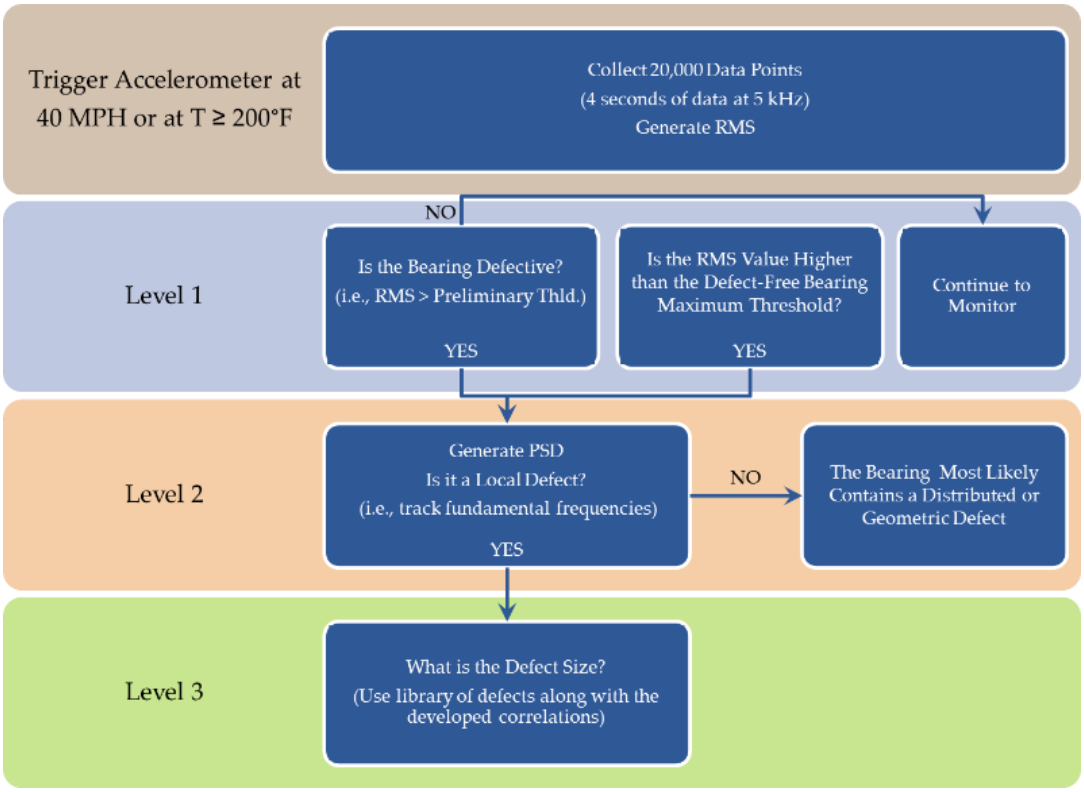

Figure 19: Defect detection algorithm flowchart [2]

CHAPTER IV

RESULTS AND DISCUSSIONS

In this chapter, the results of the testing performed to assess the validity of the ECA method in identifying potentially problematic bearings that the common practice reconditioning process might have missed will be shared and discussed.

4.1 Indicated Bearings

The reconditioned bearing cups for this batch consisted of eight bearings removed from service under *Why Made Code 11*, each having indicated subsurface defect(s) from the ECA scanner. The overall goal of the dynamic accelerated service life testing of the indicated bearings was to assess whether the suspect locations output by the ECA scanner result in the formation and propagation of spalls before the target mileage of 120,000 mi (193,121 km). To that end, the test bearings were positioned with the indicated regions directly under the applied load (i.e., top-dead-center position) and run uninterrupted until the vibration and/or thermal sensors indicated that a spall has developed or the bearings have reached 60,000 mi of continuous operation. A full teardown and visual inspection were conducted every 60,000 mi (96,560 km) or when the defect detection algorithm (Figure 19) indicated that a defect has developed. If no defect was present post teardown, the bearings were rebuilt and retested until the 120,000 mi (193,121 km) target was reached. If any abnormal behavior was detected, testing was halted for immediate teardown and visual inspection.

The initial conditions for each tester started by simulating empty (17%) railcar conditions with the load held at 5,850 lbs (26 kN) per bearing and low speeds of 25 mph (40 km/h). These

conditions were held until steady state conditions were reached, usually taking a period of a few hours. The testing conditions were then increased to 85 mph (137 km/h) and full load (34,400 lbs or 153 kN per bearing). These operating conditions were maintained for the duration of the accelerated service life test.

The experiments conducted at the UTCRS are archived using the following naming scheme: an experiment number followed by a letter denoting the current iteration of the experiment. An example of this would be experiment 200A. For this study, different letters indicated that a teardown and inspection occurred. The number is cataloged sequentially. Whenever a new experiment starts, the next number is assigned to it. Given that experiments last for weeks, it is likely that two correlating experiments will not be within one integer of each other. The labels used for the experiments involving the indicated reconditioned bearings are: Experiment 286A, Experiment 287A, Experiment 289A&B, Experiment290A, Experiment 292A, and Experiment 293A. The results for the experiments without a dedicated section are available in APPENDIX A. Results for Experiment 286A and Experiment 292A are similar to those presented in sections 4.1.1 and 4.1.2.

The test bearings were labeled using the following scheme: the number two to indicate that this is the second round of testing conducted at the UTCRS in collaboration with MxV Rail, followed by MxV and a number denoting the order in which the bearings were scanned. The labels for the eight indicated bearings are: 2MxV1, 2MxV2, 2MxV3, 2MxV4, 2MxV5, 2MxV6, 2MxV7, and 2MxV8.

4.1.1 Experiment 287A: 2MxV5 and 2MxV6

Experiment 287A featured two bearings, 2MxV5 and 2MxV6. Only 2MxV6 developed a spall during this experiment. An ECA scan of 2MxV6 is shown in Figure 20(A). The scan

outputs a C-scan image that highlights an indicated anomaly, implying a potential defect within the region of that cup raceway. The red markings in Figure 20(A) indicate localized changes in the probe impedance caused by defects that interfere with the flow of eddy currents through the conductive material. The corresponding region is displayed on the visually inspected surface of the reconditioned bearing cup, displayed in Figure 20(B). It should be noted that the defect was not discernible on the surface of the cup.

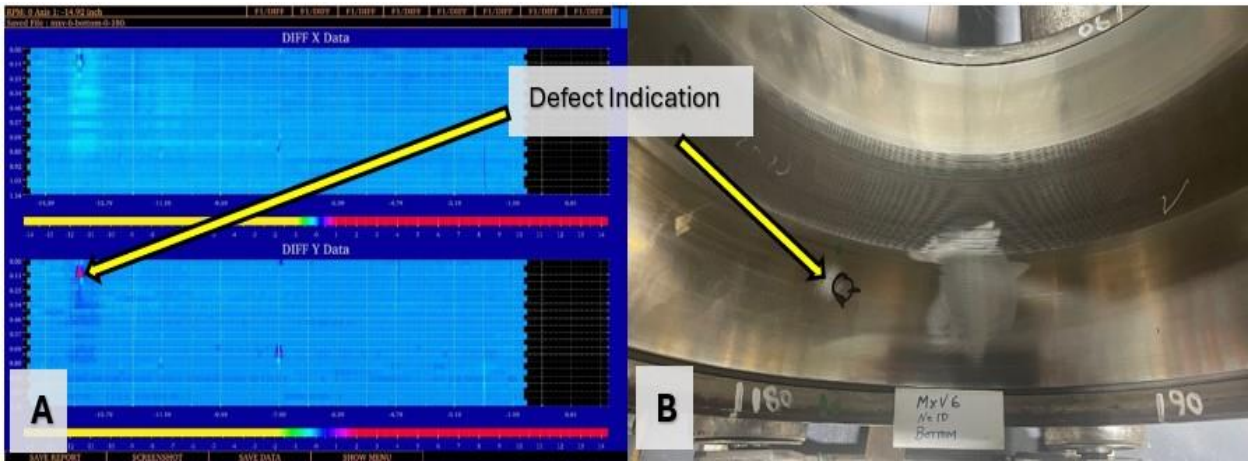

Figure 20: (A) ECA indication on the bottom raceway of 2MxV6, (B) Visual inspection of the bottom raceway of 2MxV6

A magnified scan was performed to closely display the indication on the cup raceway, as depicted in Figure 21(A). Further validation regarding whether the observed ECA indication corresponds to a defect is shown in Figure 21(B), which is the associated A-scan. This signal provides additional diagnostic insight by visualizing impedance changes across the scanned region. Signal analysis is useful not only for identifying discontinuities or defects but also for distinguishing between near-surface anomalies and signal noise caused by variations in material permeability or other factors. Additionally, this evaluation helps determine whether the indication may result from man-made dimples or tooling marks possibly introduced during the reconditioning process. The means in which the A-scan can measure impedance is through the

capacitive interaction between the conductive material and the defect, implying the presence of a dielectric and a space between two parallel plates. Peaks that arise on the left-hand side of the graph are defined to be due to the permeability or the presence of man-made dimples in the region. Peaks on the right-hand side correlate to defects in that region. The amplitude of the peaks do not define the severity of the defect as seen in other results, where peak amplitudes were smaller but developed larger defect sizes than others with larger peaks. The graph assists only in defining whether the indication is a potential defect or not.

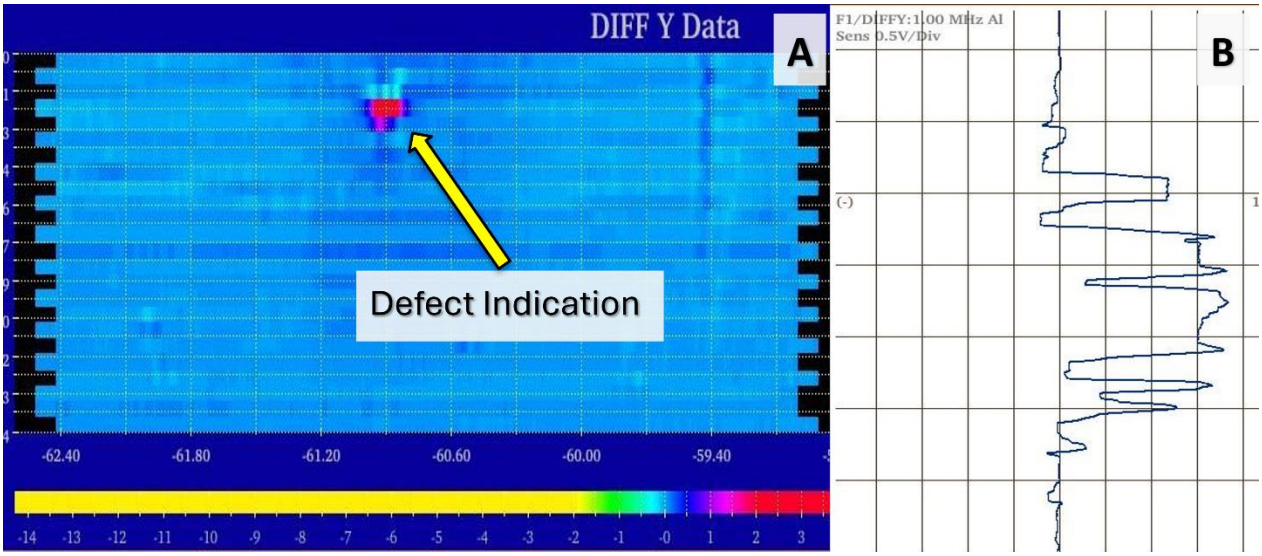

Figure 21: (A) Magnified C-scan of 2MxV6, (B) A-scan for the defect indication of 2MxV6

Since the goal of the accelerated service life testing is to simulate worst-case operation conditions, the two test bearings were loaded on the indicated regions output by the ECA. The test was carried out on the UTCRS Chamber Four-Bearing Tester (C4BT), and the experiment was stopped after the bearings had run for a total of 38,056 mi (61,245 km) as the condition monitoring system indicated that a defect had developed on the 2MxV6 bearing.

The vibration and temperature profiles for the test bearings are provided in Figure 22. The temperature data presents no characteristics associated with those of bearings in distress as the operating temperature of the defective bearing exhibited normal operating conditions at

100% load and 85 mph (137 km/h). In fact, the operating temperature for the 2MxV6 bearing, which averaged around 21.5°C (38.7°F) above ambient, was well below the average temperature for healthy bearings operating at the same load and speed conditions (indicated by the control bearing correlation in Figure 22), and significantly lower than the recommended AAR Hot-Bearing Detector (HBD) alarm threshold, which is 94.4°C (170°F) above ambient. The control bearing correlation is a statistical average temperature for a healthy bearing at those operating conditions as determined by prior work at the UTCRS [31]. It should be noted that experiments were stopped when the defect detection algorithm used would indicate that a defect had developed. The HBD alarm threshold is usually exceeded after significant damage has developed within the bearing, which may not allow for early intervention to mitigate catastrophic bearing failure.

The acceleration (G_{RMS}) levels of 2MxV6 displayed control bearing conditions at the beginning of the experiment. Nearing the 380 hour-mark (32,725 mi or 52,666 km), the defect detection algorithm indicated that a defect had initiated. The acceleration values exceeded the preliminary threshold, signifying that a possible defect had initiated. Within the following 6,000 mi (9,656 km), the acceleration surpassed the maximum threshold meaning that a spall had fully developed on one of the components of the bearing. Vibration analysis enables detection of early-stage defects through correlations to the empirical defined thresholds [2]. As for the 2MxV5 bearing, the acceleration values were below the preliminary threshold, implying that it was still healthy at this point.

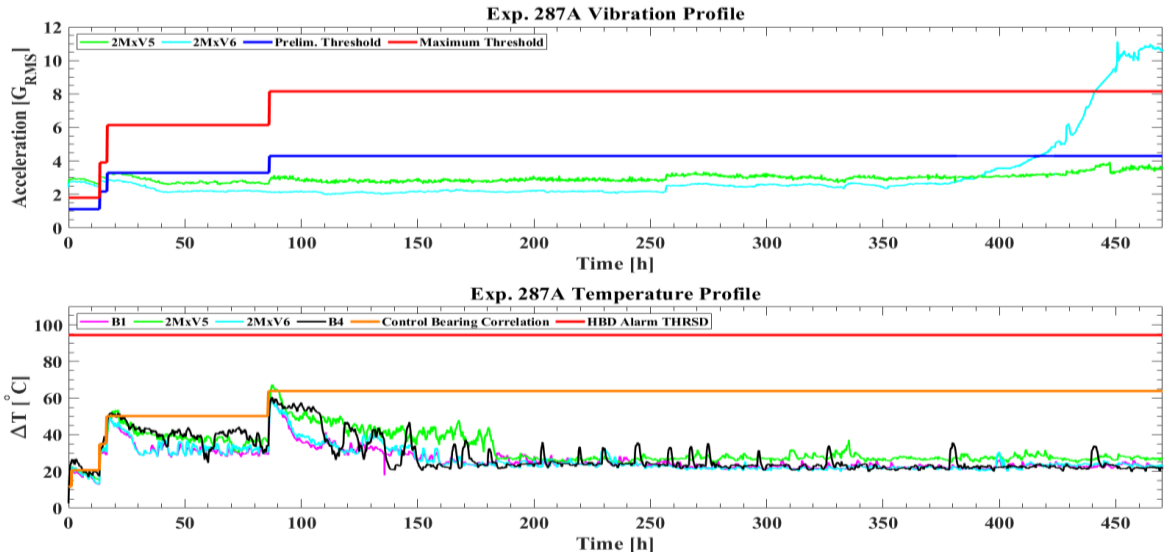

Figure 22: Vibration and temperature profiles for Experiment 287A

Table 3 provides the Level 1 analysis results for 2MxV6 as output by the defect detection algorithm. Displayed is the highest acceleration that was recorded from the Top-Dead-Center (TDC) mounted accelerometer for 2MxV6. The value in **bold** exceeds the maximum threshold, signifying that a defect has developed on one of the components. The algorithm then advances to Level 2 analysis, where it identifies the defective component by calculating the defect frequencies based on the operating conditions.

Table 3. Level 1 analysis for 2MxV6

Cup ID:	Test Bearing 2MxV6
Load [%]	100
Speed [RPM]/[MPH]	796/85
Maximum TDC Acceleration [G_{RMS}]	**11.12**
Prelim. Thld. [G_{RMS}]	4.29
Max. Thld. [G_{RMS}]	8.15

Level 2 analysis quantifies the defect energy associated with each bearing component and expresses it as a percentage relative to the component exhibiting the highest certainty. Table 4

displays results of Level 2 analysis for 2MxV6. The maximum percentage in **bold** indicates that 2MxV6 has a cup defect with 99% certainty.

Table 4. Level 2 analysis for 2MxV6

Test Bearing 2MxV6						
	Folder	17	18	19	20	21
	Speed [RPM/MPH]	796/85	796/85	796/85	796/85	796/85
TDC Accel.	Defective Component	**Cup**	**Cup**	**Cup**	**Cup**	**Cup**
	Certainty [%]	**99**	**99**	**99**	**99**	**99**

The results of the Level 2 analysis support the ECA scans given that it specifies that the cup was the defective component as expected. To confirm that the defect developed at the location output by the ECA, a full teardown and visual inspection was conducted. Figure 23(B) shows the defect that developed in the region that the ECA indicated. For comparison, the pre-test surface of this region is pictured in Figure 23(A), which shows no surface damage.

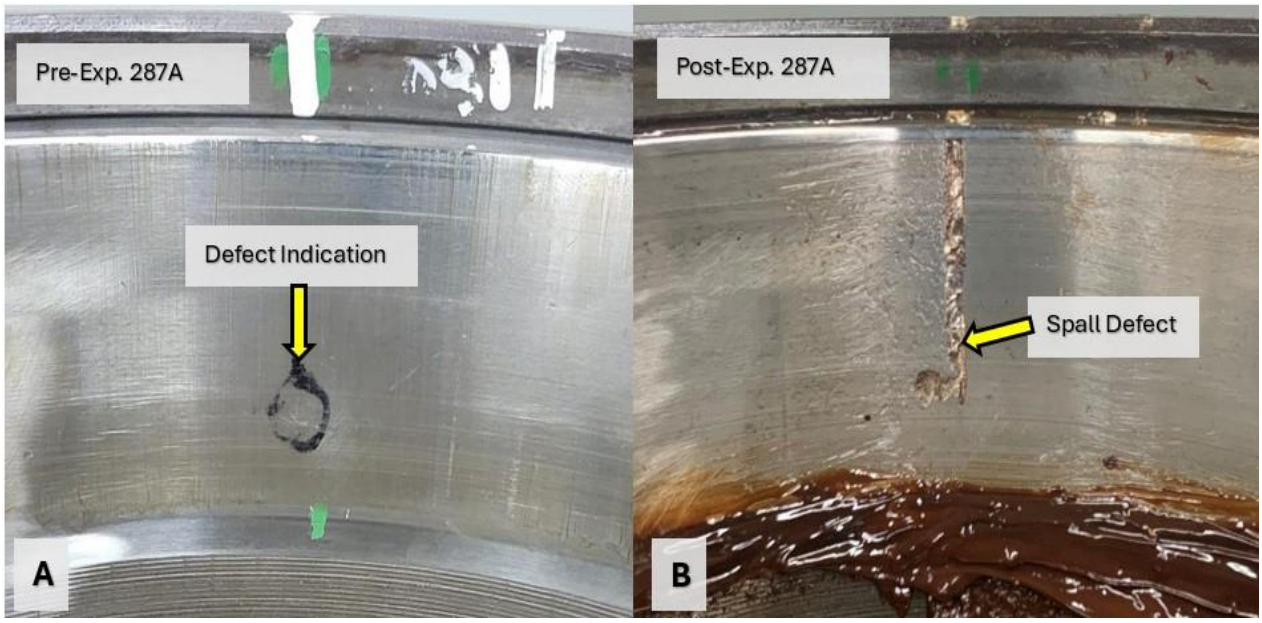

Figure 23: 2MxV6 (A) Pre-test inspection, (B) Post-test inspection

From Figure 23, it can be observed that the spall developed from the region where the ECA detected a defect and propagated towards the upper shoulder of the cup raceway. The resulting size of the spall on the cup raceway measured approximately 0.33 in^2 (2.13 cm^2). This exceeds the maximum allowable defect size (0.14 in^2 or 0.90 cm^2) for repair, meaning that this would no longer be eligible for the reconditioning process. Although the spall was small, continued operation would have likely resulted in a potential mechanical failure. It is especially important to note that 2MxV6 developed this spall after only 38,056 mi (61,245 km) of operation. To reiterate, the reconditioning process is expected to extend the service life of bearings anywhere from 50,000 mi to 250,000 mi (80,467 km to 402,336 km). The 2MxV5 bearing was also inspected, and no defects were observed in the indicated region. Thus, this bearing was rebuilt in accordance with AAR guidelines and was paired with another indicated bearing for continued testing.

4.1.2 Experiment 290A: 2MxV7 and 2MxV8

2MxV7 and 2MxV8 were the test bearings utilized in Experiment 290A. Scans of 2MxV8, depicted in Figure 24(A), output a C-scan image with a detected anomaly, indicating a potential defect on the bottom raceway. The corresponding region is displayed on the visually inspected surface of the reconditioned bearing cup, shown in Figure 24(B). The defect was not discernible on the surface of the cup.

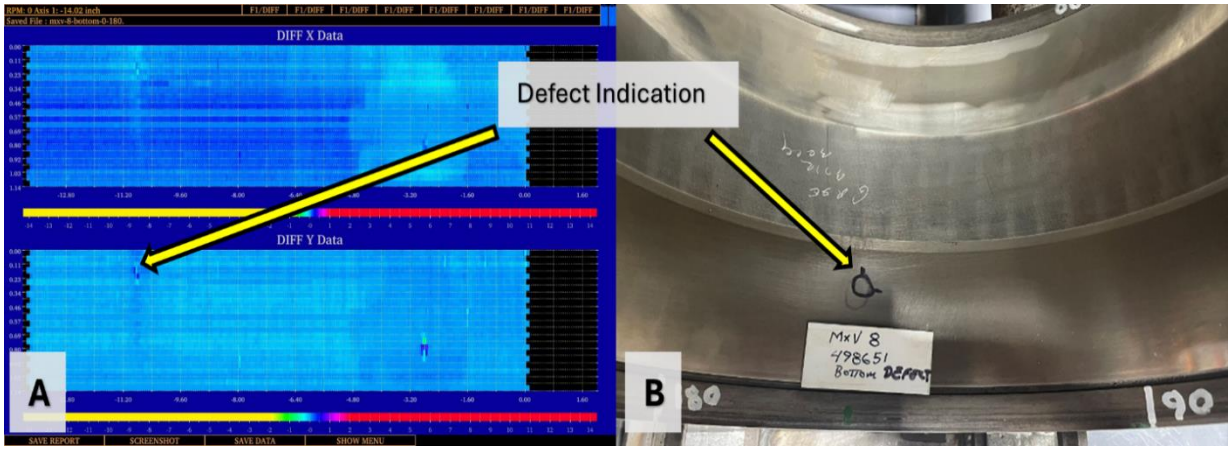

Figure 24: (A) ECA indication on the bottom raceway of 2MxV8, (B) Visual inspection of the bottom raceway of 2MxV8

Figure 25(A) provides a magnified image to better represent the indication from the ECA scan. The indication did not output as high of an amplitude as the one for 2MxV6, however the A-scan was still employed to verify that this anomaly was caused by a subsurface defect, as shown in Figure 25(B). The two major peaks observed on the right-hand side of the graph imply that the anomaly indeed correlates to the presence of a subsurface defect. While several smaller peaks appear on the left-hand side, their amplitudes do not surpass the maximum impedance observed on the right. To reiterate, Figure 25(B) distinguishes that there is a near-surface defect that has been indicated rather than the anomaly being caused by signal noise from variations in material permeability or tooling marks.

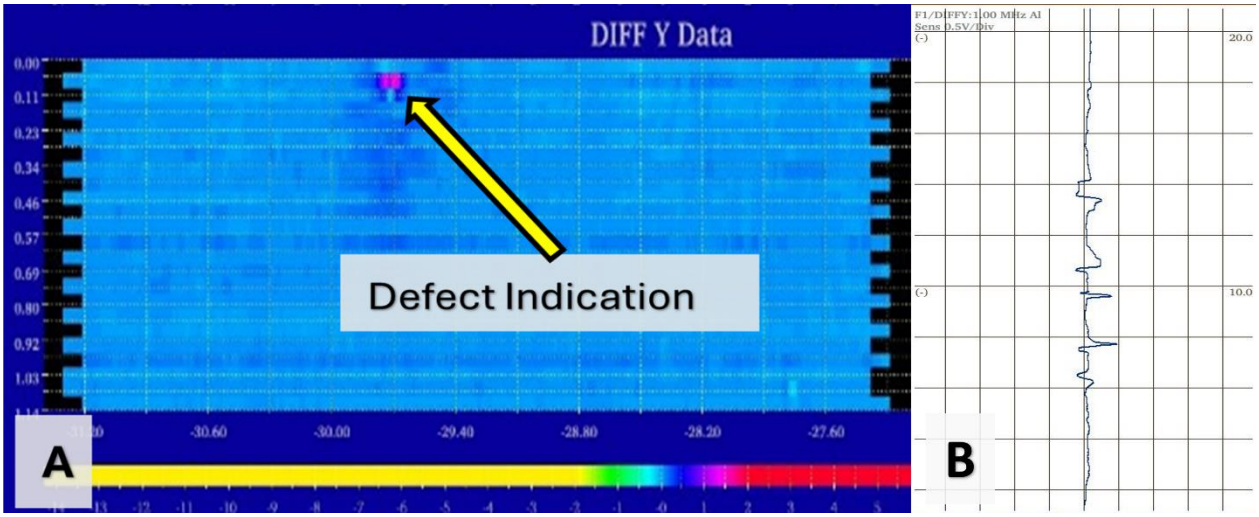

Figure 25: (A) Magnified C-scan of 2MxV8, (B) A-scan for 2MxV8

The same testing procedures followed in Experiment 287A were executed for bearings 2MxV7 and 2MxV8 in Experiment 290A. Again, the ECA indicated regions in the bearing cups were placed directly under the applied load (i.e., top-dead-center position). These bearings were run on one of the UTCRS Four-Bearing Testers (4BT) using the same accelerated service life conditions previously mentioned. This experiment ran for a total of 41,151 mi (66,226 km) of operation and was terminated early due to the onset of a spall.

Plots representing the vibration and temperature profiles of these two test bearings are given in Figure 26. The operating temperatures for both test bearings, which averaged around 39.0°C (70.2°F) above ambient, remained below the control bearing correlation for the majority of the experiment, and well below the HBD alarm threshold. The acceleration (G_{RMS}) levels for 2MxV7 ran steady and below the preliminary threshold, exhibiting healthy bearing conditions for the duration of the experiment. However, the acceleration levels for the 2MxV8 bearing started to steadily increase around the 370 hour-mark, crossing the preliminary threshold at hour 434 (31,025 mi or 49,930 km) of the experiment, thus signifying a possible defect initiation, and eventually exceeding the maximum threshold at the 41,151 mi (66,226 km) mark, which

confirmed that a defect had developed on that bearing.

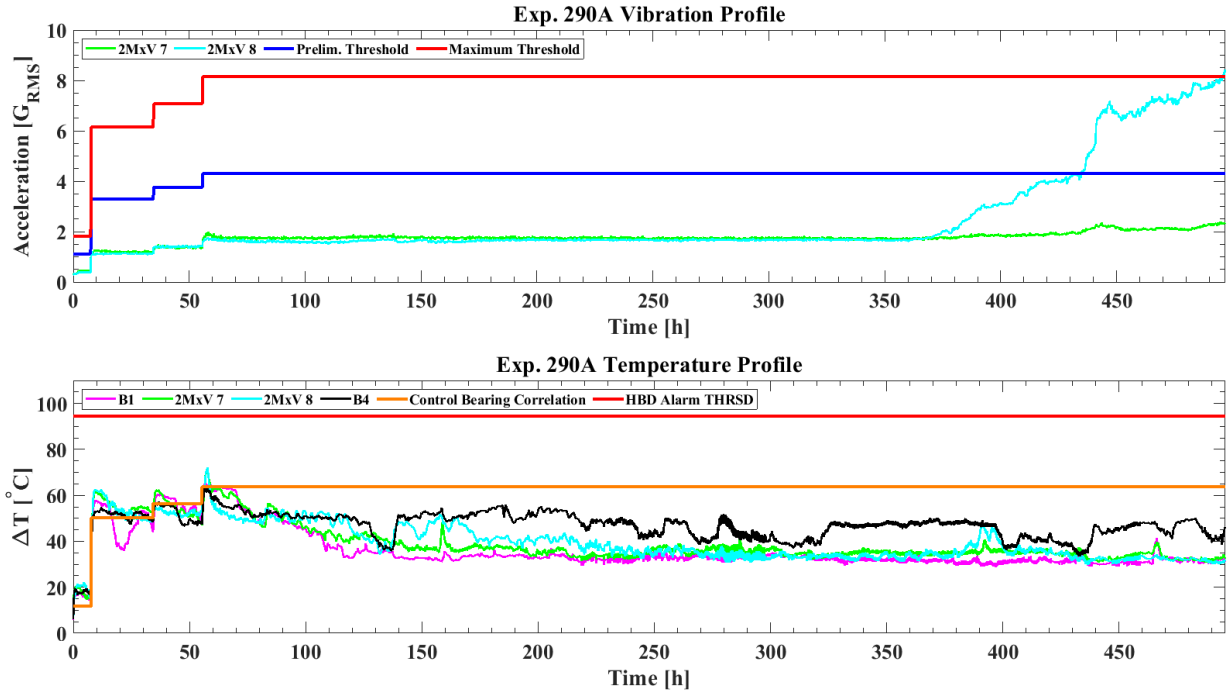

Figure 26: Vibration and temperature profiles for Experiment 290A

Table 5 displays the results from the Level 1 analysis using the vibration data output by the Top-Dead-Center (TDC) mounted accelerometer for 2MxV8. The value in **bold** exceeds the maximum threshold, signifying that one of the components of that bearing developed a defect. Level 2 analysis was then performed to identify the defective component.

Table 5. Level 1 analysis of 2MxV8

Cup ID:	Test Bearing 2MxV8
Load [%]	100
Speed [RPM]/[MPH]	796/85
Maximum TDC Acceleration [G_{RMS}]	**8.42**
Prelim. Thld. [G_{RMS}]	4.29
Max. Thld. [G_{RMS}]	8.15

Table 6 displays the output of the Level 2 analysis for 2MxV8. The value for the maximum percentage in **bold** indicates that 2MxV8 has a cup defect with 99% certainty.

Table 6. Level 2 analysis for 2MxV8

Test Bearing 2MxV8						
	Folder	14	15	16	17	18
	Speed [RPM/MPH]	796/85	796/85	796/85	796/85	796/85
TDC Accel.	Defective Component	**Cup**	**Cup**	**Cup**	**Cup**	**Cup**
	Certainty [%]	**99**	**99**	**99**	**99**	**99**

The output of the Level 2 analysis supports the indication from the ECA scan as it confirmed that the defective component was the cup. A full teardown and visual inspection were then conducted. Figure 27(B) displays a post-test image of the loaded zone with the developed defect in the same region that the ECA scan indicated. A pre-test image of this same region displayed no visible defect as shown in Figure 27(A).

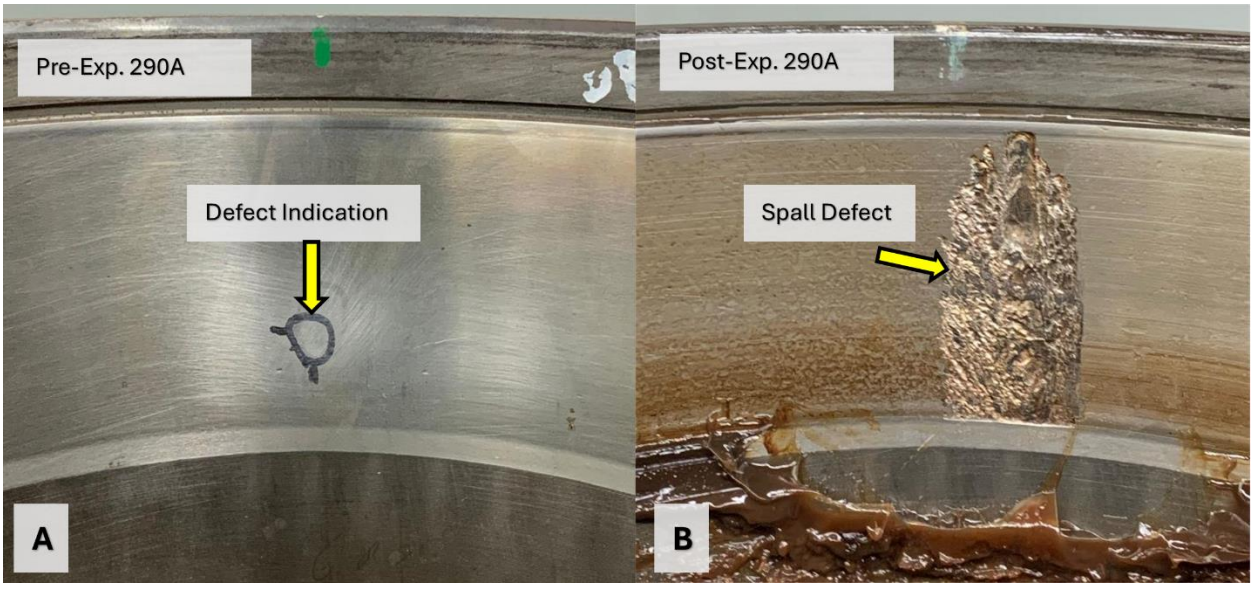

Figure 27: 2MxV8 (A) Pre-test inspection, (B) Post-test inspection

The propagated defect was approximately 1 in (2.54 cm) wide and spanned across the width of the cup raceway. The size of the spall measured approximately 1.46 in^2 (9.42 cm^2). This

area exceeds the maximum allowable defect size (0.14 in^2 or 0.90 cm^2) for repairing, making it no longer eligible for the reconditioning process. Bearing 2MxV8 developed this spall after running a total distance of 41,151 mi (66,226 km). The visual inspection revealed no defects on the 2MxV7 bearing, so, it was rebuilt in accordance with AAR guidelines and paired with another indicated bearing for continued testing.

4.1.3 Experiment 293A: 2MxV5 and 2MxV7

Following the complete teardown and thorough inspections from experiments 287A and 290A, 2MxV5 and 2MxV7 were paired for the next round of testing since they had not developed a defect in their previous test and had not yet reached the 120,000 milestone. The loading locations remained the same as they were in their respective experiments. 2MxV5 ran for two previous experiments (Experiments 287A and 292A) that terminated early due to the neighboring bearing developing a defect. Therefore, to avoid unnecessary stoppages and interruptions to this test, it was decided, in consultation with MxV Rail engineers, to allow this experiment to run until the 2MxV7 bearing reached the 120,000 mileage goal, which meant that the 2MxV5 bearing would exceed that mileage.

ECA Scans of 2MxV5 and 2MxV7 are depicted in Figure 28(A) and Figure 29(A), respectively. These figures display C-scan images of their corresponding detected anomalies. The visually inspected surfaces of these regions can be seen in Figure 28(B) for 2MxV5 and Figure 29(B) for 2MxV7. There were no discernible defects on either raceway.

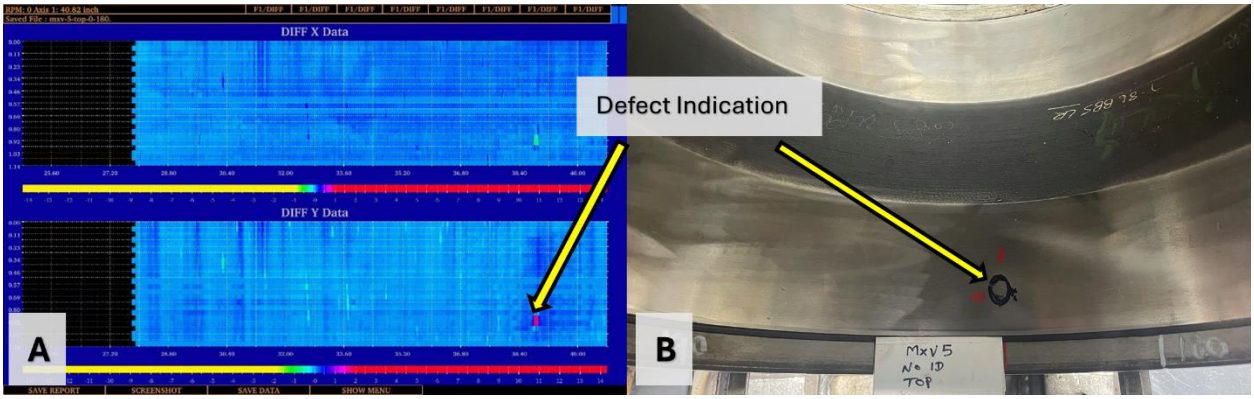

Figure 28: (A) ECA indication on the top raceway of 2MxV5, (B) Visual inspection of the top raceway of 2MxV5

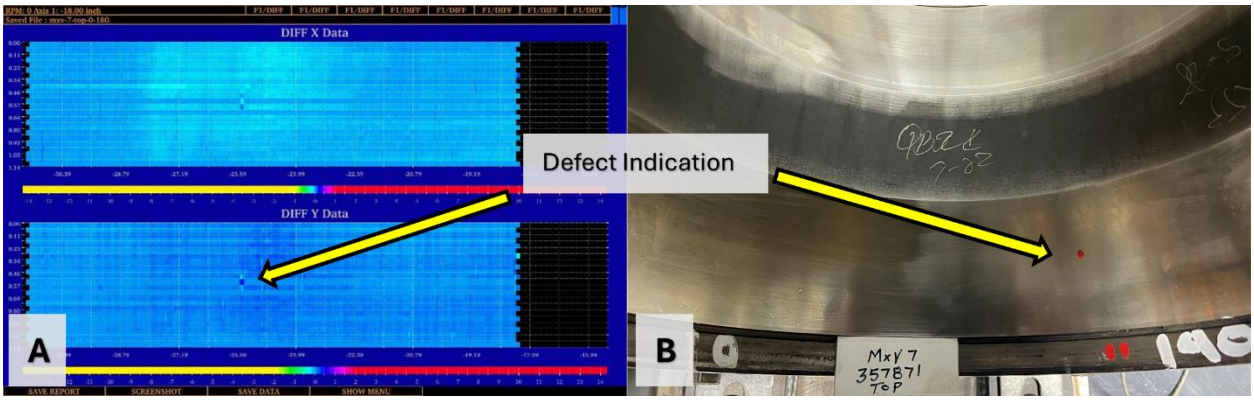

Figure 29: (A) ECA indication on the top raceway of 2MxV7, (B) Visual inspection of the top raceway of 2MxV7

2MxV5 displayed a high amplitude anomaly, while 2MxV7 had a significantly lower one. Figure 30(A) and Figure 31(A) provide magnified C-scans to better visually represent the indications output by the ECA scanner. To validate whether the indications correspond to defects, A-scans were generated via the use of a pencil probe as shown in Figure 30(B) and Figure 31(B). The A-scan output by the ECA for 2MxV5 exhibited major peaks on the right-hand side of the graph, implying that the anomaly is a defect. 2MxV7 displayed multiple peaks on both sides of the impedance plot. This is possibly explained by variations in material

permeability; however, the maximum amplitude was on the right-hand side signifying that it was likely a defect.

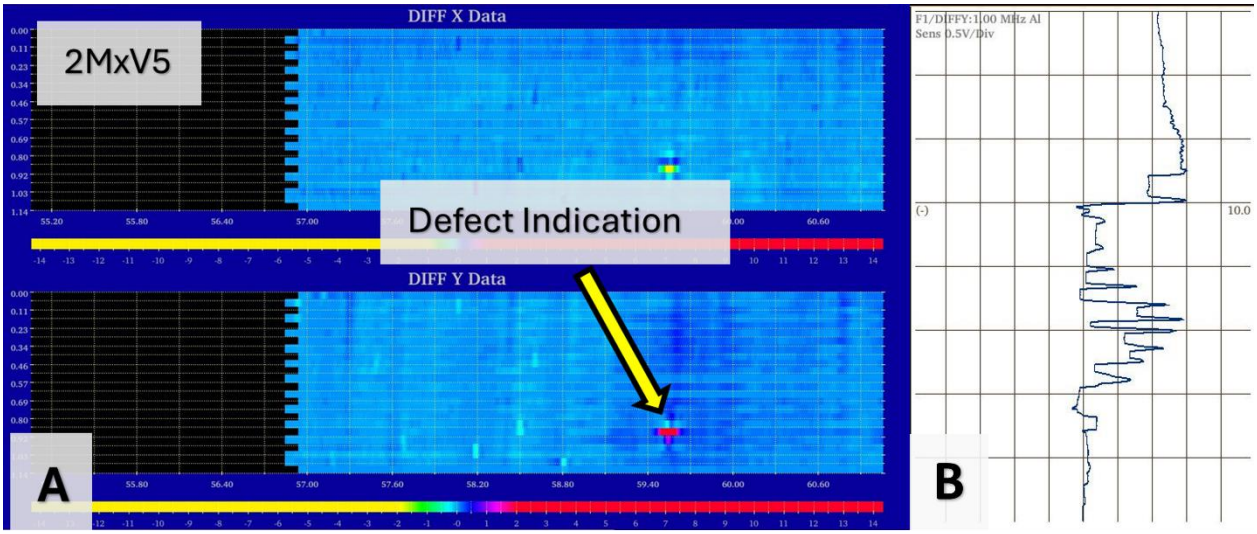

Figure 30: (A) Magnified C-scan of 2MxV5, (B) A-scan for 2MxV5

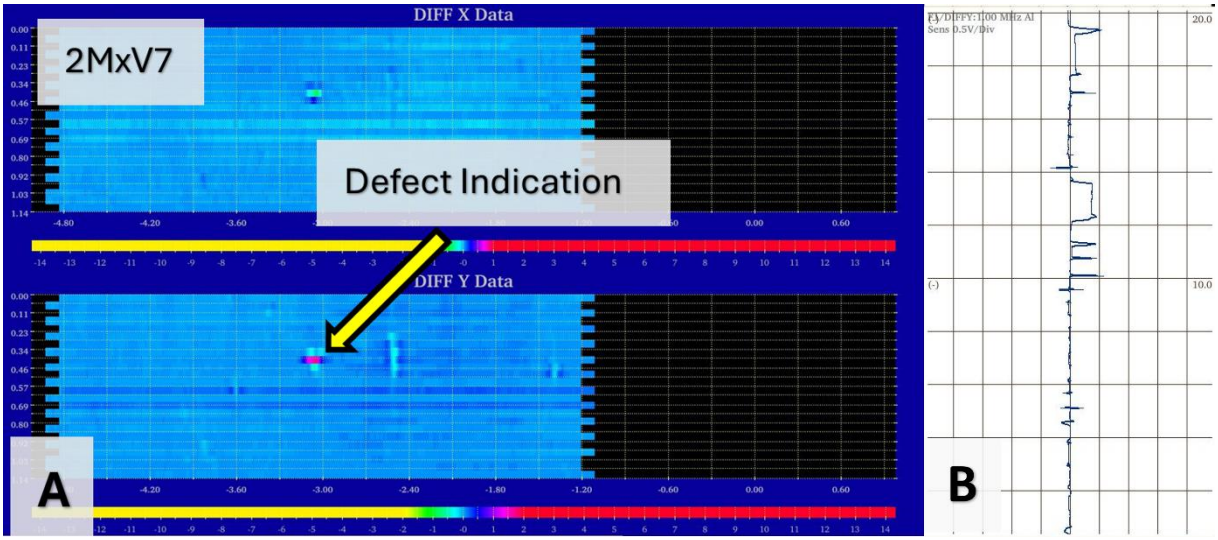

Figure 31: (A) Magnified C-scan of 2MxV7, (B) A-scan for 2MxV7

Similar procedures to those carried out in the previous experiments were followed with the bearings set up on the 4BT. Both bearings were rebuilt using the same grease used in their previous experiments, however, the spacer rings were replaced to ensure that the lateral displacement remained within suggested AAR guidelines. Again, the ECA indicated regions on

the bearing cups were placed directly under the applied load (i.e., top-dead-center position). Accelerated service life testing conditions of 85 mph (137 km/h) and full railcar load (34,400 lbs or 153 kN per bearing) were utilized for this experiment. This experiment was terminated after 2MxV7 ran for a total of 120,114 mi (193,304 km), reaching the test mileage goal. As for 2MxV5, it ran for a total of 151,108 mi (243,185 km), exceeding the mileage goal as explained earlier.

The vibration and temperature profiles for these two test bearings are plotted in Figure 32. The operating temperatures for both test bearings, which averaged around 46.9°C (84.4°F) for 2MxV5 and 61.2°C (110.2°F) for 2MxV7 above ambient, remained below the control bearing correlation for the majority of the experiment, and well below the HBD alarm threshold. The acceleration for 2MxV7 ran steady and below the preliminary threshold, signifying that it remained a healthy bearing for the duration of the experiment. However, the acceleration levels for the 2MxV5 bearing started to steadily increase around the 630 hour-mark (118,879 mi or 191,317 km) of the experiment. The vibration levels approached the maximum threshold and remained just below that threshold. The G_{RMS} values that are between the preliminary threshold (blue line), and the maximum threshold (red line) signify that the bearing is potentially defective. However, the steady increase in the G_{RMS} value exhibited by the 2MxV5 bearing is usually indicative that a spall has initiated and propagated.

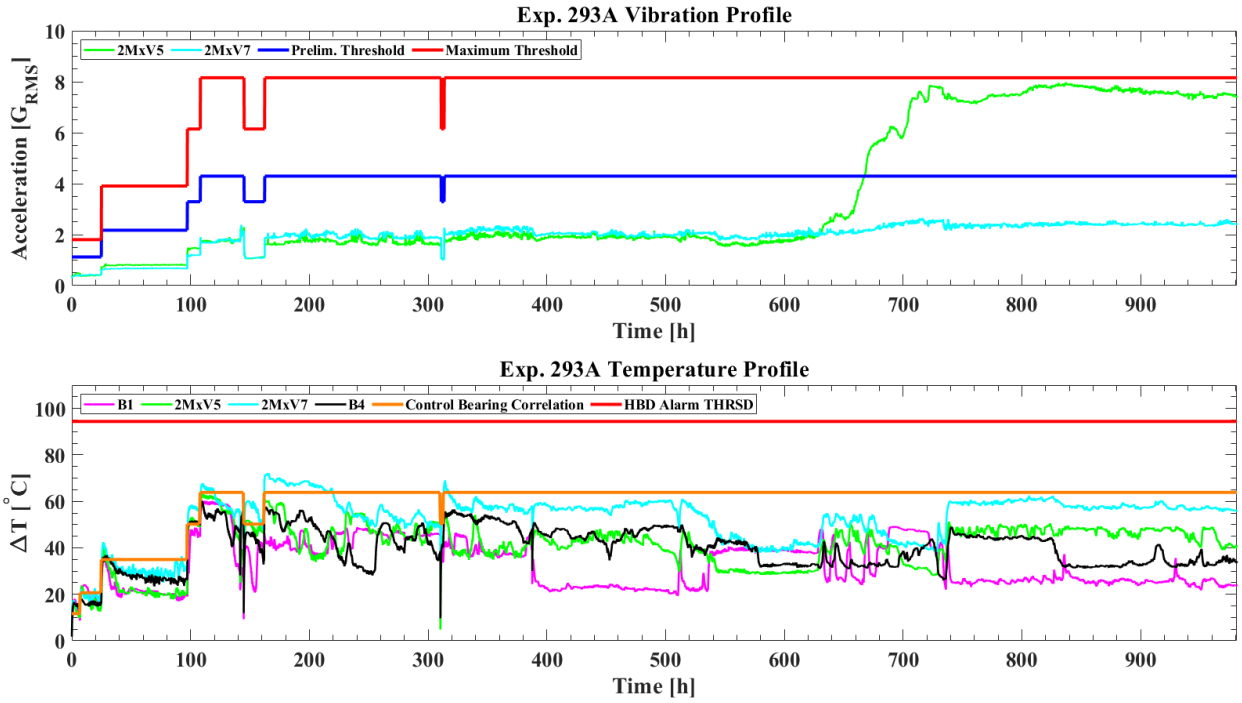

Figure 32: Vibration and temperature profiles for Experiment 293A

Table 7 displays the results from the Level 1 analysis using the vibration data output by the TDC-mounted accelerometer for 2MxV5 and 2MxV7. The value for 2MxV5 exceeded the preliminary threshold (*italicized*), signifying that the bearing has potentially developed a defect. The 2MxV7 bearing never exceeded either threshold, which implied that it was healthy (defect-free). Level 2 analysis was then performed to identify the defective component.

Table 7. Level 1 analysis for 2MxV5 and 2MxV7

Cup ID:	**Test Bearing 2MxV5**	**Test Bearing 2MxV7**
Load [%]	100	100
Speed [RPM]/[MPH]	796/85	796/85
Maximum TDC Acceleration [G_{RMS}]	*7.97*	2.65
Prelim. Thld. [G_{RMS}]	4.29	4.29
Max. Thld. [G_{RMS}]	8.15	8.15

Table 8 and

Table 9 display the output of the Level 2 analysis for 2MxV5 and 2MxV7, respectively. The value for the maximum percentage for 2MxV5 in **bold** indicates that a defect developed on the cup with 99% certainty. Level 2 analysis for 2Mxv7 also implies that a cup defect had developed with 99% certainty even though the vibration levels did not exceed the preliminary threshold. When this happens, it could mean one of two things; either the defect that initiated is very small and in its very early stages of development, or cross talk between the two test bearings occurred where the 2MxV7 bearing picked up the vibrations from the neighboring 2MxV5 bearing. The only way to ascertain what actually transpired is by performing a full teardown and visual inspection, which ensued.

Table 8. Level 2 analysis for 2MxV5

Test Bearing 2MxV5						
	Folder	38	39	40	41	42
	Speed [RPM/MPH]	796/85	796/85	796/85	796/85	796/85
TDC Accel.	Certainty [%]	**99**	**99**	**99**	**99**	**99**
	Defective Component	**Cup**	**Cup**	**Cup**	**Cup**	**Cup**

Table 9. Level 2 analysis for 2MxV7

Test Bearing 2MxV7						
	Folder	38	39	40	41	42
	Speed [RPM/MPH]	796/85	796/85	796/85	796/85	796/85
TDC Accel.	Certainty [%]	**99**	**99**	**99**	**99**	**99**
	Defective Component	**Cup**	**Cup**	**Cup**	**Cup**	**Cup**

The output of the Level 2 analysis supports the indication from the ECA scan as it confirmed that the defective components were the cups. A full teardown and visual inspection

were then conducted for both bearings since the mileage goal was reached. Figure 33(B) and Figure 34(B) display post-test images of 2MxV5 and 2MxV7, respectively. These images show the spalls that developed on both cups in the regions that had ECA scan indications. For comparison, the pre-test images of these same regions for bearings 2MxV5 and 2MxV7 are pictured in Figure 33(A) and Figure 34(A), respectively, which shows no surface damage. All corresponding test images for Experiment 292A can be found in APPENDIX A.

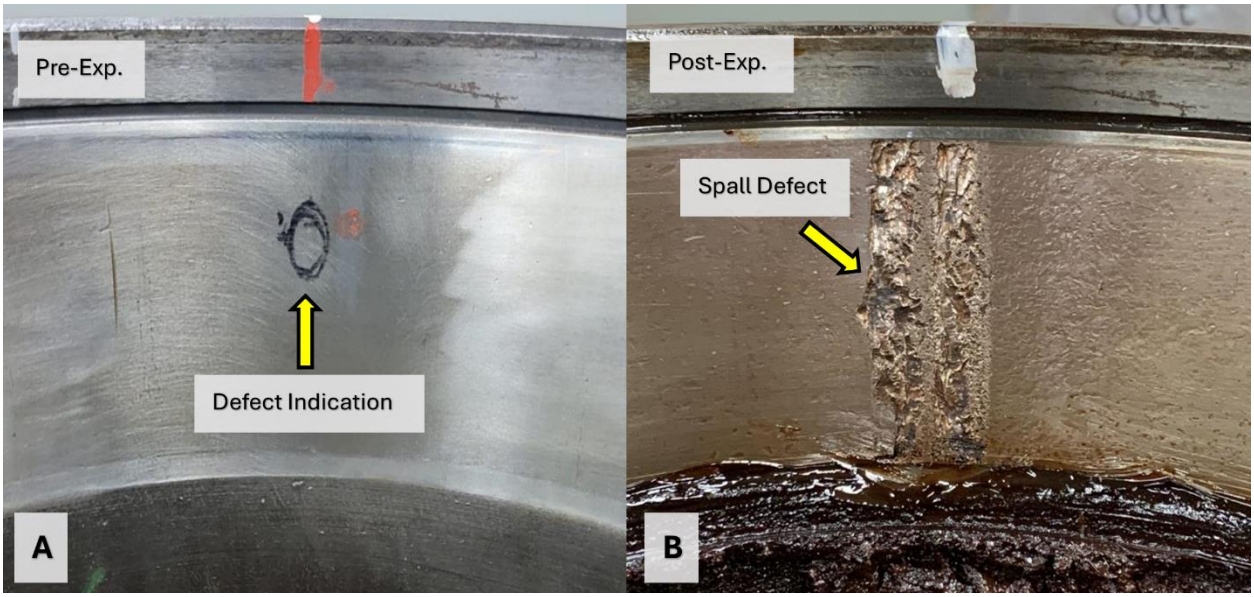

Figure 33: 2MxV5 (A) Pre-test inspection, (B) Post-test inspection

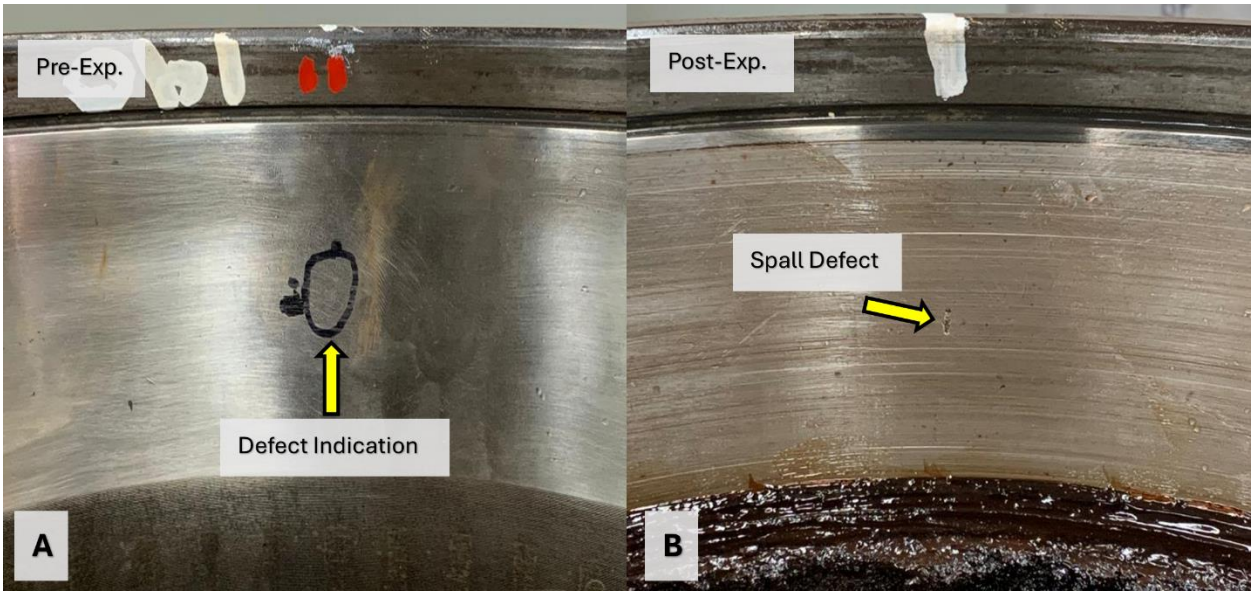

Figure 34: 2MxV7 (A) Pre-test inspection, (B) Post-test inspection

The propagated defect for 2MxV5 was approximately 0.5 in (1.27 cm) wide and spanned across the width of the cup raceway. The size of this spall measured approximately 1.51 in^2 (9.74 cm^2). This area exceeds the maximum allowable defect size (0.14 in^2 or 0.90 cm^2) for repair, making it unsuitable for the reconditioning process. Referring to the vibration profile of Figure 32, it can be seen that the spall on bearing 2MxV5 started developing after running a total

distance of 118,879 mi (191,317 km), which is just before reaching the target mileage of 120,000 mi, and propagated to the size seen in Figure 33(B) after 151,108 mi (243,185 km) of operation. Bearing 2MxV7 developed a spall that measured approximately 0.02 in^2 (0.13 cm^2) after running a total of 120,114 mi (193,304 km). This spall size does not exceed the maximum allowable defect size (0.14 in^2 or 0.90 cm^2) for repair, which means that this bearing can potentially undergo another reconditioning process before re-entry into rail revenue service. Although the spall was small, it could have resulted in a potential mechanical failure. It is important to note that the ECA scanner was still able to detect a defect that would initiate in that region.

4.1.4 Experiment 289A: 2MxV1 and 2MxV2

2MxV1 and 2MxV2 were the test bearings utilized in Experiment 289A, and the ECA scans for these two bearings are depicted in Figure 35(A) and Figure 36(A), respectively. These figures display C-scan images of their corresponding detected anomalies. For 2MxV1, multiple red indications are present, but only one represents a defect as the others were tooling marks such as repair dimples. The visually inspected surfaces of these regions can be seen in Figure 35(B) for 2MxV1 and Figure 36(B) for 2MxV2. There were no discernible defects on either raceway.

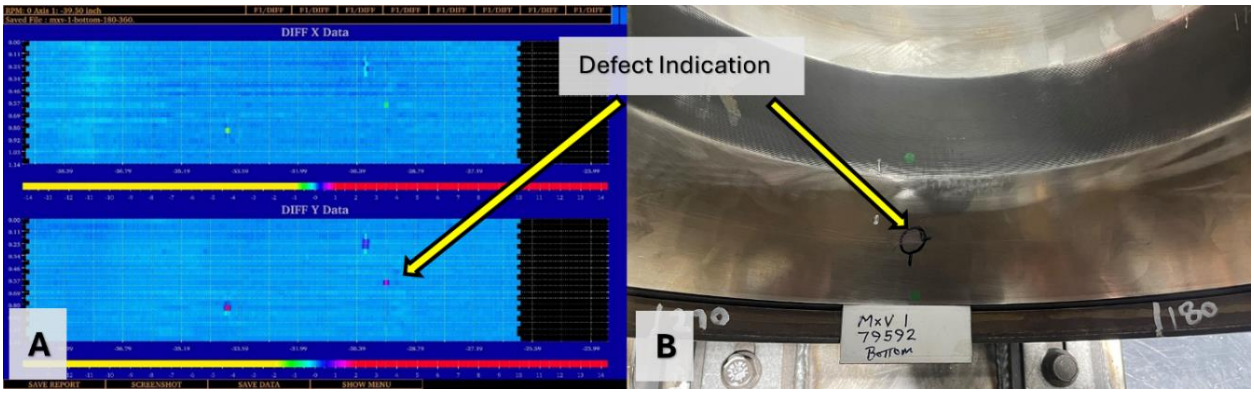

Figure 35: (A) ECA indication on the bottom raceway of 2MxV1, (B) Visual inspection of the bottom raceway of 2MxV1

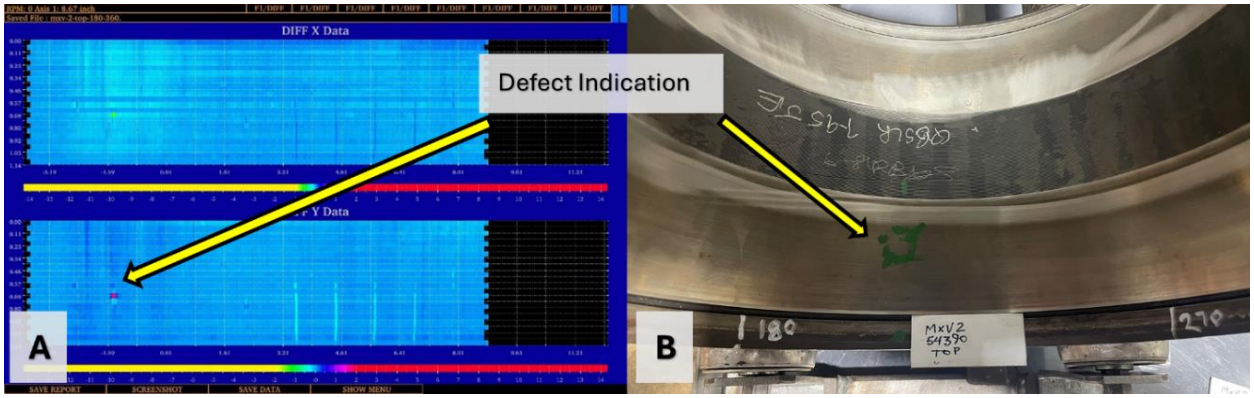

Figure 36: (A) ECA indication on the top raceway of 2MxV2, (B) Visual inspection of the top raceway of 2MxV2

2MxV1 displayed multiple anomalies as pictured in Figure 37(A). This image provides a magnified C-scan to better visually represent the indications output by the ECA scanner. The C-scan displays two high amplitudes on the image but one represents a man-made dimple that was located on the surface. To validate whether the indications correspond to defects, A-scans were generated via the use of a pencil probe as shown in Figure 37(B). The A-scan output by the ECA for 2MxV1 exhibited small peaks that were mainly seen on the right-hand side of the scan, implying that the anomaly is a defect.

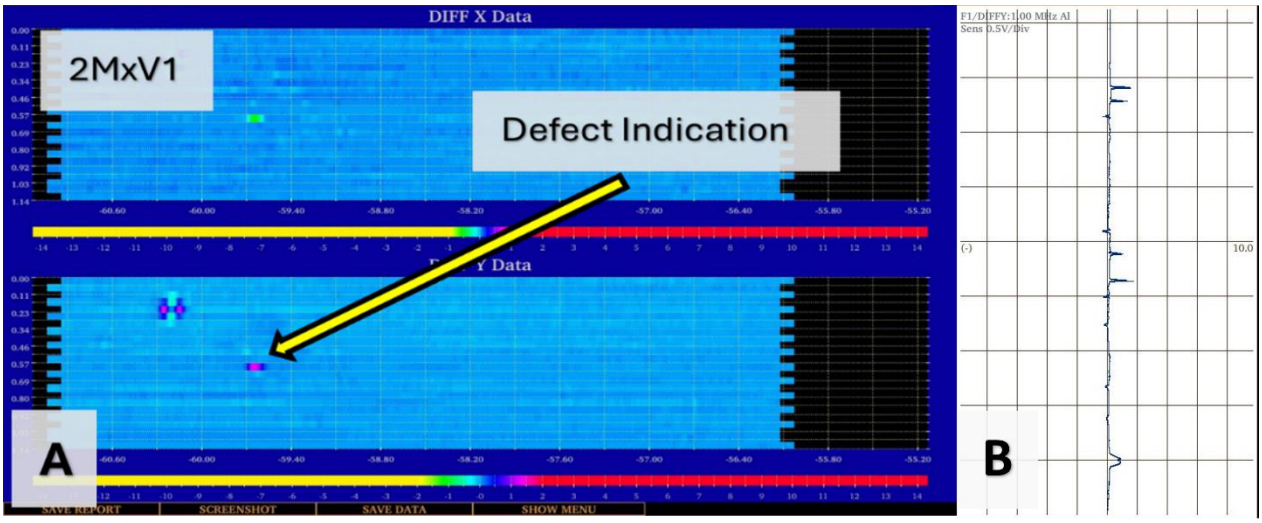

Figure 37: (A) Magnified C-scan of 2MxV1, (B) A-scan for 2MxV1

Figure 38(A) provides a magnified image for 2MxV2 to better represent the indication. Only one indication was displayed on the C-scan image for 2MxV2. To validate whether the indication corresponded to a defect, an A-scan was generated via the use of a pencil probe, as shown in Figure 38(B). Larger peaks can be observed on the right-hand side, meaning that the indication is a defect. To reiterate, the change in impedance is not a measure of the severity of the defect but rather denotes the existence of one near the surface.

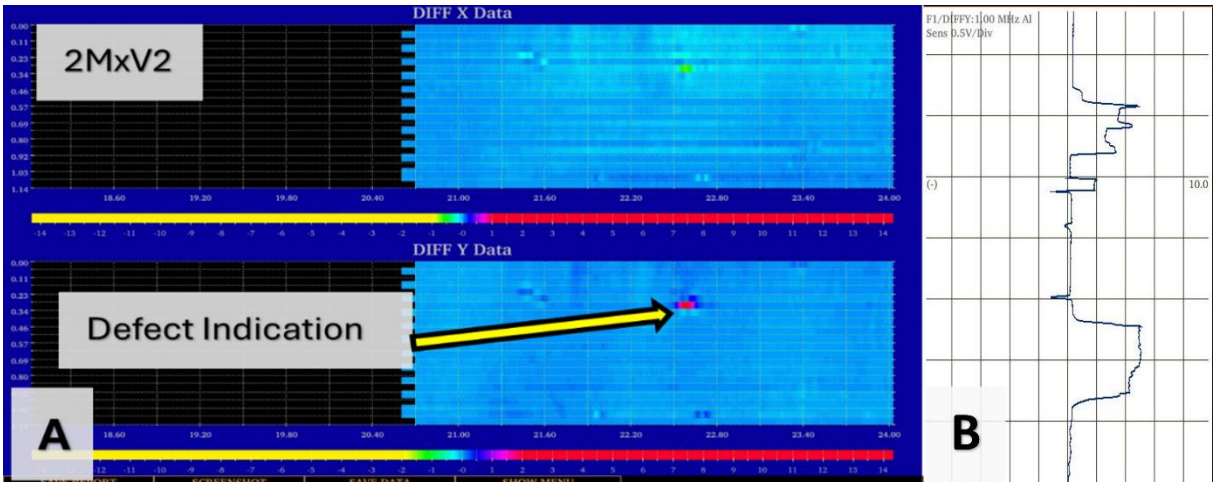

Figure 38: (A) Magnified C-scan of 2MxV2, (B) A-scan for 2MxV2

Similar procedures to those carried out in the previous experiments were followed with the bearings set up on the 4BT. Again, the ECA indicated regions on the bearing cups were placed directly under the applied load (i.e., top-dead-center position). Accelerated service life testing conditions of 85 mph (137 km/h) and full railcar load (34,400 lbs or 153 kN per bearing) were utilized for this experiment. This experiment was terminated after 2MxV1 and 2MxV2 ran for a total of 60,496 mi (97,359 km), reaching the halfway mark. Plots representing the vibration and temperature profiles of these two test bearings are given in Figure 39. The operating temperatures for both test bearings, which averaged around 48.7°C (87.7°F) for 2MxV1 and 53.5°C (96.3°F) for 2MxV2 above ambient, remained below the control bearing correlation for the majority of the experiment, and well below the HBD alarm threshold. The acceleration levels for 2MxV2 ran steady and below the preliminary threshold, exhibiting healthy bearing conditions for the duration of the experiment. However, the acceleration levels for 2MxV1 increased to the preliminary threshold and remained at that level, signifying that the bearing is potentially defective. The acceleration then experienced an impulse due to electrical issues that occurred during the experiment.

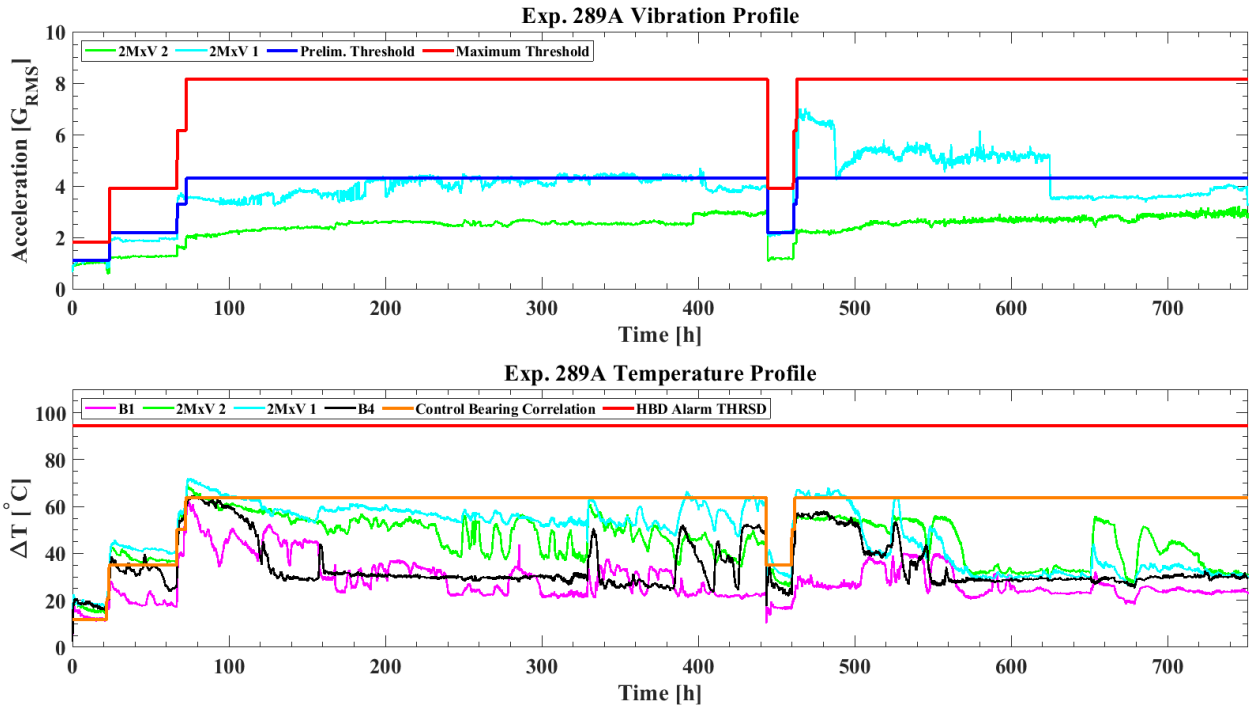

Figure 39: Vibration and temperature profiles for Experiment 289A

Table 10 displays the results from the Level 1 analysis using the vibration data output by the TDC-mounted accelerometer for 2MxV1 and 2MxV2. The value for 2MxV1 only exceeded the preliminary threshold (*italicized*), signifying that the bearing potentially developed a defect. 2MxV2 never exceeded either threshold. Level 2 analysis was then performed to identify the defective component.

Table 10. Level 1 analysis for 2MxV1 and 2MxV2

Cup ID:	Test Bearing 2MxV1	Test Bearing 2MxV2
Load [%]	100	100
Speed [RPM]/[MPH]	796/85	796/85
Maximum TDC Acceleration [G_{RMS}]	*4.71*	2.97
Prelim. Thld. [G_{RMS}]	4.29	4.29
Max. Thld. [G_{RMS}]	8.15	8.15

Table 11 and

Table 12 display the output of the Level 2 analysis for 2MxV1 and 2MxV2, respectively. The value for the maximum percentage for 2MxV1 in **bold** indicates that a defect developed on the cup with 99% certainty. Level 2 analysis for 2MxV2 also implies that a cup defect had developed with an average certainty of 98% even though the vibration levels did not exceed the preliminary threshold.

Table 11. Level 2 analysis for 2MxV1

Test Bearing 2MxV1						
	Folder	29	30	31	32	33
	Speed [RPM/MPH]	796/85	796/85	796/85	796/85	796/85
TDC Accel.	Defective Component	**Cup**	**Cup**	**Cup**	**Cup**	**Cup**
	Certainty [%]	**99**	**99**	**99**	**99**	**99**

Table 12. Level 2 analysis for 2MxV2

Test Bearing 2MxV1						
	Folder	29	30	31	32	33
	Speed [RPM/MPH]	796/85	796/85	796/85	796/85	796/85
TDC Accel.	Defective Component	**Cup**	**Cup**	**Cup**	**Cup**	**Cup**
	Certainty [%]	**98**	**98**	**99**	**99**	**98**

The output of the Level 2 analysis supports the indication from the ECA scan as it confirmed that the defective components were the cups. A full teardown and visual inspection were then conducted for both bearings. Pre- and post-images of the 2MxV1 bearing for this experiment are depicted in Figure 40(A) and Figure 40(B), respectively. A small defect can be observed on the surface of the raceway. Moreover, the post-test image for the 2MxV2 bearing, shown in Figure 41(B), also shows that a very small defect in its early stages of development has initiated in the region where the C-scan identified a defect.

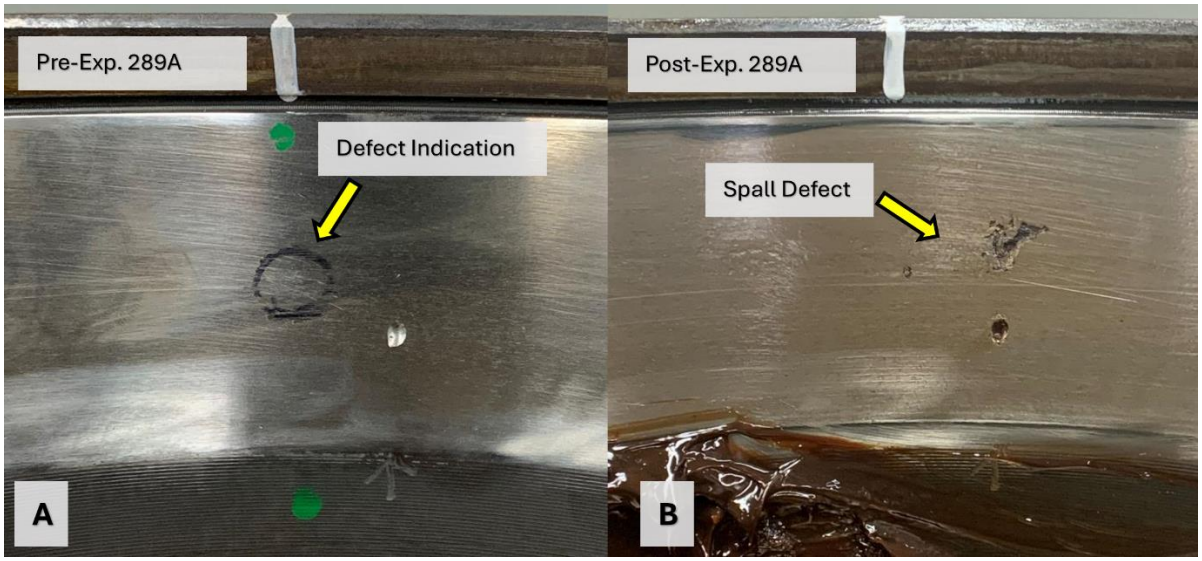

Figure 40: 2MxV1 (A) Pre-test inspection for 2MxV1, (B) Post-test inspection

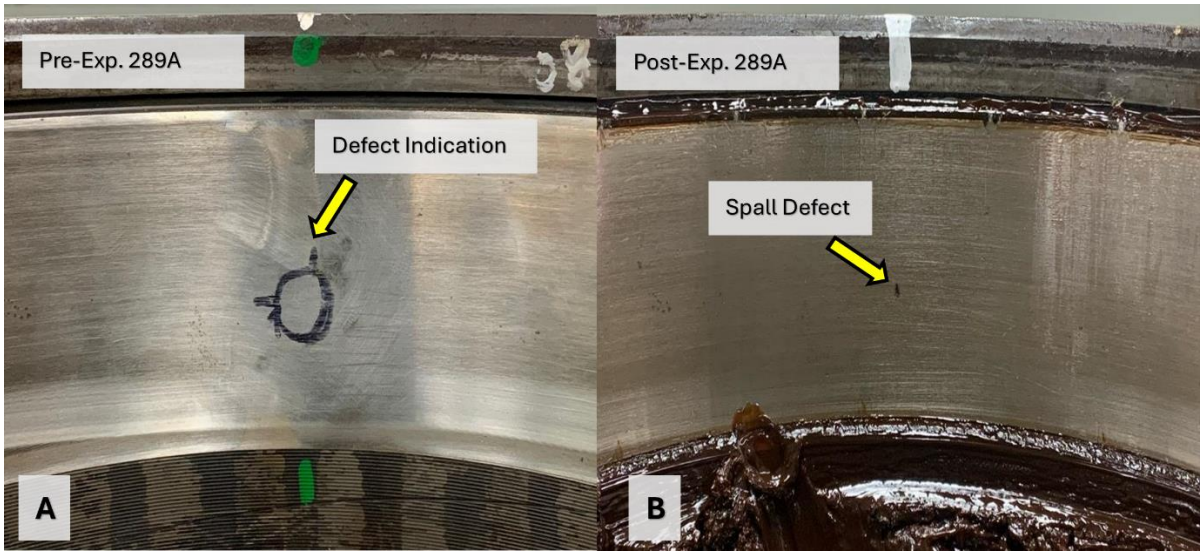

Figure 41: 2MxV2 (A) Pre-test inspection for 2MxV2, (B) Post-test inspection

Both bearings developed a defect, albeit small, in the regions indicated by the ECA scans. The resulting defect size for 2MxV1 measured approximately 0.08 in^2 (0.52 cm^2). 2MxV2 developed a defect that measured approximately 0.01 in^2 (0.06 cm^2). Both these defects are below the maximum allowable defect size (0.14 in^2 or 0.90 cm^2) for repair, however, it should be noted that the ECA scans were still able to detect suspect regions on the cup raceways that are susceptible to defect initiation. Both bearings developed these spalls after running for 60,496 mi

(97,359 km). Since the defect areas were small, both 2MxV1 and 2MxV2 were reassembled in accordance with AAR guidelines and set up for continued testing to observe the growth of these defects.

4.1.5 Experiment 289B: 2MxV1 and 2MxV2

Following the complete teardown and thorough visual inspections from Experiment 289A, 2MxV1 and 2MxV2 were reassembled using the same grease. The spacer rings needed to be replaced to ensure that the lateral displacement remained within recommended AAR guidelines. The bearings were mounted onto the 4BT exactly as they were in the previous Experiment 289A, and the testing was resumed. Again, the ECA indicated regions in the bearing cups were placed directly under the applied load just as they were in the previous test.

The experiment was stopped after the bearings had run for a total of 120,258 mi (193,536 km), reaching the target mileage. Figure 42 presents the vibration and temperature profiles for this experiment. The operating temperatures for both test bearings, which averaged around 50.3°C (90.5°F) for 2MxV1 and 54.8°C (98.6°F) for 2MxV2 above ambient, remained below the control bearing correlation for the majority of the experiment, and well below the HBD alarm threshold. The acceleration levels for 2MxV2 were steady and below the preliminary threshold, exhibiting healthy bearing conditions for the duration of the experiment. The acceleration levels for 2MxV1 remained around the preliminary threshold.

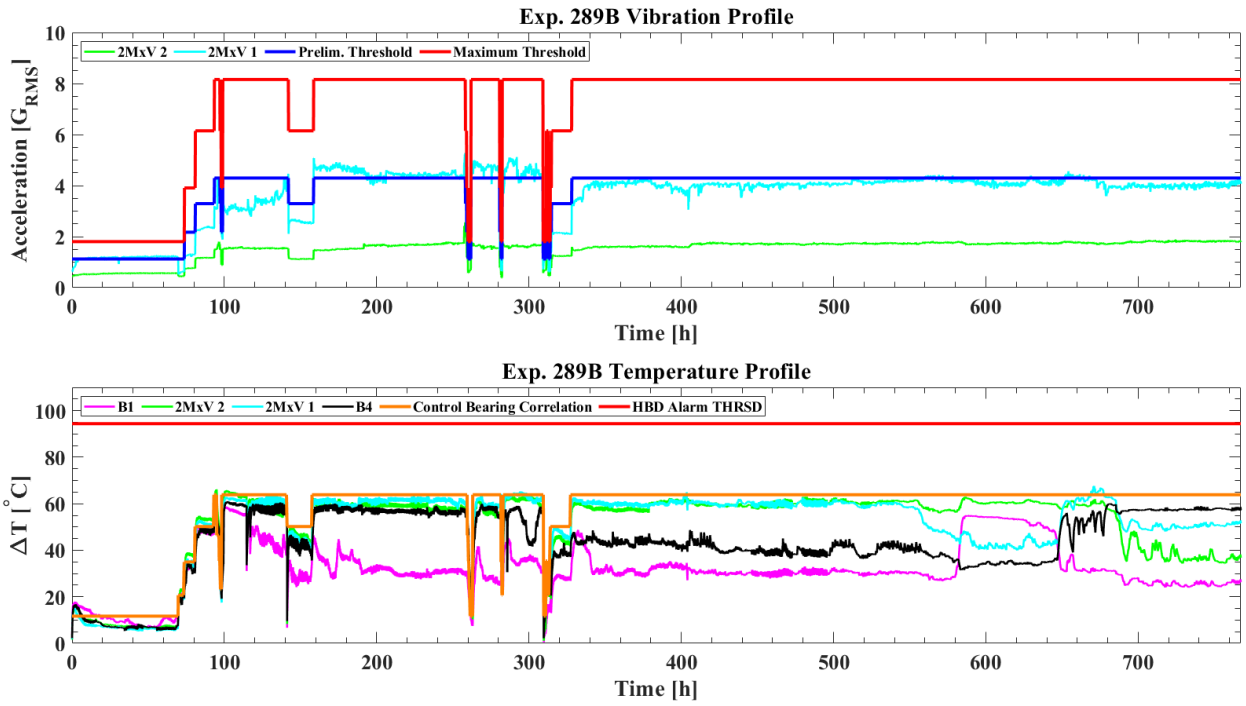

Figure 42: Vibration and temperature profiles for Experiment 289B

Table 13 presents the results of Level 1 analysis for 2MxV1 and 2MxV2. These results were obtained from the TDC-mounted accelerometer. The values for 2MxV1 only exceeded the preliminary threshold (*italicized*), signifying that the bearing potentially developed a defect. 2MxV2 never exceeded either threshold.

Table 13. Level 1 analysis for 2MxV1 and 2MxV2

Cup ID:	Test Bearing 2MxV1	Test Bearing 2MxV2
Load [%]	100	100
Speed [RPM]/[MPH]	796/85	796/85
Maximum TDC Acceleration [G_{RMS}]	*5.11*	1.86
Prelim. Thld. [G_{RMS}]	4.29	4.29
Max. Thld. [G_{RMS}]	8.15	8.15

Table 14 and

Table 15 present the Level 2 analysis results for 2MxV1 and 2MxV2, respectively. Results for 2MxV1 in **bold** indicate that a defect developed on the cup with 99% certainty. Level 2 analysis for 2MxV2 implies that a cup defect had developed with an average certainty of 93%.

Table 14. Level 2 analysis for 2MxV1

Test Bearing 2MxV1						
	Folder	48	49	50	51	52
	Speed [RPM/MPH]	796/85	796/85	796/85	796/85	796/85
TDC Accel.	Defective Component	**Cup**	**Cup**	**Cup**	**Cup**	**Cup**
	Certainty [%]	**99**	**99**	**99**	**99**	**99**

Table 15. Level 2 analysis for 2MxV2

Test Bearing 2MxV2						
	Folder	48	49	50	51	52
	Speed [RPM/MPH]	796/85	796/85	796/85	796/85	796/85
TDC Accel.	Defective Component	**Cup**	**Cup**	**Cup**	**Cup**	**Cup**
	Certainty [%]	**94**	**92**	**92**	**93**	**94**

A full teardown and visual inspection ensued after both bearings reached the mileage goal of 120,258 mi (193,536 km) to see if the defects have grown in surface area. Images of pre- and post-test for 2MxV1 are depicted in Figure 43. Looking at Figure 43(B), it can be seen that the spall on the 2MxV1 bearing exhibited growth toward the upper shoulder and towards the repair dimple. This behavior is typical of spall growth on cup raceways where any defects that initiate in the middle region of the raceway tend to grow across the raceway width before expanding circumferentially. The spall area after this iteration measured approximately 0.36 in^2 (2.06 cm^2), which represents an increase in surface area that is four times its previous size (0.08 in^2 or 0.52 cm^2). Figure 44 presents the defect from both iterations for 2MxV2. The picture

shows that the spall area remained at the same size after both iterations and measured approximately 0.01 in^2 (0.06 cm^2).

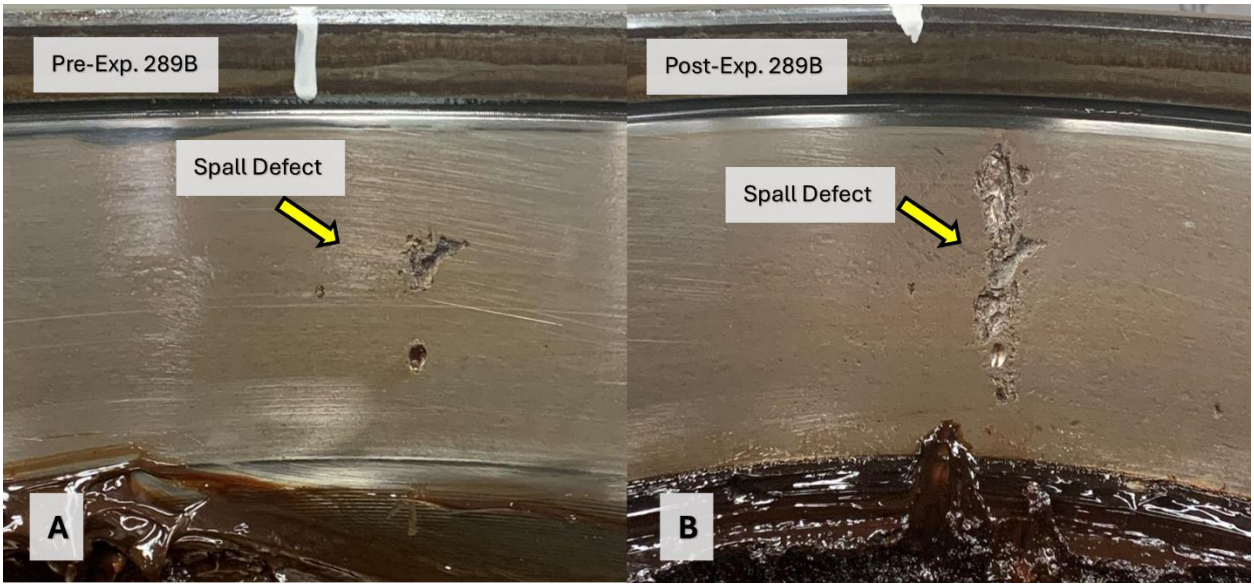

Figure 43: 2MxV1 (A) Pre-test inspection, (B) Post-test inspection

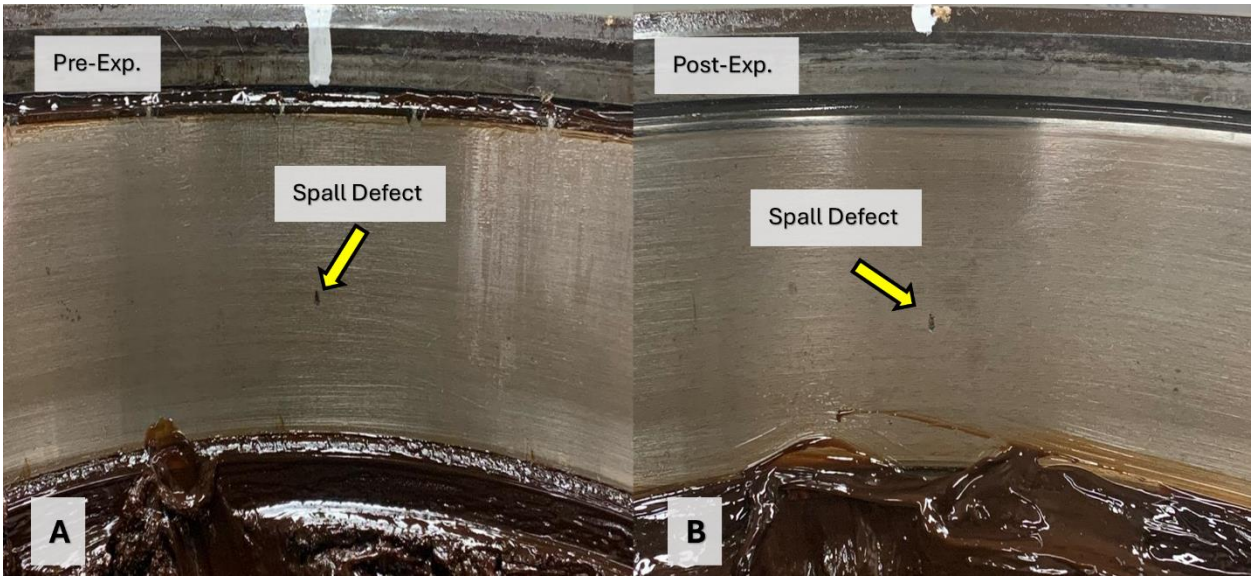

Figure 44: 2MxV2 (A) Pre-test inspection, (B) Post-test inspection

4.2 Summary of the indicated bearings

The results for all the indicated bearings are summarized in Table 16 and Table 17. In Table 16, the acceleration G_{RMS} and the operating temperatures above ambient are listed for each bearing.

The acceleration and operating temperature values were obtained from the steady-state data while the bearings were operating at 100% load (simulating a fully loaded railcar) and 85 mph (137 km/h). The acceleration values that only exceeded the preliminary threshold are *italicized* whereas the values that exceeded the maximum threshold are **bolded**. Similarly, the operating temperatures that exceeded the control (healthy) bearing correlation were also **bolded**. Note that all of the operating temperatures were well below the AAR recommended HBD alarm threshold. Table 17 displays the total distance that each bearing traveled (in kilometers and miles), as well as a brief description of the performance outcome.

Table 16. Summary of indicated bearing vibration and temperature profiles

Reconditioned Cups	Acceleration [G_{RMS}]			Temperature above ambient [ΔT]		
	Avg. [G_{RMS}]	Max. [G_{RMS}]	Min. [G_{RMS}]	Avg. [°C]	Max. [°C]	Min. [°C]
2MxV1	3.89	*5.11*	3.62	50.3	**68.0**	40.0
2MxV2	1.78	1.86	1.45	54.8	**66.0**	34.3
2MxV3	6.03	**9.00**	1.35	39.0	**65.0**	25.5
2MxV4	2.97	*5.10*	1.05	36.0	**68.8**	28.0
2MxV5	4.35	*7.97*	1.51	46.9	63.3	28.2
2MxV6	2.62	**11.12**	1.99	21.5	59.3	19.8
2MxV7	2.46	2.65	1.76	61.2	**72.2**	37.8
2MxV8	3.84	**8.42**	1.49	39.0	**72.1**	29.9

Table 17. Summary of the total distance traveled and performance outcome for each of the eight indicated bearings

Reconditioned Cup	Total Distance Traveled [km]/[mi]	Performance Outcome
2MxV1	193,536/ 120,258	Testing was terminated after reaching the 120,000-mile mark. A teardown and inspection were conducted revealing a cup defect of 0.36 in^2 located on the region that the C-scan indicated, validating the accuracy of the ECA scanner.
2MxV2	193,536 / 120,258	Testing was terminated after reaching the 120,000-mile mark. A teardown and inspection were conducted revealing a small cup defect of 0.01 in^2 located on the region that the C-scan indicated, validating the accuracy of the ECA scanner.
2MxV3	155,065 / 96,353	Testing was terminated when the acceleration exceeded the maximum threshold. A teardown and inspection were conducted revealing a cup spall of 1.19 in^2 in size located on the region that the C-scan indicated, validating the accuracy of the ECA scanner.
2MxV4	100,204 / 62,264	Testing was terminated when reaching the 60,000-mile mark to perform a teardown and inspection. The inspection revealed a cup spall of 0.96 in^2 in size located on the region that the C-scan indicated, validating the accuracy of the ECA scanner.
2MxV5	243,185 / 151,108	Testing was terminated after the 120,000-mile mark was reached for a final teardown and inspection. The acceleration increased just before the 120,000-mile mark was reached but the bearing continued to run until its paired bearing reached the mileage goal. The inspection revealed a cup spall of 1.51 in^2 in size located on the region that the C-scan indicated, validating the accuracy of the ECA scanner.
2MxV6	61,245 / 38,056	Testing was terminated when the acceleration exceeded the maximum threshold. A teardown and inspection were conducted revealing a cup spall of 0.33 in^2 in size located on the region that the C-scan indicated, validating the accuracy of the ECA scanner.
2MxV7	193,304 / 120,114	Testing was terminated after reaching the 120,000-mile mark. The post-test inspection revealed a small cup defect of 0.02 in^2 in size located on the region that the C-scan indicated, validating the accuracy of the ECA scanner.
2MxV8	66,226 / 41,151	Testing was terminated when the acceleration exceeded the maximum threshold. The post-test inspection revealed a cup spall of 1.46 in^2 in size located on the region that the C-scan indicated, validating the accuracy of the ECA scanner.

Ultimately, bearings 2MxV2 and 2MxV7 were the only two bearings from the indicated batch of bearings that completed the service life test without exhibiting discernible signs of a spall propagating mid-operation. The acceleration G_{RMS} for these bearings was within the normal thresholds for healthy bearings even though post-test inspection revealed small defects on the indicated areas. This can be explained by the fact that these defects were smaller than the AAR maximum allowable defect size (0.14 in^2 or 0.90 cm^2) for repair, and hence, they can undergo another reconditioning cycle before re-entry into rail revenue service. Nevertheless, the main takeaway is that the ECA scanner was able to detect suspect regions that could potentially initiate defects for all eight bearings tested.

4.3 Non-indicated Bearings

The reconditioned bearing cups for this batch consisted of eight bearings removed from service under *Why Made Code 11*, each having no indicated subsurface defect(s) from the ECA scanner. The overall goal of the dynamic accelerated service life testing of the non-indicated bearings was to verify that no defect(s) would develop during the set target mileage of 120,000 mi (193,121 km) of operation.

To that end, the test bearings were loaded on the cup raceway regions that correlated to statistical outliers output by ultrasonic scans provided by the research team at the Quantitative Ultrasonic Inspection for Structural Prognosis laboratory (QUISP) located at the University of Nebraska-Lincoln (UNL). For bearings with no statistical outliers detected, the loading zone was selected to be a region significantly away from repair dimples or other tooling marks. The test bearings were run uninterrupted until the vibration and/or thermal sensors indicated that a spall has developed or the bearings have reached 60,000 mi of continuous operation (i.e., halfway through the target mileage), at which point, a full teardown and visual inspection were

conducted. If no defect(s) were present post teardown, the bearings were rebuilt and testing resumed until the 120,000 mi (193,121 km) target was reached. If any abnormal behavior was detected, testing was halted for immediate teardown and visual inspection.

The initial conditions for each test started by simulating an empty railcar load (i.e., 17% of full AAR load capacity for class F bearings), which corresponds to 5,850 lbs (26 kN) per bearing, and low speeds of 25 mph (40 km/h). These conditions were held until steady state operation was achieved, usually taking a period of a few hours. The testing conditions were then increased to 85 mph (137 km/h) and full load (34,400 lbs or 153 kN per bearing). These operating conditions were maintained for the duration of the accelerated service life test.

The same naming convention explained earlier in this chapter was followed to label the experiments conducted for this batch of test bearings. The labels used for the experiments involving the non-indicated reconditioned bearings are: Experiment 297A&B, Experiment 298A, Experiment 300A&B, Experiment 301A, Experiment 302A, and Experiment 303A. The results for the experiments without a dedicated section are available in APPENDIX A. Results for Experiment 297A, Experiment 300A, and Experiment 302A are similar to those presented in sections 4.3.1 and 4.3.4.

The test bearings were labeled using the following scheme: the number two to indicate that this is the second round of testing conducted at the UTCRS in collaboration with MxV Rail, followed by MxV and a number denoting the order in which the bearings were scanned. The labels for the eight non-indicated bearings are: 2MxV9, 2MxV10, 2MxV11, 2MxV12, 2MxV13, 2MxV14, 2MxV15, and 2MxV16.

4.3.1 Experiment 297B: 2MxV12 and 2MxV13

Experiment 297B featured two bearings, 2MxV12 and 2MxV13. The ECA scanner output C-scan images of these two cups can be seen in Figure 45(A) and Figure 46(A), respectively. No defects were identified by the ECA, signifying that the eddy current was not disrupted and there were no subsurface defects in this focal depth. Pictures of the visually inspected surfaces of the reconditioned bearing cups are displayed in Figure 45(B) and Figure 46(B) for bearings 2MxV12 and 2MxV13, respectively. No defects were visible on the surface of the cups.

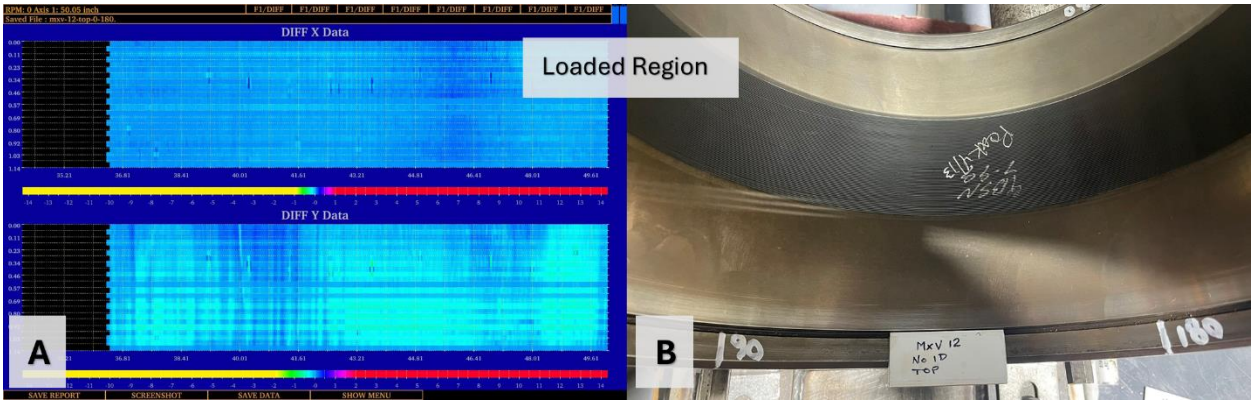

Figure 45: (A) C-scan image of the raceway of 2MxV12, (B) Visual inspection of the raceway of 2MxV12

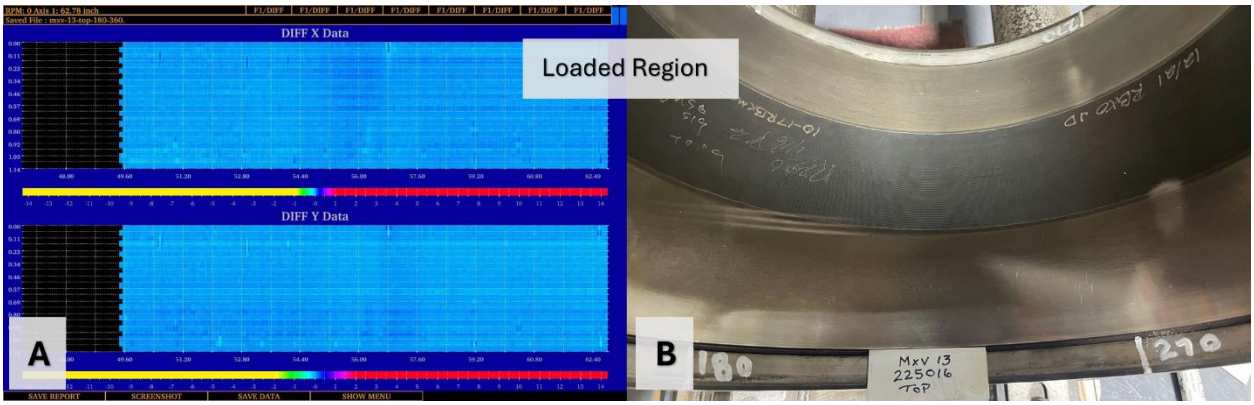

Figure 46: (A) C-scan image of the raceway of 2MxV13, (B) Visual inspection of the raceway of 2MxV13

The test was carried out on the UTCRS Four-Bearing Tester (4BT), and the experiment was terminated after the bearings ran for a total of 120,798 mi (194,405 km), reaching the mileage goal.

The vibration and temperature profiles of the two test bearings for the last 60,000 mi of operation are provided in Figure 47. The operating temperatures for both test bearings, which averaged around 42.6°C (76.7°F) for 2MxV12 and 46.9°C (84.4°F) for 2MxV13 above ambient, remained below the control bearing correlation for the majority of the experiment, and well below the AAR Hot-Bearing Detector (HBD) alarm threshold. The acceleration (G_{RMS}) levels for

both bearings also displayed healthy conditions, running below the preliminary threshold. A full teardown and visual inspection were conducted after both bearings reached the mileage goal. The pre- and post-test images are pictured in Figure 48 for 2MxV12 and Figure 49 for 2MxV13, and show no defects or any discernible damage on the cup raceways other than normal wear after running 120,000 mi.

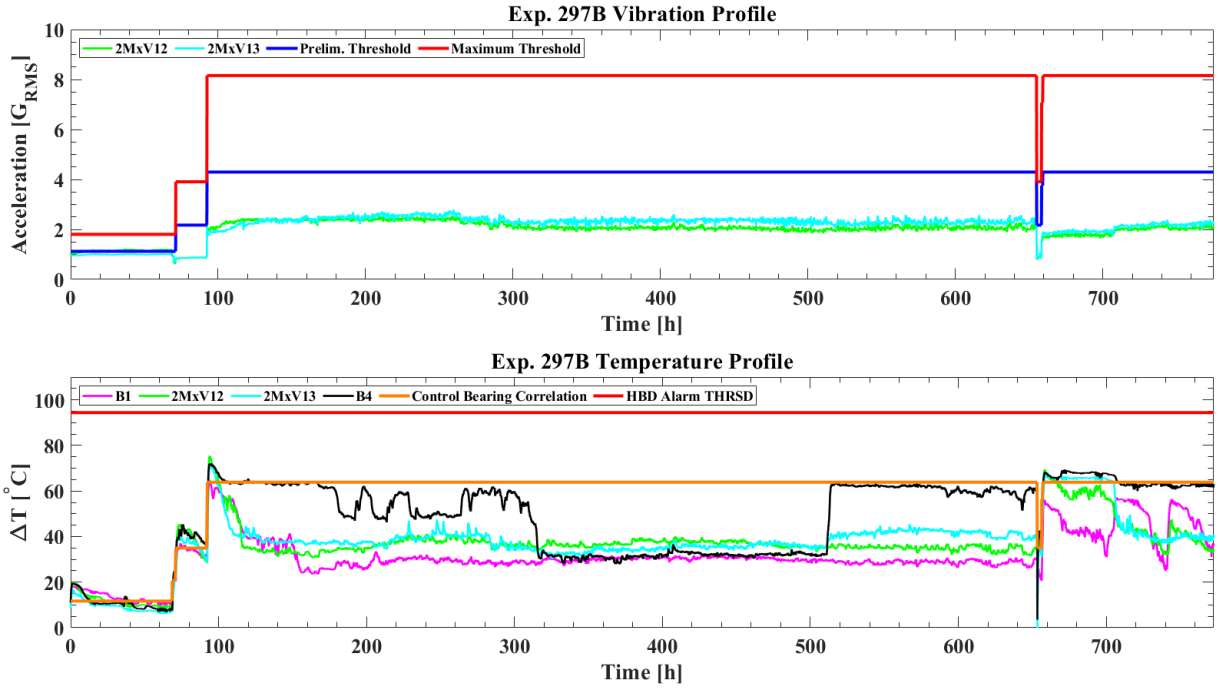

Figure 47: Vibration and temperature profiles for Experiment 297B

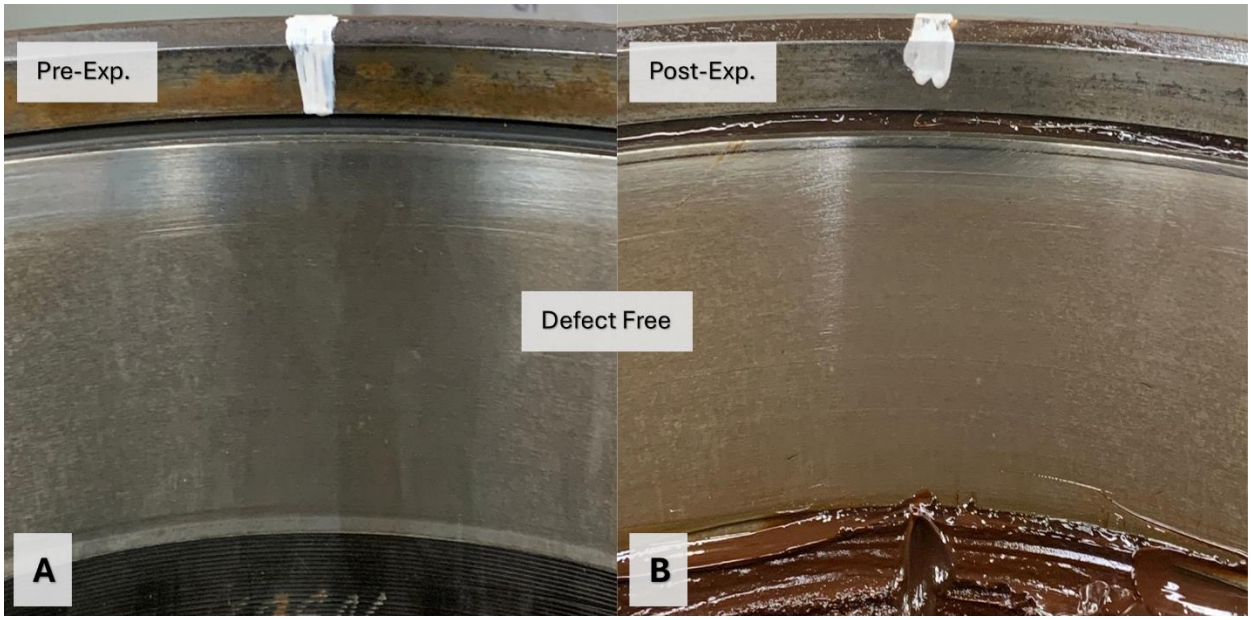

Figure 48: 2MxV12 (A) Pre-test inspection, (B) Post-test inspection

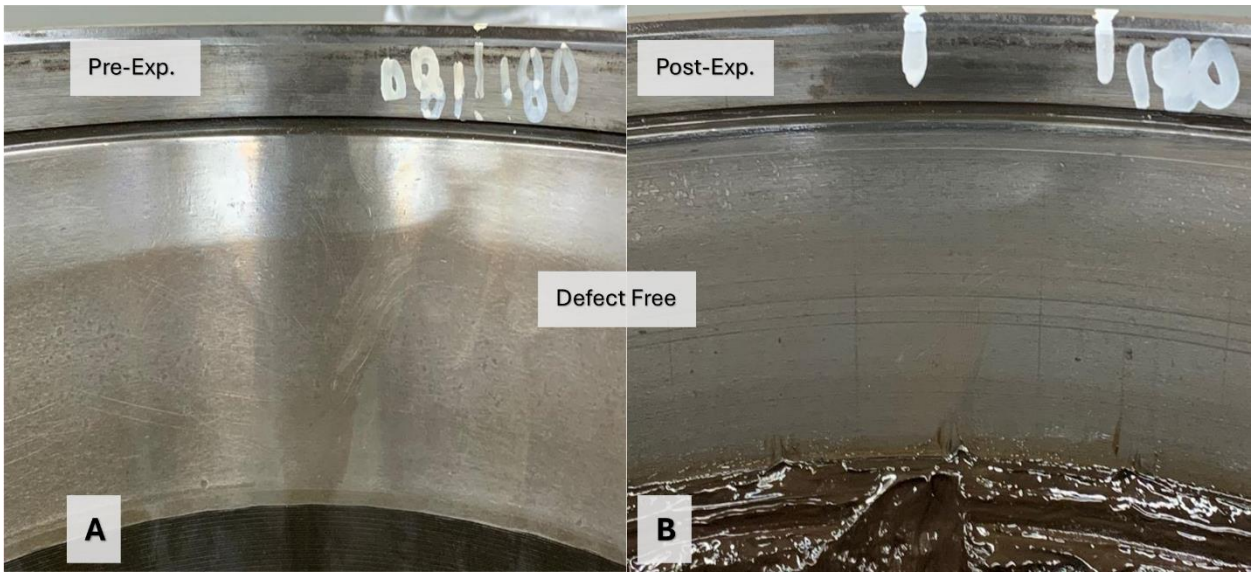

Figure 49: 2MxV13 (A) Pre-test inspection, (B) Post-test inspection

4.3.2 Experiment 298A: 2MxV9 and 2MxV10

Experiment 298A featured two bearings, 2MxV9 and 2MxV10. An ECA scan of 2MxV10 can be pictured in Figure 50(A). The ECA scan detected no anomalies as shown in the C-scan image, signifying that there are no subsurface defects at this focal depth. The corresponding region is displayed on the visually inspected surface of the reconditioned bearing cup pictured in Figure 50(B), which showed no defects were present on the cup raceway.

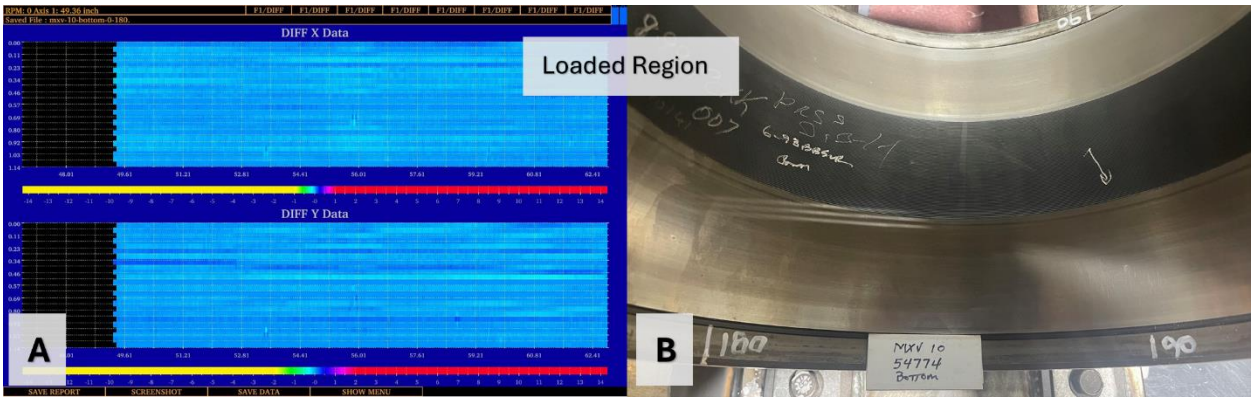

Figure 50: A) C-scan image of the raceway of 2MxV10 B) Visual inspection of the raceway of 2MxV10

The same testing procedures followed in Experiment 297B were executed for bearings 2MxV9 and 2MxV10 in Experiment 298A. Again, the two test bearings were loaded on the regions that correlated with the ultrasonic scans provided from QUISP and away from repair dimples. These bearings were run using the same accelerated service life test conditions previously mentioned. The experiment was stopped after the bearings ran for 60,916 mi (98,034 km), reaching the halfway mark.

Plots representing the vibration and temperature profiles of the two test bearings are given in Figure 51. The operating temperatures for both test bearings, which averaged around 35.6°C (64.1°F) for 2MxV9 and 45.9°C (82.6°F) for 2MxV10 above ambient, remained below the control bearing correlation for the majority of the experiment, and well below the HBD alarm threshold. The acceleration levels for 2MxV9 demonstrated healthy bearing conditions, running below the preliminary threshold. However, the acceleration levels for the 2MxV10 bearing started to increase around the 190 hour-mark (12,470 mi or 20,068 km) of the experiment, thus signifying a possible defect initiation, and eventually exceeding the maximum threshold, confirming that a defect had developed. To avoid unnecessary stoppage to this test, it was

decided to allow this experiment to run until the 2MxV9 bearing reached the halfway mark mileage before performing a full teardown and visual inspection.

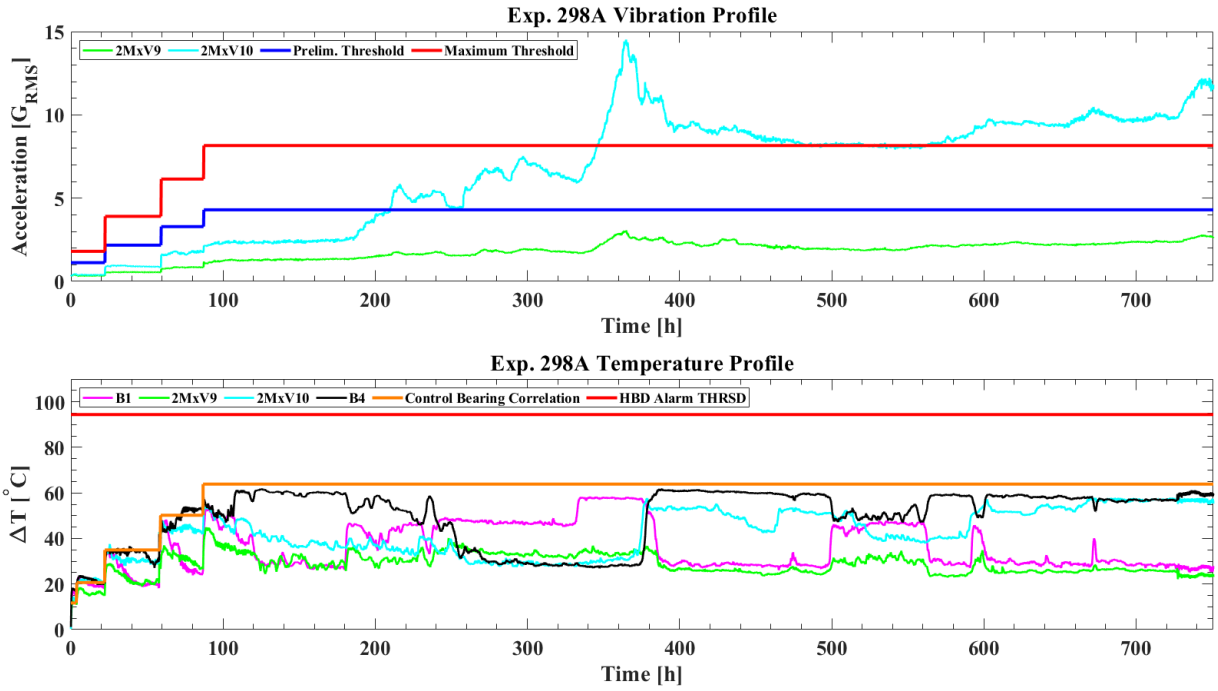

Figure 51: Vibration and temperature profiles for Experiment 298A

Table 18 presents the results from the Level 1 analysis using the vibration data output by the TDC-mounted accelerometer for 2MxV10. The value in **bold** exceeded the maximum threshold, signifying that one of the components of that bearing developed a defect. Level 2 analysis was then performed to identify the defective component.

Table 18. Level 1 analysis for 2MxV10

Cup ID:	Test Bearing 2MxV10
Load [%]	100
Speed [RPM]/[MPH]	796/85
Maximum TDC Acceleration [G_{RMS}]	**14.52**
Prelim. Thld. [G_{RMS}]	4.29
Max. Thld. [G_{RMS}]	8.15

Table 19 presents the output from the Level 2 analysis which indicated that the 2MxV10 bearing developed a cup defect with 99% certainty.

Table 19. Level 2 analysis for 2MxV10

Test Bearing 2MxV10						
	Folder	23	24	25	26	27
	Speed [RPM/MPH]	796/85	796/85	796/85	796/85	796/85
TDC Accel.	Defective Component	**Cup**	**Cup**	**Cup**	**Cup**	**Cup**
	Certainty [%]	**99**	**99**	**99**	**99**	**99**

A full teardown and visual inspection were conducted after both bearings reached the halfway mark. The visual inspection revealed no defects on the 2MxV9 bearing, so it was reassembled in accordance with suggested AAR guidelines and paired with another non-indicated bearing for continued testing. Figure 52(B) displays a post-test image of the loaded zone with the developed defect on the surface of 2MxV10. The pre-test image of that same surface is illustrated in Figure 52(A) and shows no discernible damage.

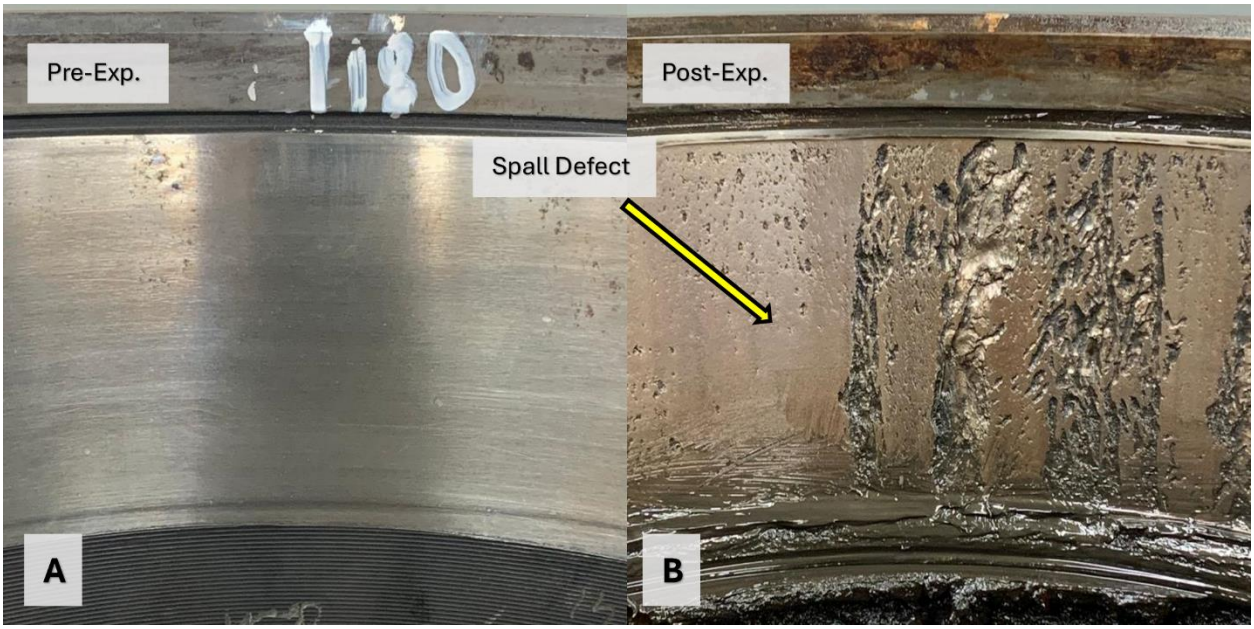

Figure 52: (A) Pre-test inspection, (B) Post-test inspection

The defect propagated across the entire width of the cup raceway and measured approximately 3.11 in^2 (20.06 cm^2) in area, as seen in Figure 53. This spall exceeded the maximum allowable defect size (0.14 in^2 or 0.90 cm^2) for repair, making it unsuitable for the reconditioning process. This defect was located around the 180° mark of the bottom raceway (refer to Figure 54) and was not detected by the ECA scans. However, the research team at QUISP provided ultrasonic scans that were able to detect that defect, as depicted in Figure 54 [32]. This reiterates the point that NDE technology can detect this defect but was likely missed due to the focal zone or the lack of overlapping scans of the ECA. That is, there is a chance that the defect was not properly scanned given that the scanning profiles from the ECA scanner were taken from approximately 0° to 180° and from 180° to 360° and that the defect initiated around the 180° region. Implementing scanning profiles taken from 90° to 270° and from 270° to 90° alongside the original scans would provide overlapping that would minimize the likelihood of this potential false negative. This practice would also ensure that the ECA scanned the entire raceway, for a total of eight scans per bearing cup (four per raceway).

Figure 53: 2MxV10 bottom raceway (loaded zone)

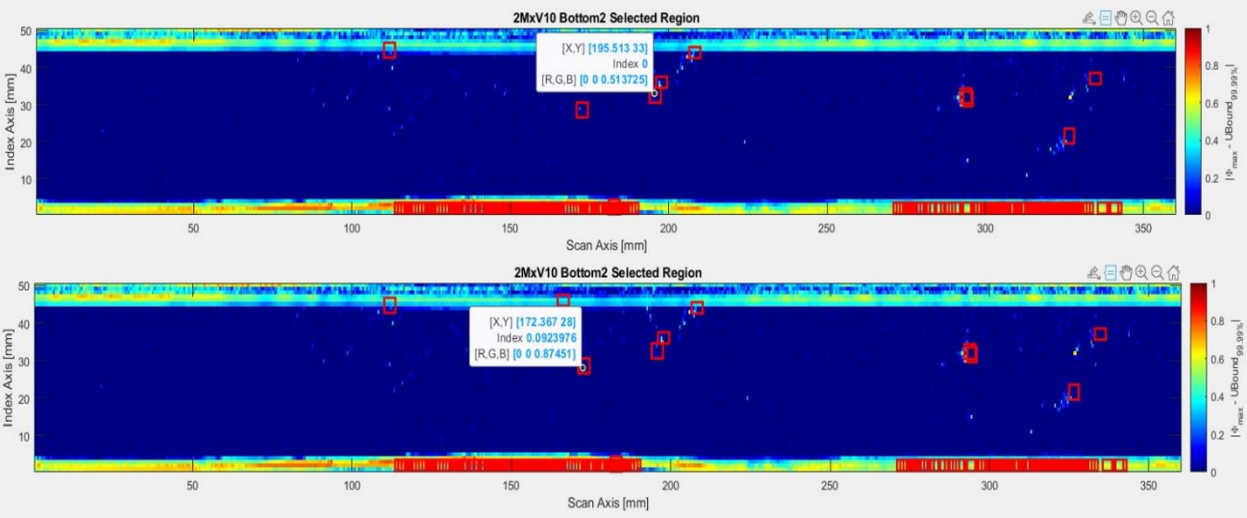

Figure 54: 2MxV10 ultrasonic scans [32]

4.3.3 Experiment 301A: 2MxV9 and 2MxV11

The 2MxV9 bearing was paired with the 2MxV11 bearing for Experiment 301A, as 2MxV9 had not yet reached the 120,000 milestone following its complete teardown and visual inspection. The experiment was allowed to continue until the 2MxV11 bearing reached the halfway mark of 60,000 mi (96,560 km) of operation and the 2MxV9 bearing reached the target milestone, avoiding any unnecessary stoppages or delays.

The C-scan image produced by the ECA scanner for the2MxV9 bearing is provided in Figure 55(A). The ECA scans detected no potential defects on either raceway. This finding was confirmed by the picture of the visually inspected surface of the reconditioned bearing cup, seen in Figure 55(B), which showed no damage on the raceway surface.

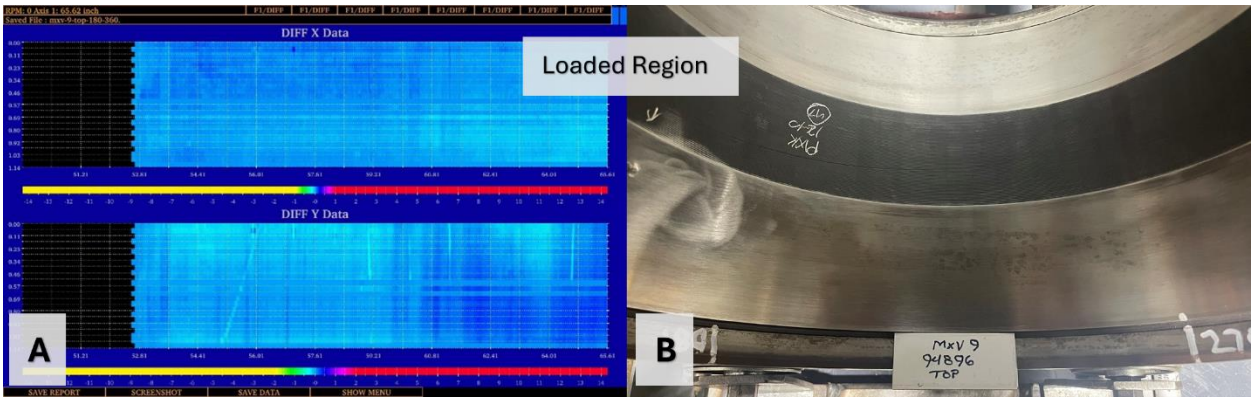

Figure 55: (A) C-scan image of the raceway of 2MxV9, (B) Visual inspection of the raceway of 2MxV9

Similar procedures to those carried out in the previous experiments were followed with the bearings set up on the 4BT. The 2MxV9 bearing was rebuilt using the same grease used in its previous experiment, but the spacer ring was replaced to ensure that the lateral displacement remained within suggested AAR guidelines. Again, the two test bearings were loaded on the regions that correlated with the ultrasonic scans provided from QUISP and away from any repair dimples. For the 2MxV9 bearing, the loaded zone remained the same as in Experiment 298A. This experiment was terminated after 2MxV9 ran for a total of 120,923 mi (194,606 km), reaching the milestone, and 2MxV11 ran for 60,007 mi (96,572 km), reaching the halfway point.

The vibration and temperature profiles for 2MxV9 and 2MxV11 are provided in Figure 56. The operating temperatures for both test bearings, which averaged around 32.6°C (58.7°F) for 2MxV9 and 36.5°C (65.7°F) for 2MxV11 above ambient, remained below the control bearing correlation for the majority of the experiment, and well below the HBD alarm threshold. The acceleration levels for 2MxV11 were below the preliminary threshold, signifying that it remained healthy (defect-free) for the duration of the experiment. However, the acceleration levels for the 2MxV9 bearing started to increase around the 120 hour-mark (68,226 mi or

109,799 km) of the experiment and surpassed the preliminary threshold, suggesting a potential defect initiation on one of the bearing components.

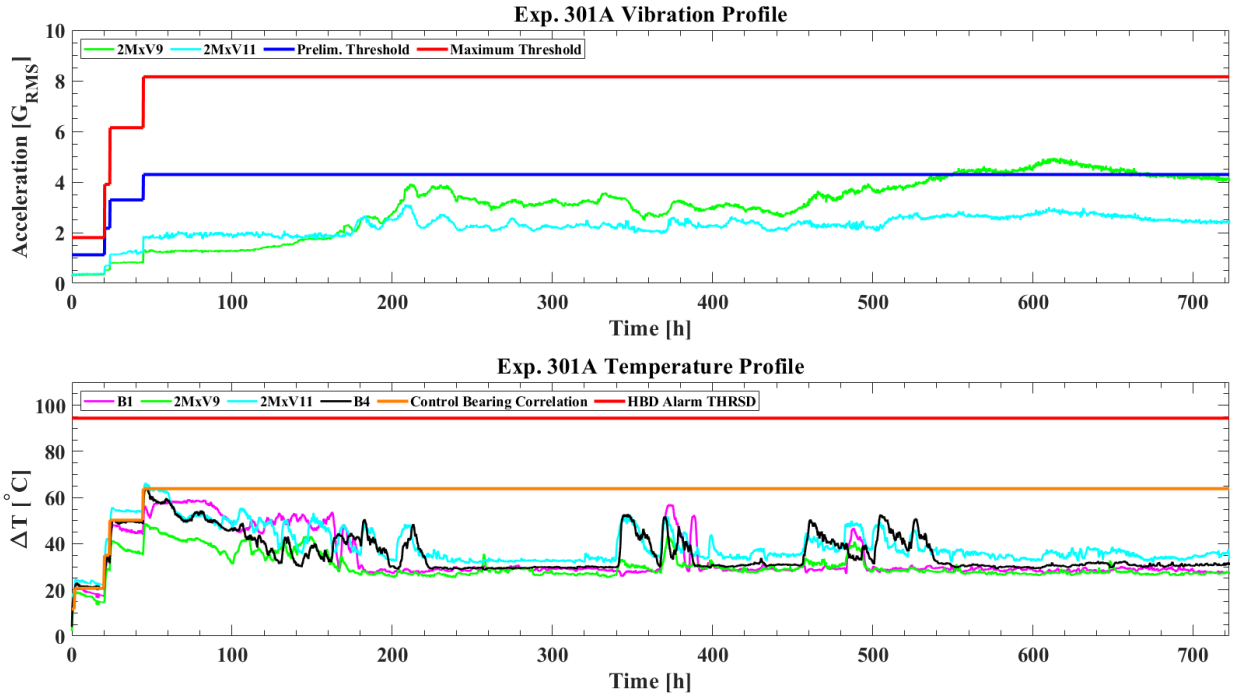

Figure 56: Vibration and temperature profiles for Experiment 301A

Table 20 presents the results from the Level 1 analysis using the vibration data output by the TDC-mounted accelerometer for 2MxV9. The value exceeded the preliminary threshold (*italicized*), signifying that one of the components of that bearing may have developed a defect. Level 2 analysis was then performed to identify the defective component.

Table 20. Level 1 analysis for 2MxV9

Cup ID:	**Test Bearing 2MxV9**
Load [%]	100
Speed [RPM]/[MPH]	796/85
Maximum TDC Acceleration [G_{RMS}]	*4.95*
Prelim. Thld. [G_{RMS}]	4.29
Max. Thld. [G_{RMS}]	8.15

Table 21 presents the output of the Level 2 analysis for 2MxV9 which indicated that the bearing developed a roller defect with an average certainty of 60%. This finding was interesting as roller defects are not common in railroad tapered roller bearings. Hence, this necessitated a full teardown and visual inspection.

Table 21. Level 2 analysis for 2MxV9

Test Bearing 2MxV9						
	Folder	21	22	23	24	25
	Speed [RPM/MPH]	796/85	796/85	796/85	796/85	796/85
TDC Accel.	Defective Component	**Roller**	**Roller**	**Roller**	**Roller**	**Roller**
	Certainty [%]	**48**	**59**	**62**	**67**	**66**

The visual inspection revealed that no defects developed on the 2MxV11 bearing, so it was reassembled in accordance with suggested AAR guidelines and paired with another non-indicated bearing for continued testing. Pre- and post-test images for the 2MxV9 bearing are depicted in Figure 57, showing that no defect(s) had developed on the cup raceway. The minor abrasions that can be seen are likely due to the small metal fragments introduced to the raceway from the spalled roller(s). To confirm this observation, the cone assembly was cleaned and disassembled to enable the visual inspection of the rollers.

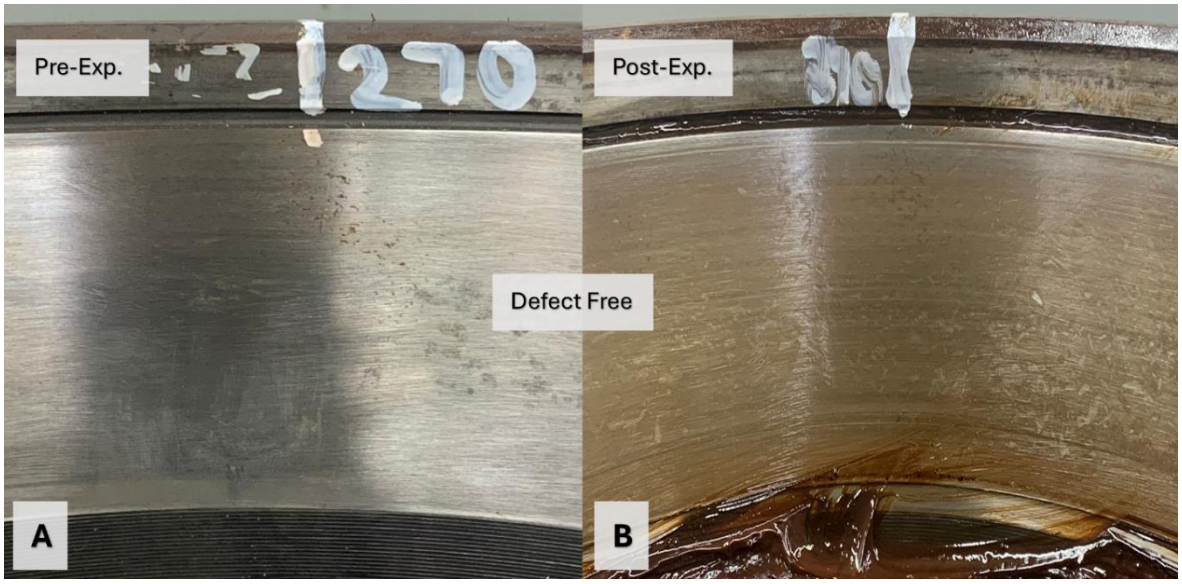

Figure 57: 2MxV9 (A) Pre-test inspection, (B) Post-test inspection

One of the rollers developed a spall that covered half of its surface area as pictured in Figure 58. This roller defect was responsible for the increase in the acceleration levels observed for 2MxV9, and the Level 2 analysis was able to correctly identify the damaged component. Since the reconditioned component to be assessed was the cup of the 2MxV9 bearing and the other components used to build this bearing were not art of this study, it was concluded that this bearing successfully completed its accelerated service life test without propagating a defect.

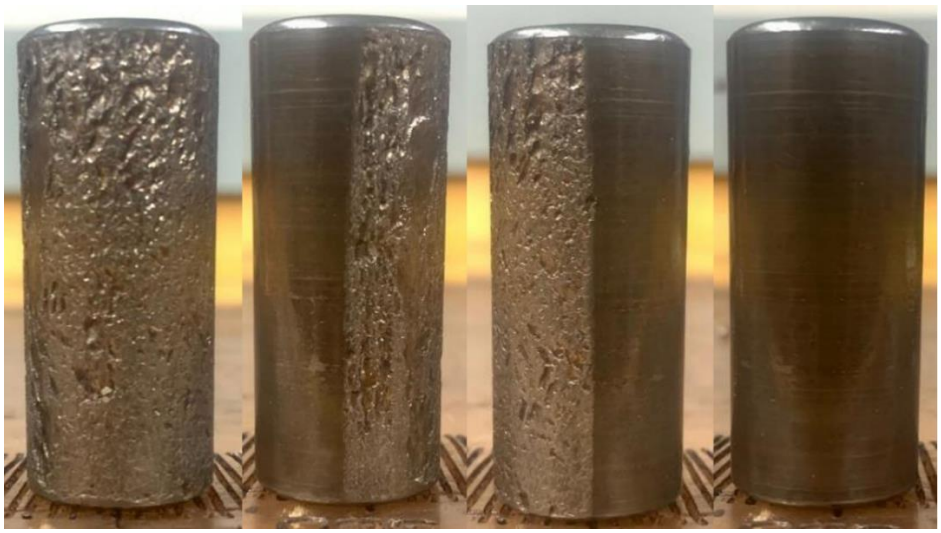

Figure 58: 2MxV9 roller defect

4.3.4 Experiment 300B: 2MxV15 and 2MxV16

Experiment 300B featured two bearings, 2MxV15 and 2MxV16. The ECA C-scan images of these two cups can be seen in Figure 59(A) and Figure 60(A), respectively. The ECA scans detected no potential defects on these cups. Pictures of the visually inspected surfaces of the reconditioned bearing cups are displayed in Figure 59(B) and Figure 60(B), for bearings 2MxV15 and 2MxV16, respectively. It should be noted that surfaces of the cups looked clean and free from any damage.

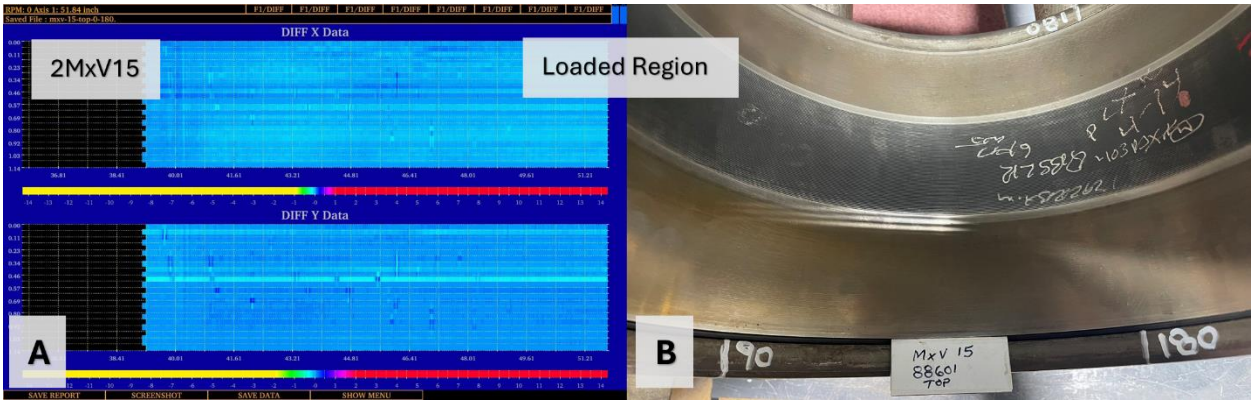

Figure 59: (A) C-scan of the raceway of 2MxV15, (B) Visual inspection of the raceway of 2MxV15

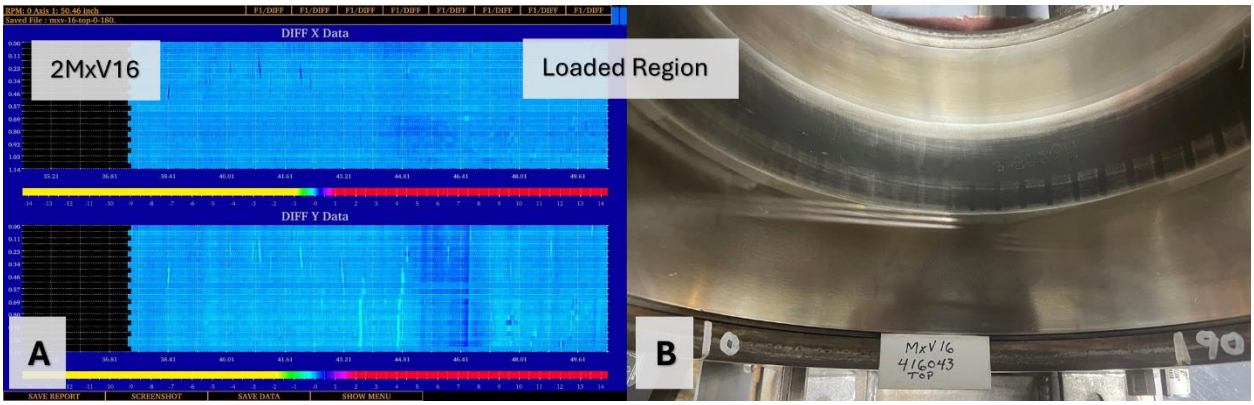

Figure 60: (A) C-scan of the raceway of 2MxV16, (B) Visual inspection of the raceway of 2MxV16

The test was carried out on the 4BT, and the experiment was stopped after the bearings ran for a total of 120,009 mi (193,135 km), reaching the mileage goal.

The vibration and temperature profiles for the two test bearings for the last 60,000 mi of operation are provided in Figure 61. The operating temperatures for both test bearings, which averaged around 40.2°C (72.4°F) for 2MxV15 and 42.8°C (77.0°F) for 2MxV16 above ambient, remained below the control bearing correlation for the majority of the experiment, and well below the HBD alarm threshold. The acceleration levels for both bearings also displayed healthy conditions, running below the preliminary threshold. The square wave signal behavior exhibited

by the vibration profile of the 2MxV15 bearing was caused by minor electrical interference issues that occurred during the experiment. A full teardown and visual inspection were conducted after both bearings reached the mileage goal. The pre- and post-test images are depicted in Figure 62 for 2MxV15 and Figure 63 for 2MxV16, and show no defects or any discernible damage on the cup raceways other than normal wear after running 120,000 mi.

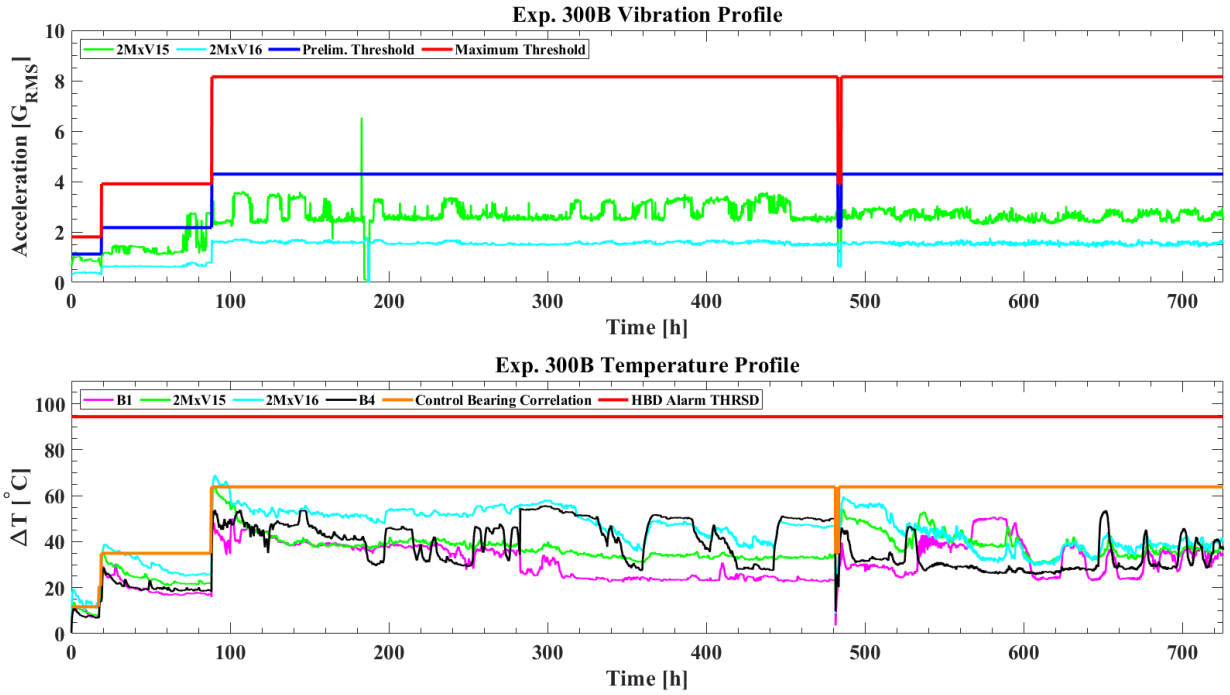

Figure 61: Vibration and temperature profiles for Experiment 300B

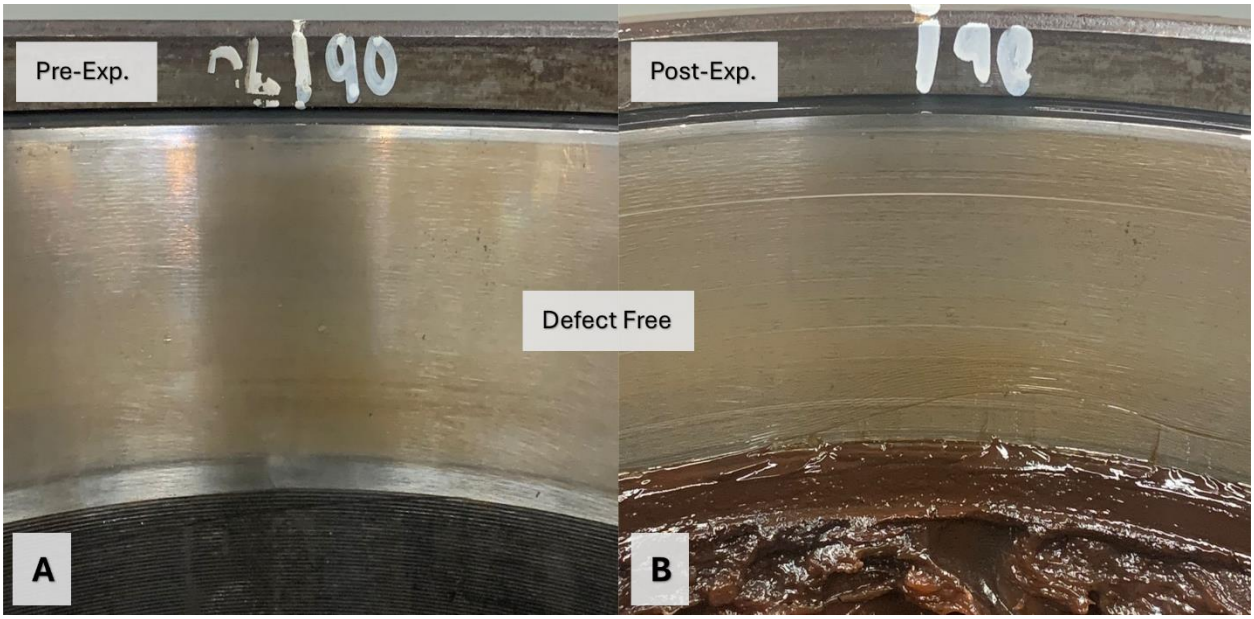

Figure 62: 2MxV15 (A) Pre-test inspection, (B) Post-test inspection

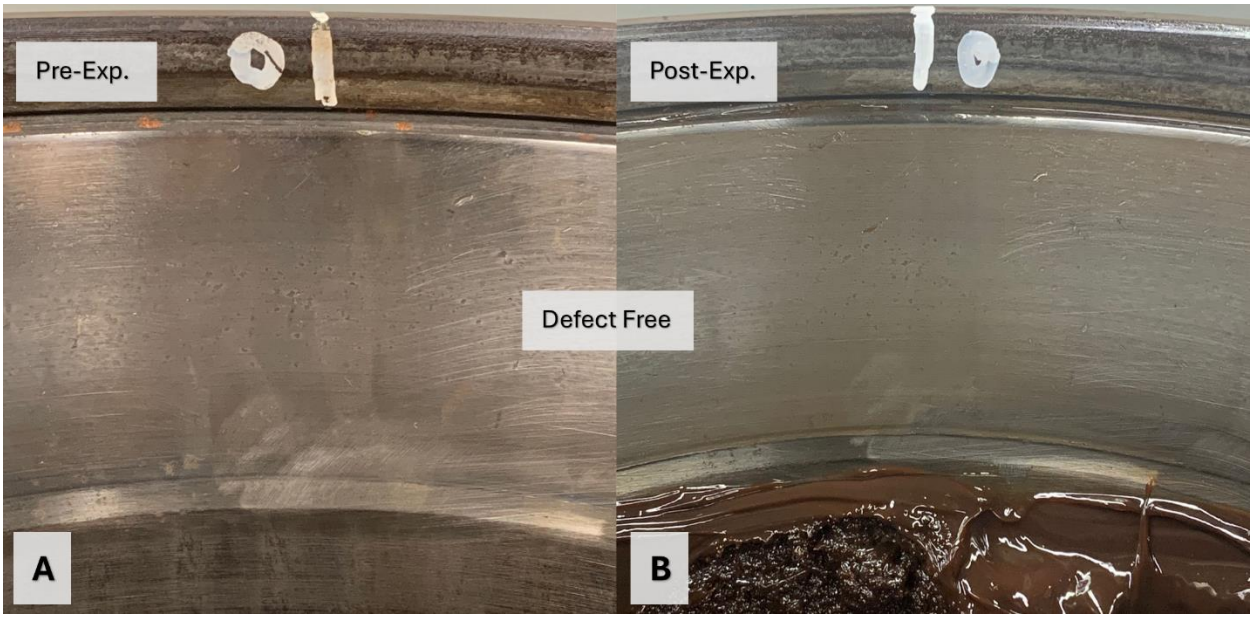

Figure 63: 2MxV16 (A) Pre-test inspection, (B) Post-test inspection

4.4 Summary of the non-indicated bearings

The testing results for all the non-indicated bearings are summarized in Table 22 and Table 23. In Table 22, the acceleration G_{RMS} and the operating temperature above ambient are listed for each bearing. The acceleration and operating temperature values were obtained from the steady-state data while the bearings were operating at 100% load (simulating a fully loaded railcar) and 85 mph (137 km/h). The acceleration values that only exceeded the preliminary threshold are *italicized* whereas the values that exceeded the maximum threshold are **bolded**. Similarly, the operating temperatures that exceeded the control (healthy) bearing correlation were also **bolded**. Note that all the operating temperatures were well below the AAR recommended HBD alarm threshold. Table 23 displays the total distance that each bearing traveled (in kilometers and miles), as well as a brief description of the performance outcome.

Table 22. Summary of non-indicated bearing vibration and temperature profiles

	Acceleration [G_{RMS}]	**Temperature above ambient [ΔT]**

Reconditioned Cups	Avg. [GRMS]	Max. [GRMS]	Min. [GRMS]	Avg. [°C]	Max. [°C]	Min. [°C]
2MxV9	2.89	*4.95*	1.20	32.6	48.9	25.2
2MxV10	7.42	**14.52**	2.21	45.9	59.0	27.4
2MxV11	1.86	2.08	1.48	34.6	61.1	27.3
2MxV12	2.06	2.54	1.69	42.6	**75.5**	30.7
2MxV13	2.21	2.79	1.76	46.9	**70.8**	30.1
2MxV14	1.65	1.93	1.11	31.3	63.4	25.9
2MxV15	2.82	3.52	2.30	40.2	**64.4**	30.8
2MxV16	1.58	1.77	1.37	42.8	**68.9**	29.3

Table 23. Summary of the total distance traveled and performance outcome for each of the eight non-indicated bearings

Reconditioned Cup	Total Distance Traveled [km]/[mi]	Performance Outcome
2MxV9	194,606 / 120,923	Testing was terminated after reaching the120,000-mile mark. A teardown and inspection were conducted revealing no cup defect on either raceway, validating the accuracy of the ECA scanner. A roller defect developed within this bearing.
2MxV10	98,034 / 60,916	Testing was terminated after reaching the 60,000-mile mark to perform a teardown and inspection. The inspection conducted revealed a cup defect of 3.11 in^2 in size located on the loaded region. The spall started propagating at hour 190 of the experiment.
2MxV11	193,898 / 120,483	Testing was terminated after reaching the 120,000-mile mark. A teardown and inspection were conducted revealing no cup defect on either raceway, validating the accuracy of the ECA scanner.
2MxV12	194,405 / 120,798	Testing was terminated after reaching the 120,000-mile mark. A teardown and inspection were conducted revealing no cup defect on either raceway, validating the accuracy of the ECA scanner.
2MxV13	194,405 / 120,798	Testing was terminated after reaching the 120,000-mile mark. A teardown and inspection were conducted revealing no cup defect on either raceway, validating the accuracy of the ECA scanner.
2MxV14	193,409 / 120,179	Testing was terminated after reaching the 120,000-mile mark. A teardown and inspection were conducted revealing no cup defect on either raceway, validating the accuracy of the ECA scanner.
2MxV15	193,135 / 120,009	Testing was terminated after reaching the 120,000-mile mark. A teardown and inspection were conducted revealing no cup defect on either raceway, validating the accuracy of the ECA scanner.
2MxV16	193,135 / 120,009	Testing was terminated after reaching the 120,000-mile mark. A teardown and inspection were conducted revealing no cup defect on either raceway, validating the accuracy of the ECA scanner.

Ultimately, bearing 2MxV10 was the only bearing from the non-indicated batch of bearings that developed a cup defect during the accelerated service life test. The ECA scans did

not detect this defect, however, ultrasonic scans provided by the research team at QUISP were able to detect it. Bearing 2MxV9 developed a roller defect during the service life test without causing any discernible damage to the cup other than normal wear.

CHAPTER V

CONCLUSIONS

The implementation of nondestructive evaluation (NDE) techniques in reconditioning facilities would provide a means to detect suspect subsurface defects in bearing raceways that could potentially compromise the remaining service life of these components. Preventing these bearings from returning to rail revenue service, costly and unnecessary delays associated with removing bearings from service can be avoided. More importantly, potentially catastrophic derailments that could result from bearings initiating and propagating large spalls from these surface defects can be mitigated, which greatly enhances the safety of the rail network.

The data presented and summarized on the indicated bearing cups supports the reliability of using eddy current methods to detect these underlying defects. The ECA scanner accurately indicated the region in which a spall would develop for all eight bearings in that test group (i.e., 100% accuracy). Although two of the tested bearings did not develop spalls that would compromise performance (i.e., spall size was noticeably smaller than the maximum allowable spall size for repair), the ECA scanner was still able to accurately detect these suspect regions where these small defects initiated. As for the non-indicated cups scanned, the operating temperatures displayed characteristics of healthy bearings at 85 mph (137 km/h) and 100% (34,400 lbs or 153 kN per bearing) load conditions. The vibration profiles exhibited abnormal readings for two of the eight bearings. Upon inspection, a defect developed on the 2MxV10 bearing, signifying that the ECA scans did not detect that defect (i.e., false negative). However, ultrasonic scans provided by the research team at QUISP were able to detect it. Potential reasons

for the ECA scans not detecting this defect include initiation outside of the focal depth, and the fact that it propagated at one of the scanning profile bounds. Recommended corrective actions for the ECA scanning procedure would be to supplement the current scans of 0° to 180° and 180° to 360° with additional scans from 90° to 270° and from 270° to 90°, which would provide overlapping scans of the entire raceway. The second bearing that developed a defect was 2MxV9, in which one of the rollers spalled. Post inspection revealed that the cup raceway did not develop a defect, validating the output from the ECA scanner. Hence, seven of the eight non-indicated cups did not develop a spall, resulting in an ECA accuracy of 87.5% for this batch.

The vibration and temperature profiles acquired from all sixteen bearings tested in this study provide overwhelming evidence that the bearing operating temperature is a reactive measure of bearing health and cannot capture small to mid-size defects that develop within the bearing. In contrast, the vibration signatures of the bearing can be used to detect the onset of spall or defect initiation within the bearing, which provides rail operators with advance notice to mitigate potential bearing failure consequences. The UTCRS condition monitoring algorithm used in this study was able to accurately and reliably predict the bearing health and correctly identify the defective component within the bearing with high certainty.

Ultimately, the integration of ECA scanners in reconditioning facilities would serve to aid in the level 1 process of inspection to ensure that there are no underlying defects that may otherwise go undetected. The ECA scanner is efficient, with the scanning process only taking two to five minutes per bearing. In this study, the total accuracy of the ECA was 93.75%, which lends credence to the use of this technology to improve and optimize current bearing reconditioning practices.

APPENDIX A

APPENDIX A

TEMPERATURES FOR RECONDTIIONED BEARINGS

Table 24. Number of reconditioning cycles for the indicated bearings

Reconditioned Cups	Reconditioning markings	Temperature above ambient [ΔT]		
		Avg. [°C]	Max. [°C]	Min. [°C]
2MxV1	5	50.3	**68.0**	40.0
2MxV2	3	54.8	**66.0**	34.3
2MxV3	4	39.0	**65.0**	25.5
2MxV4	2	36.0	**68.8**	28.0
2MxV5	5	46.9	63.3	28.2
2MxV6	4	21.5	59.3	19.8
2MxV7	4	61.2	**72.2**	37.8
2MxV8	4	39.0	**72.1**	29.9

Table 25. Number of reconditioning cycles for the non-indicated bearings

Reconditioned Cups	Reconditioning markings	Temperature above ambient [ΔT]		
		Avg. [°C]	Max. [°C]	Min. [°C]
2MxV9	3	32.6	48.9	25.2
2MxV10	5	45.9	59.0	27.4
2MxV11	2	34.6	61.1	27.3
2MxV12	3	42.6	**75.5**	30.7
2MxV13	5	46.9	**70.8**	30.1
2MxV14	1	31.3	63.4	25.9
2MxV15	5	40.2	**64.4**	30.8
2MxV16	4	42.8	**68.9**	29.3

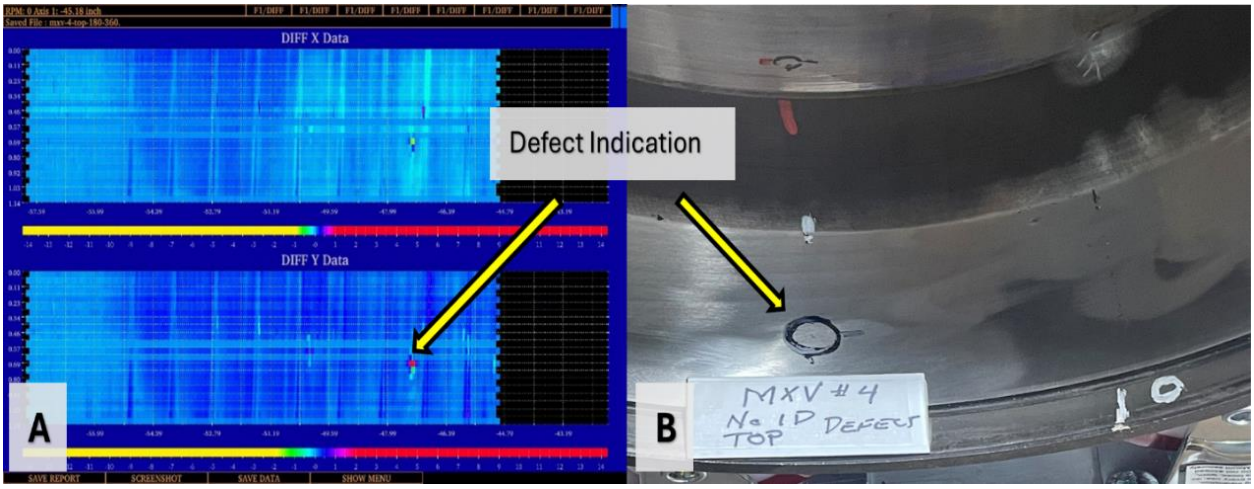

Figure 64: (A) ECA indication on the top raceway of 2MxV4, (B) Visual inspection of the top raceway of 2MxV4

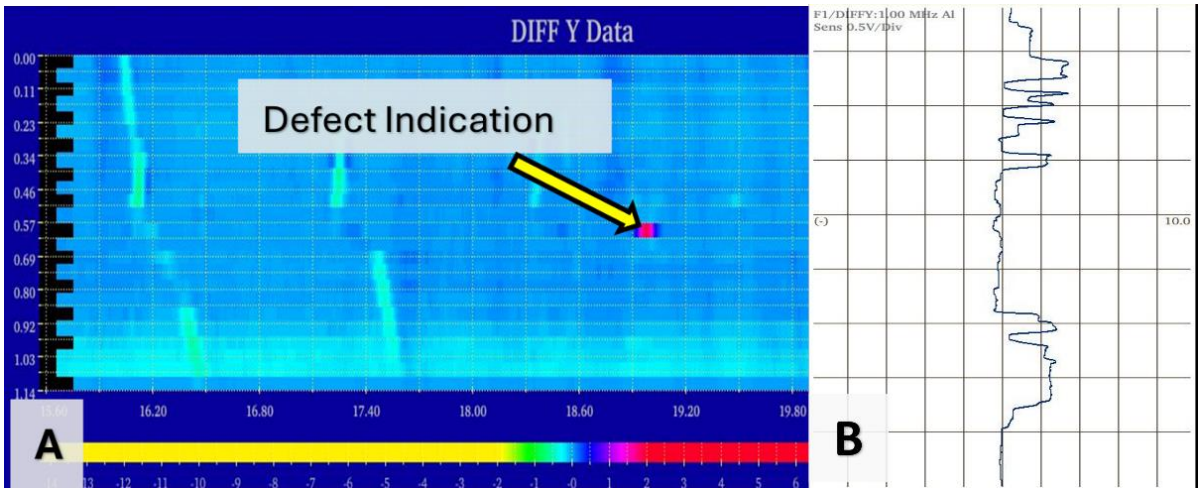

Figure 65: (A) Magnified C-scan of 2MxV4, (B) A-scan for the defect indication of 2MxV4

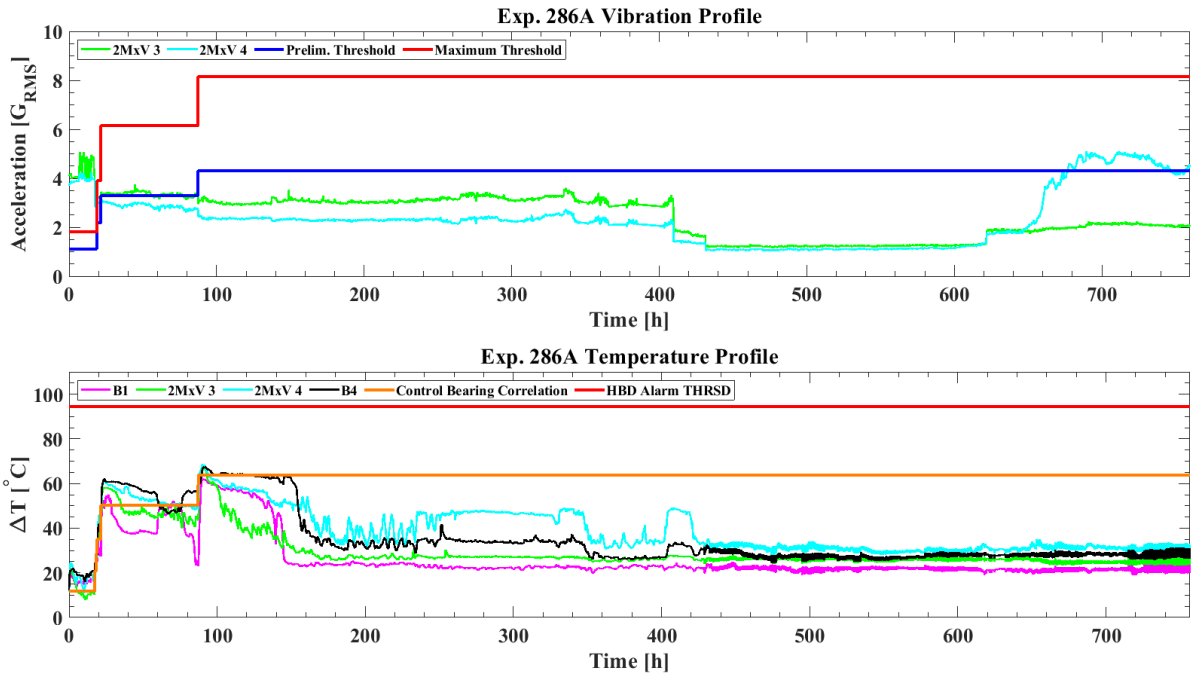

Figure 66: Vibration and temperature profiles for Experiment 286A

Table 26. Level 1 analysis for 2MxV4

Cup ID:	**Test Bearing 2MxV4**
Load [%]	100
Speed [RPM]/[MPH]	796/85
Maximum TDC Acceleration [G_{RMS}]	*5.10*
Prelim. Thld. [G_{RMS}]	4.29
Max. Thld. [G_{RMS}]	8.15

Table 27. Level 2 analysis for 2MxV4

Test Bearing 2MxV4						
	Folder	25	26	27	28	29
	Speed [RPM/MPH]	796/85	796/85	796/85	796/85	796/85
TDC Accel.	Defective Component	**Cup**	**Cup**	**Cup**	**Cup**	**Cup**
	Certainty [%]	**99**	**99**	**99**	**99**	**99**

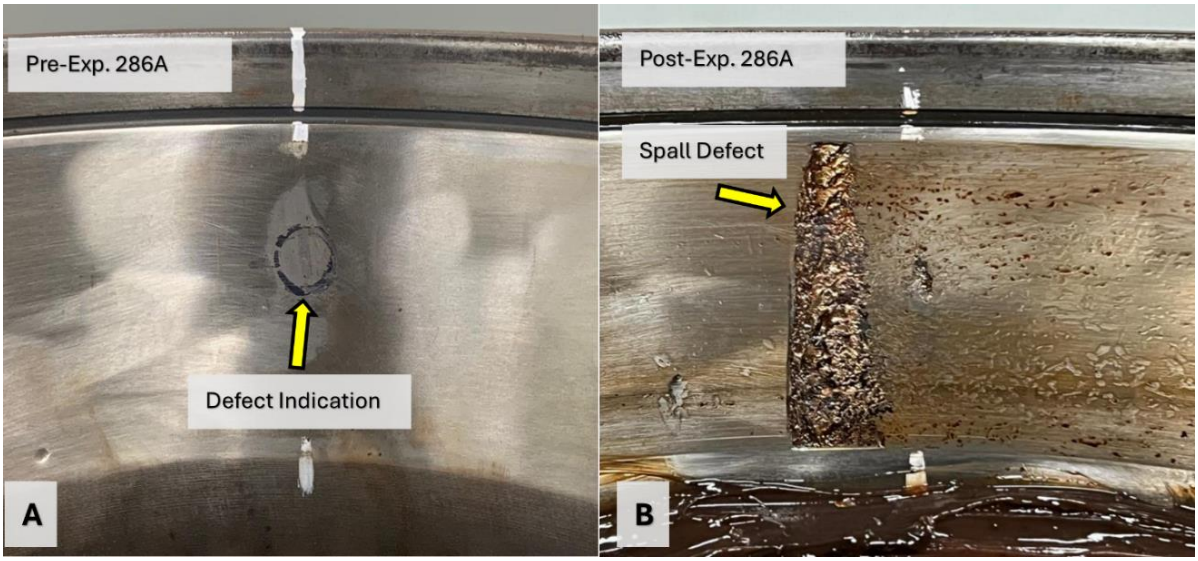

Figure 67: 2MxV4 (A) Pre-test inspection, (B) Post-test inspection: Spall size 0.96 in^2 (6.19 cm^2)

2MxV3 ECA SCANS, PLOTS, AND POST TEST IMAGES

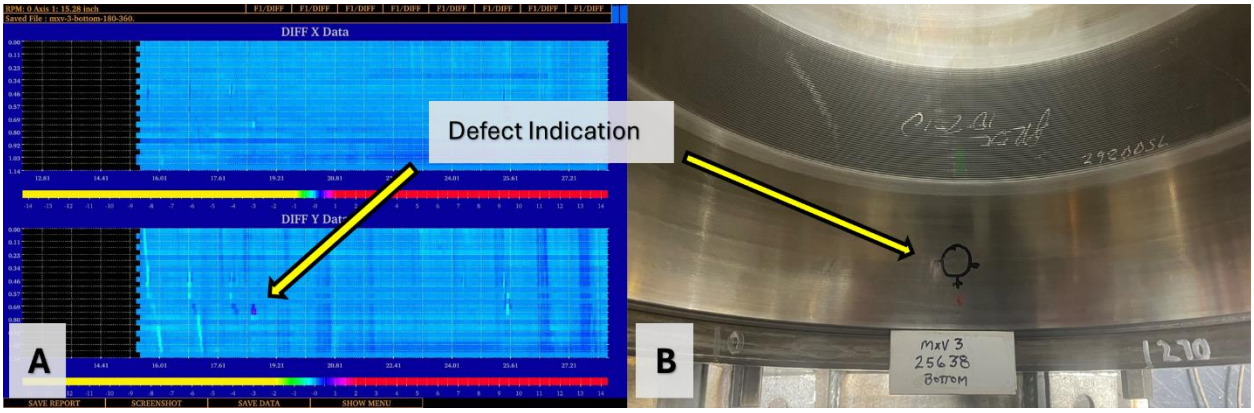

Figure 68: (A) ECA indication on the bottom raceway of 2MxV3, (B) Visual inspection of the bottom raceway of 2MxV3

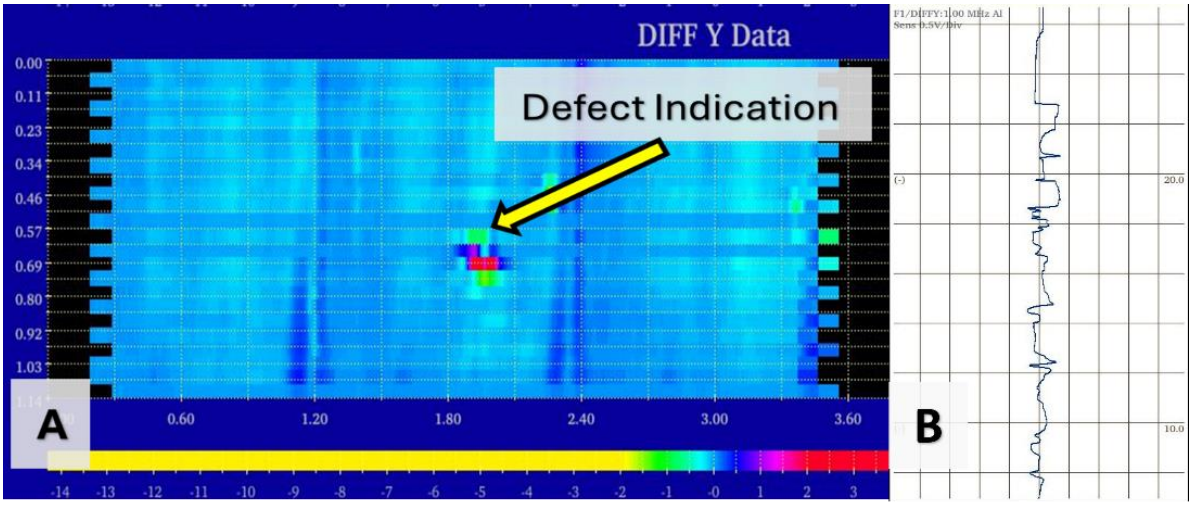

Figure 69: (A) Magnified C-scan of 2MxV3, (B) A-scan for the defect indication of 2MxV3

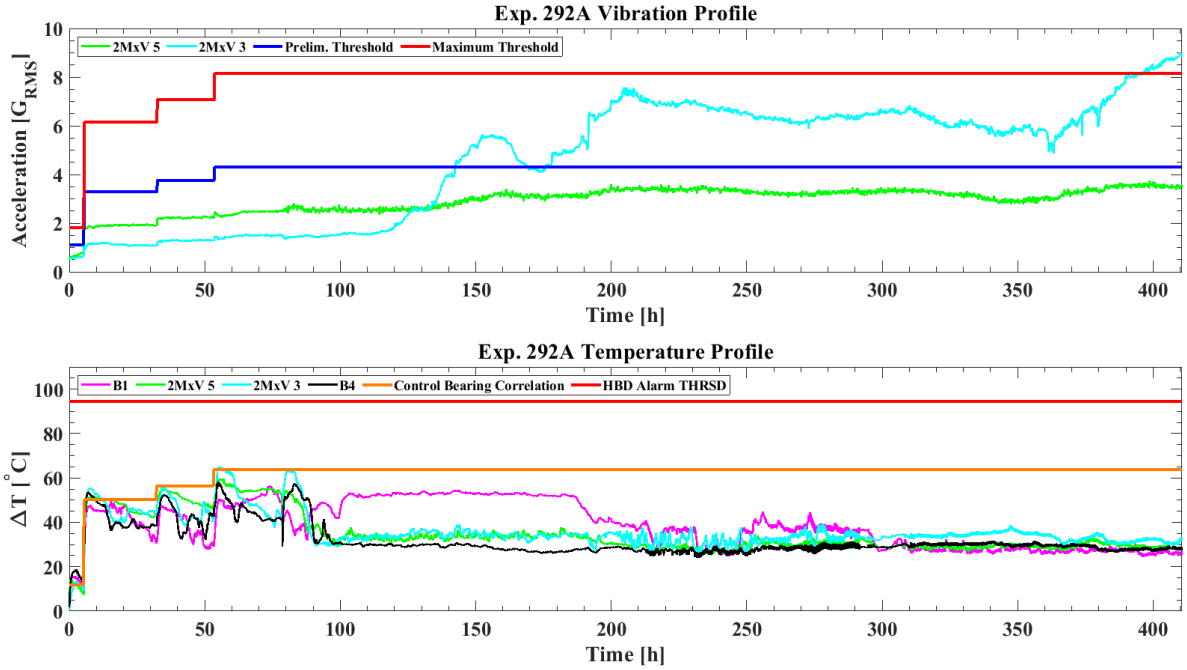

Figure 70: Vibration and temperature profiles for Experiment 292A

Table 28. Level 1 analysis for 2MxV3

Cup ID:	**Test Bearing 2MxV3**
Load [%]	100
Speed [RPM]/[MPH]	796/85
Maximum TDC Acceleration [G_{RMS}]	**9.00**
Prelim. Thld. [G_{RMS}]	4.29
Max. Thld. [G_{RMS}]	8.15

Table 29. Level 2 analysis for 2MxV3

Test Bearing 2MxV3						
	Folder	15	16	17	18	19
	Speed [RPM/MPH]	796/85	796/85	796/85	796/85	796/85
TDC Accel.	Defective Component	**Cup**	**Cup**	**Cup**	**Cup**	**Cup**
	Certainty [%]	**99**	**99**	**99**	**99**	**99**

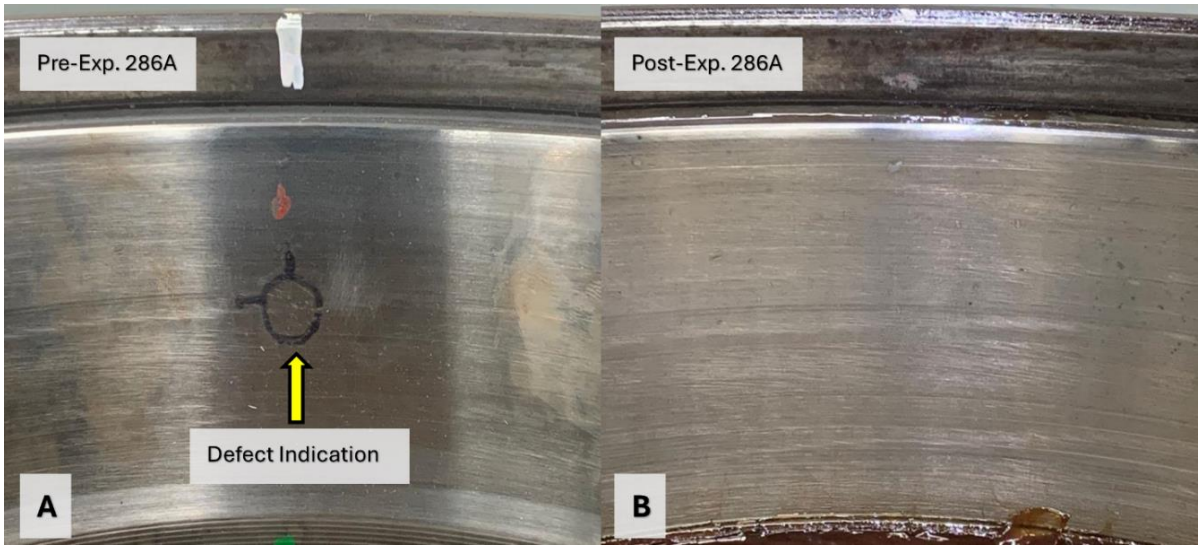

Figure 71: Exp.286A 2MxV5 (A) Pre-test inspection, (B) Post-test inspection

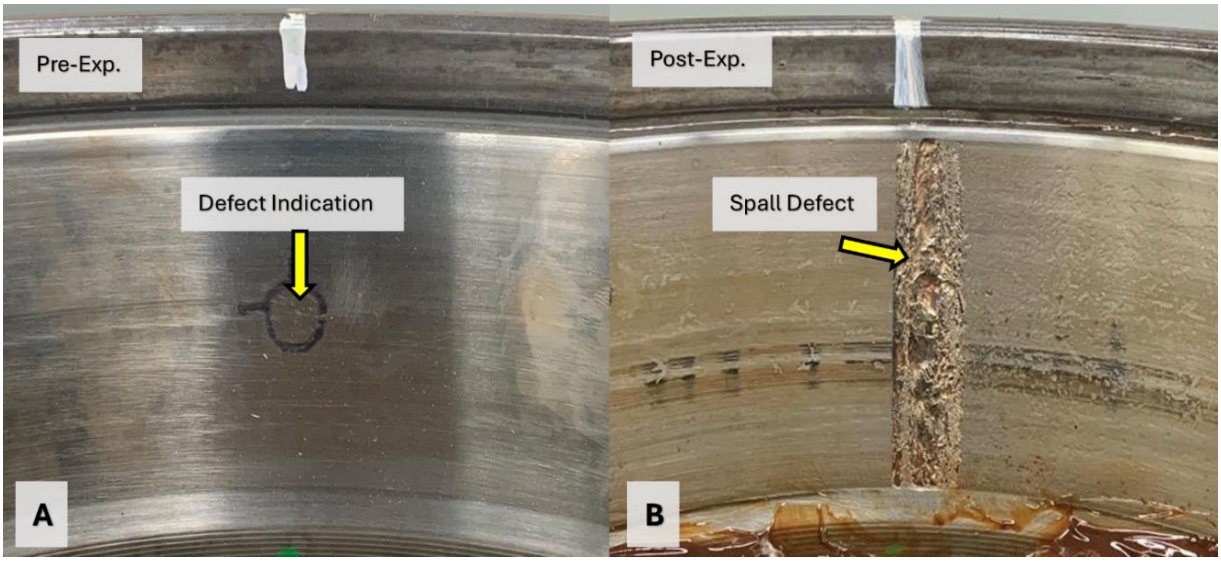

Figure 72: Exp.292A 2MxV5 (A) Pre-test inspection, (B) Post-test inspection: Spall size 1.19 in^2 (7.68 cm^2)

2MxV5 EXPERIMENT 287A PRE- AND POST-TEST INSPECTION

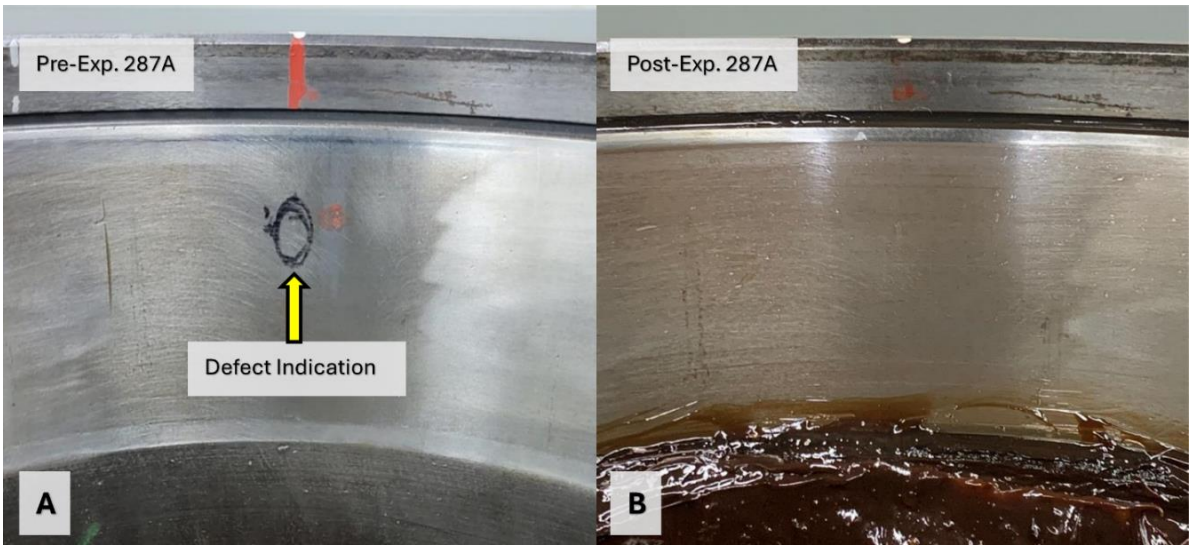

Figure 73: 2MxV5 (A) Pre-test inspection, (B) Post-test inspection

2MxV7 EXPERIMENT 290A PRE- AND POST-TEST INSPECTION

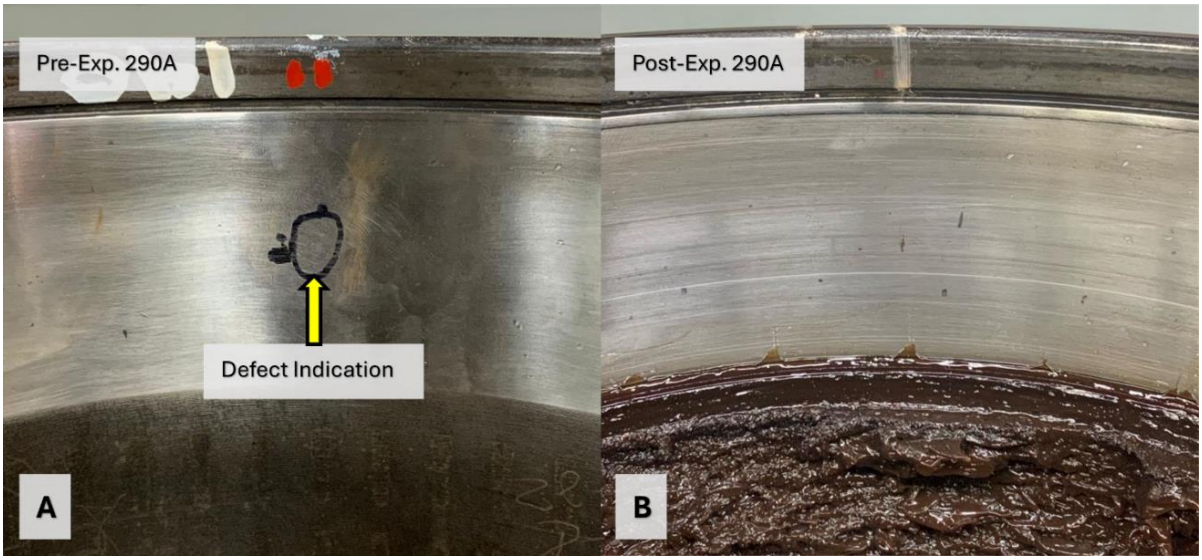

Figure 74: 2MxV7 (A) Pre-test inspection, (B) Post-test inspection

EXPERIMENT 297A: 2MxV12 AND 2MxV13

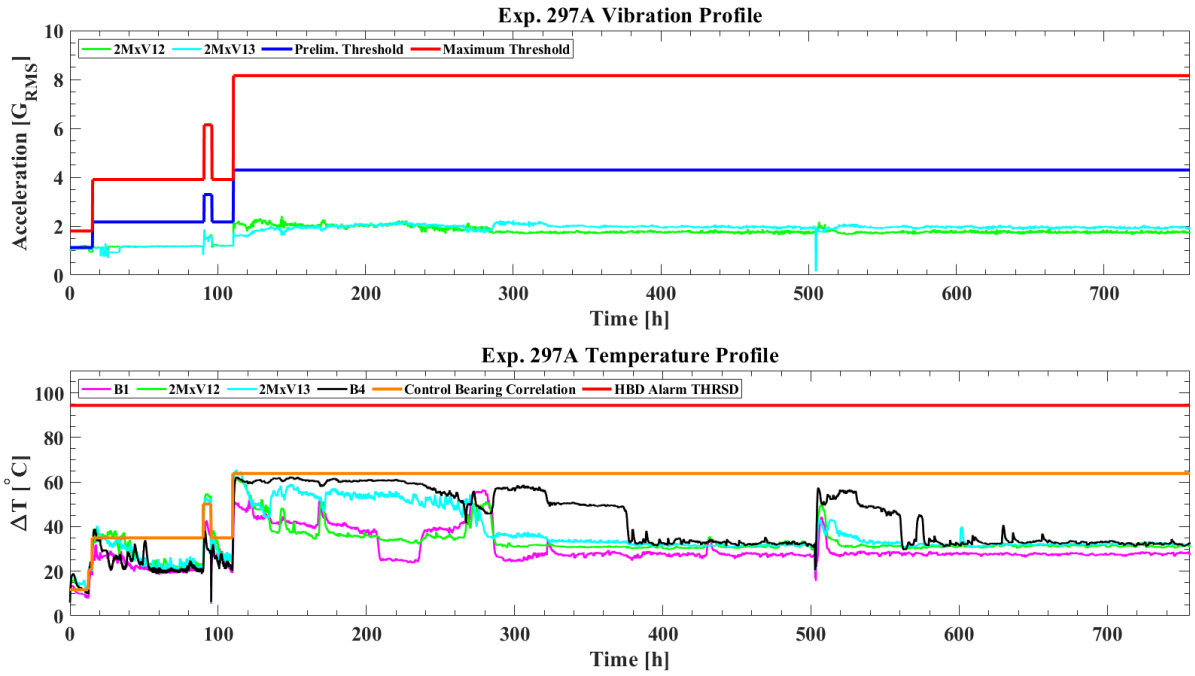

Figure 75: Vibration and temperature profiles for Experiment 297A

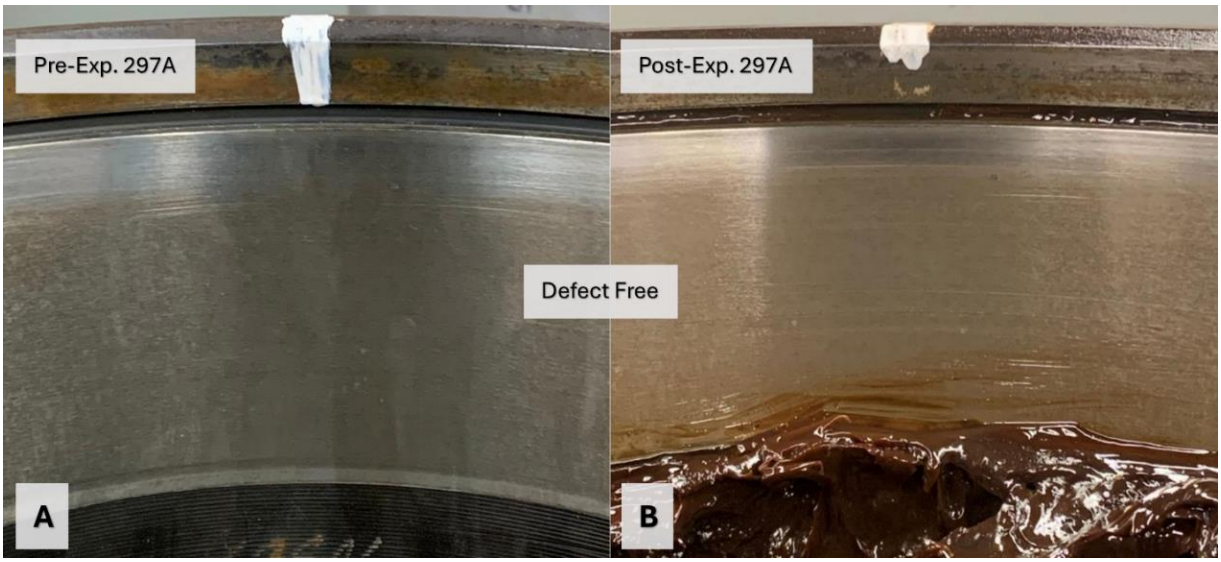

Figure 76: 2MxV12 (A) Pre-test inspection, (B) Post-test inspection

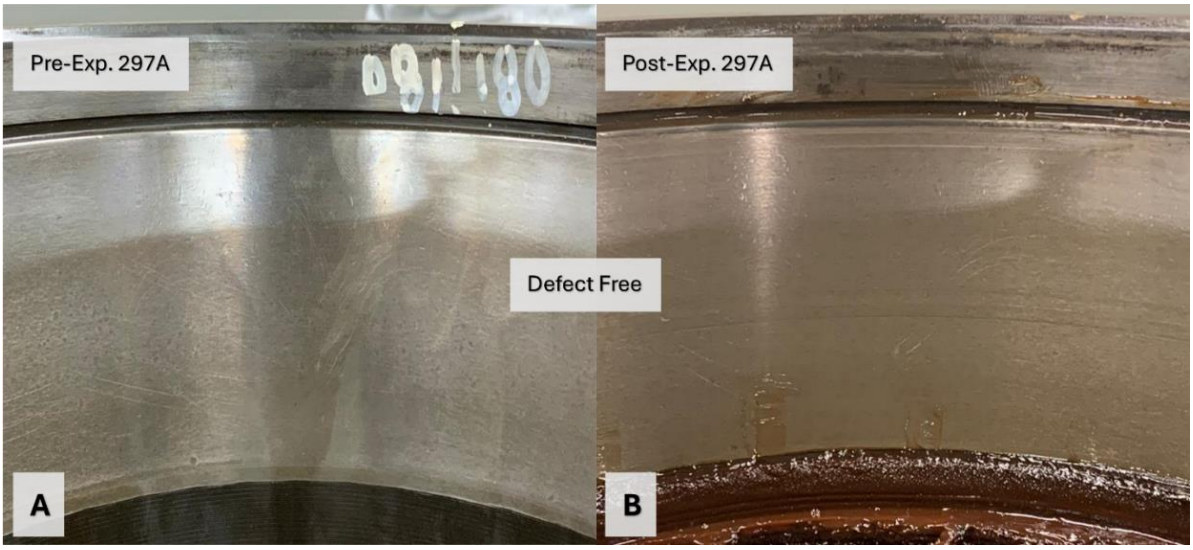

Figure 77: 2MxV13 (A) Pre-test inspection, (B) Post-test inspection

EXPERIMENT 300A: 2MxV15 AND 2MxV16

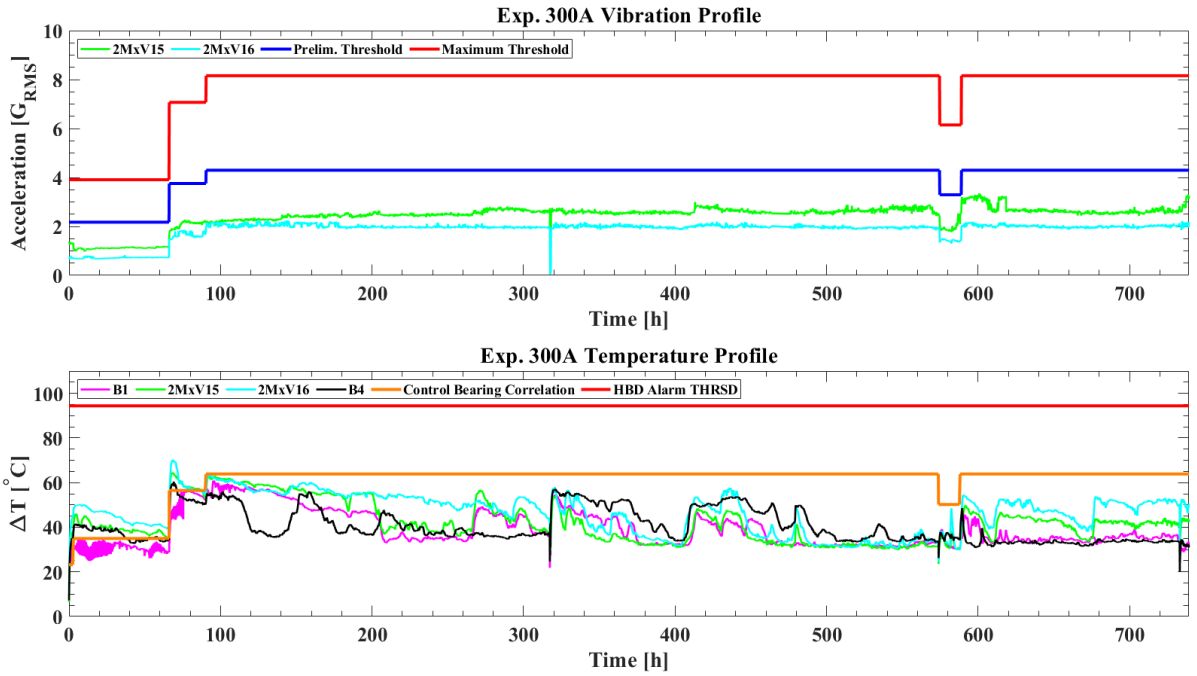

Figure 78: Vibration and temperature profiles for Experiment 300A

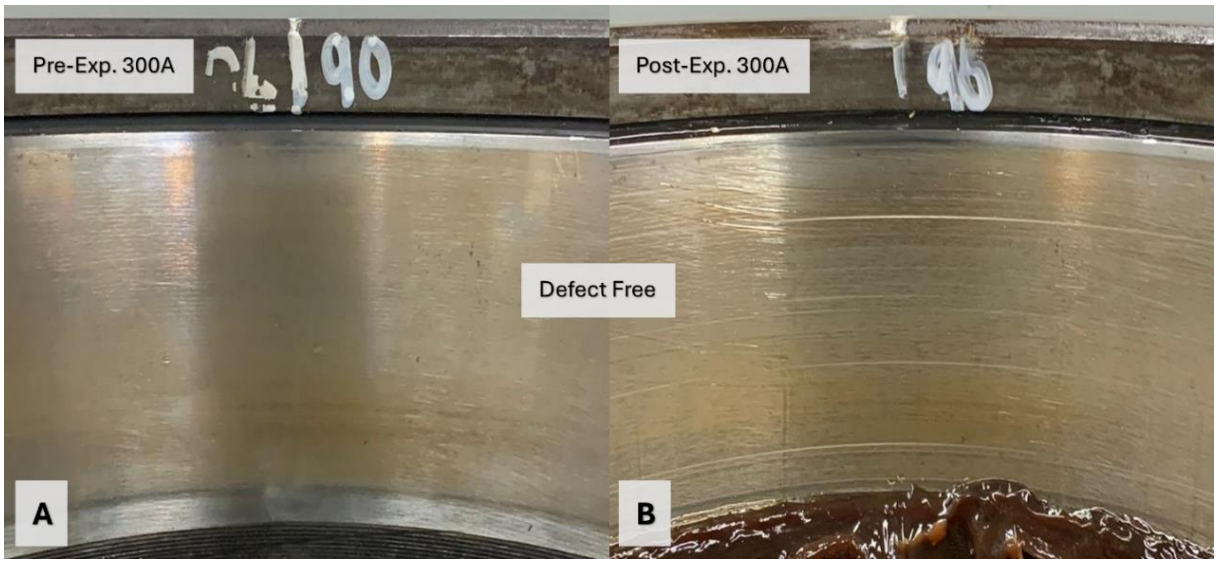

Figure 79: 2MxV15 (A) Pre-test inspection, (B) Post-test inspection

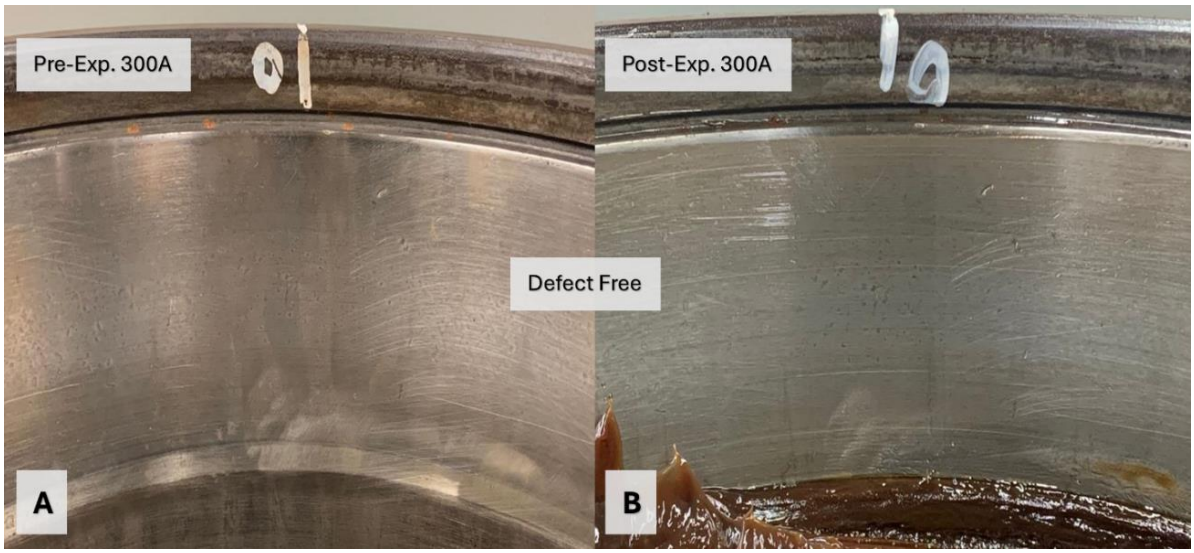

Figure 80: 2MxV16 (A) Pre-test inspection, (B) Post-test inspection

2MxV11 ECA SCANS, PLOTS, AND INPECTION

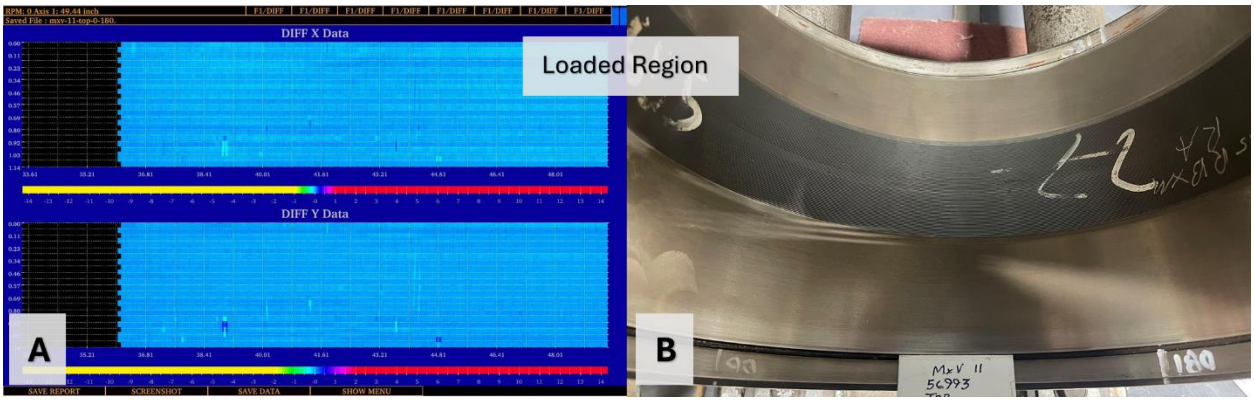

Figure 81: (A) C-scan of the top raceway of 2MxV11, (B) Visual inspection of the top raceway of 2MxV11

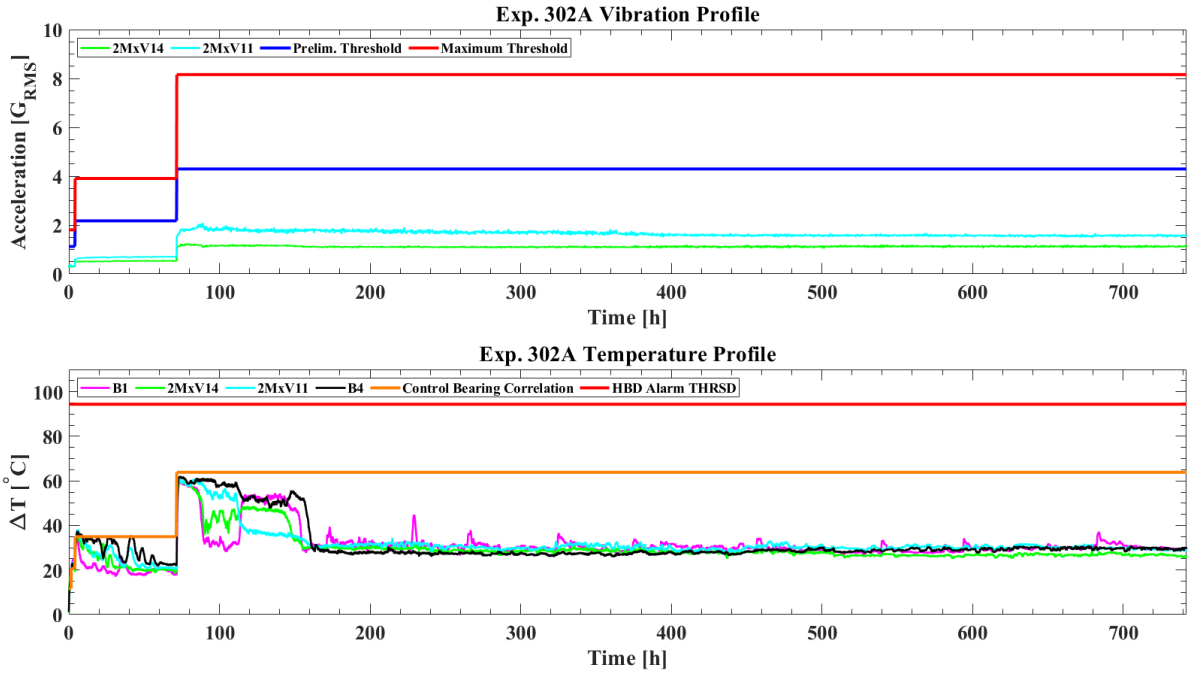

Figure 82: Vibration and temperature profiles for Experiment 302A

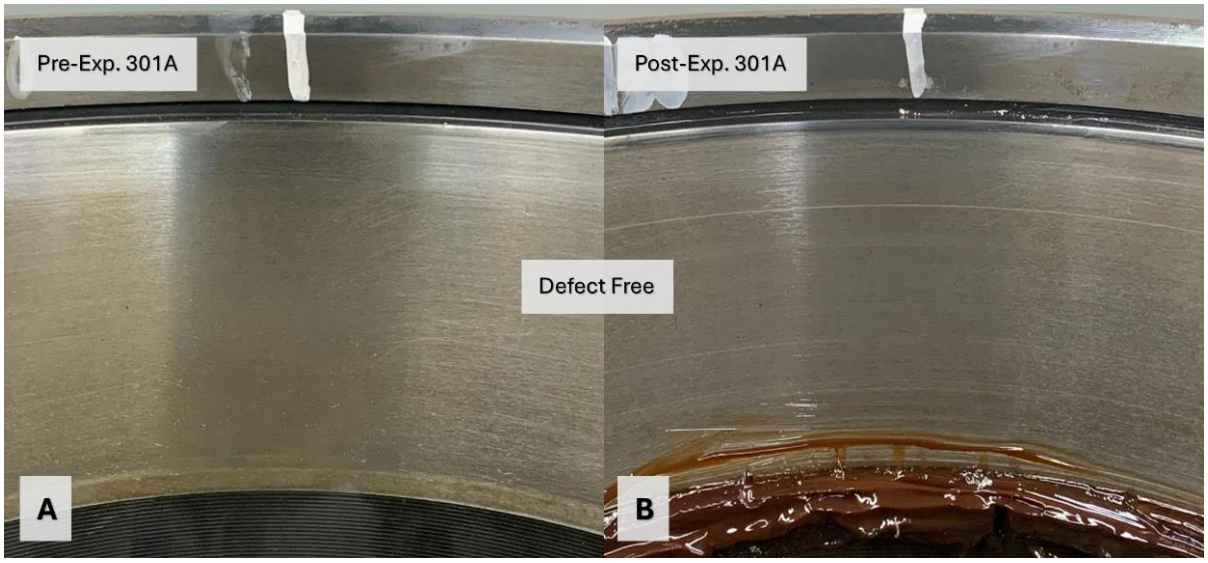

Figure 83: Exp.301A 2MxV11 (A) Pre-test inspection, (B) Post-test inspection

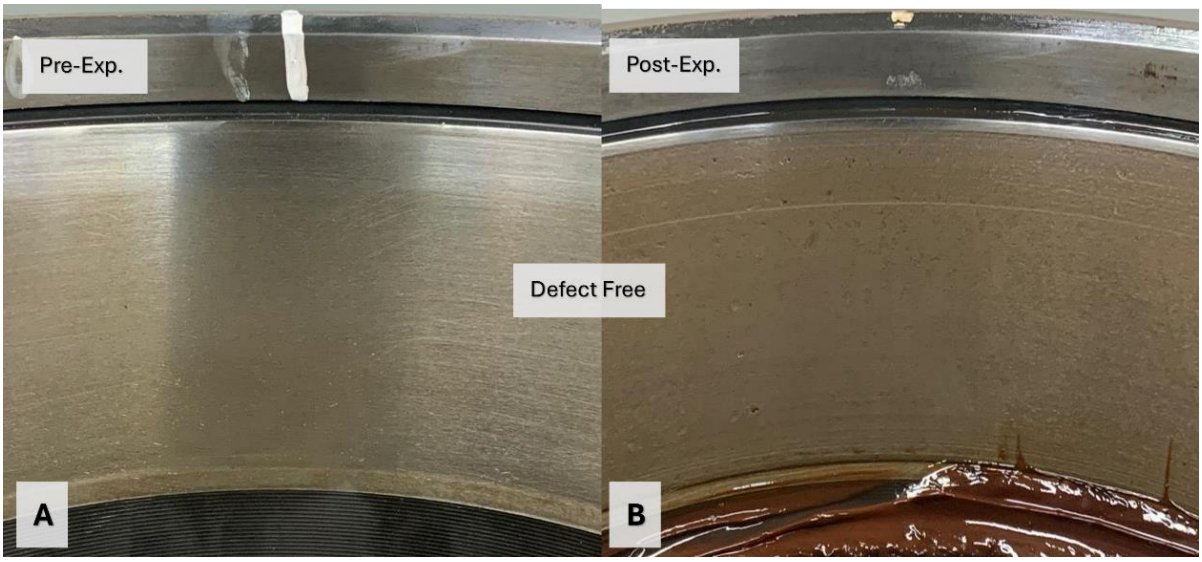

Figure 84: Exp.302A 2MxV11 (A) Pre-test inspection, (B) Post-test inspection

2MxV14 ECA SCANS, PLOTS, AND INPECTION

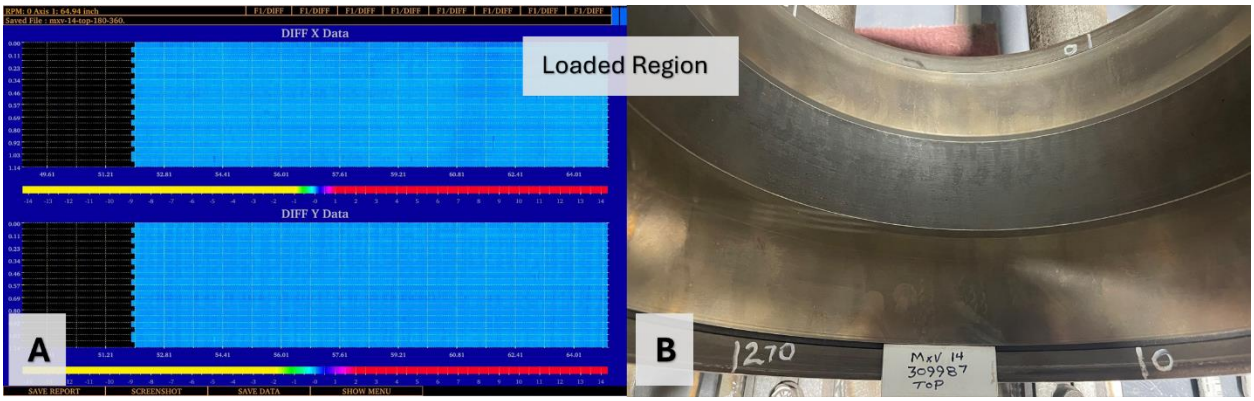

Figure 85: (A) C-scan of the top raceway of 2MxV14, (B) Visual inspection of the top raceway of 2MxV14

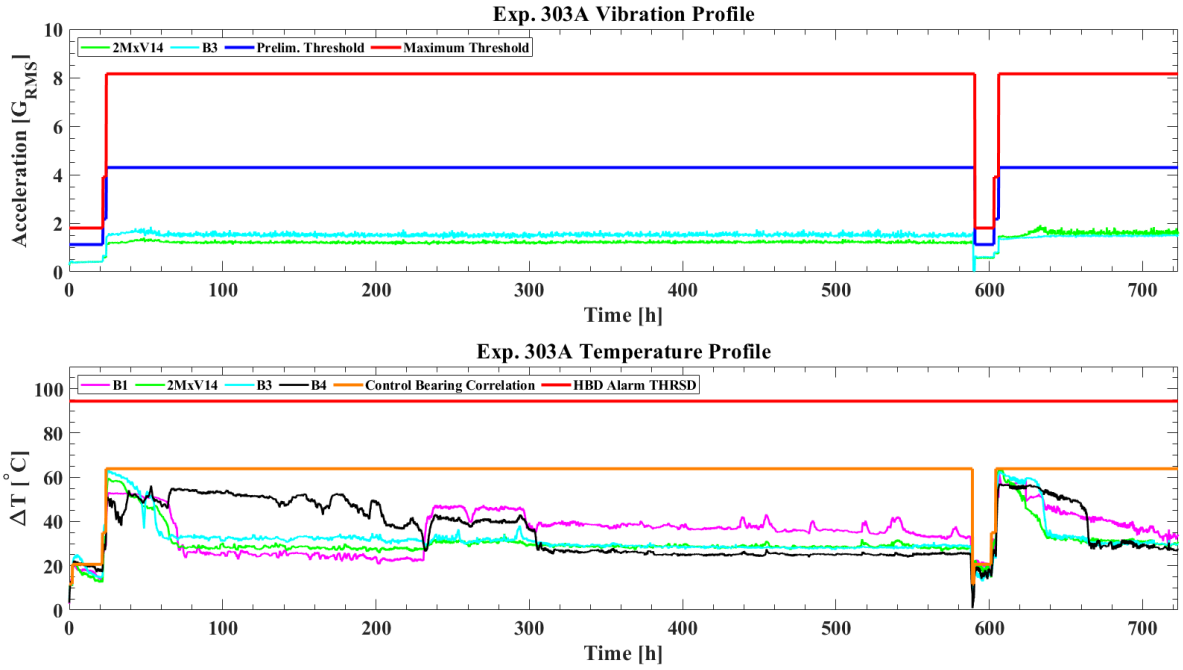

Figure 86: Vibration and temperature profiles for Experiment 303A

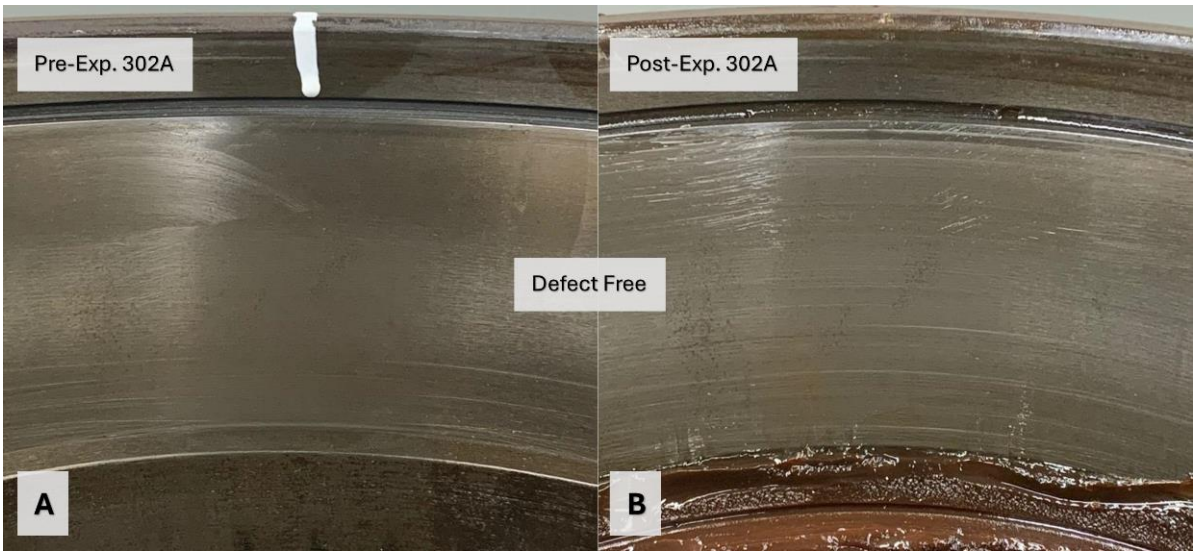

Figure 87: Exp.302A 2MxV14 (A) Pre-test inspection, (B) Post-test inspection

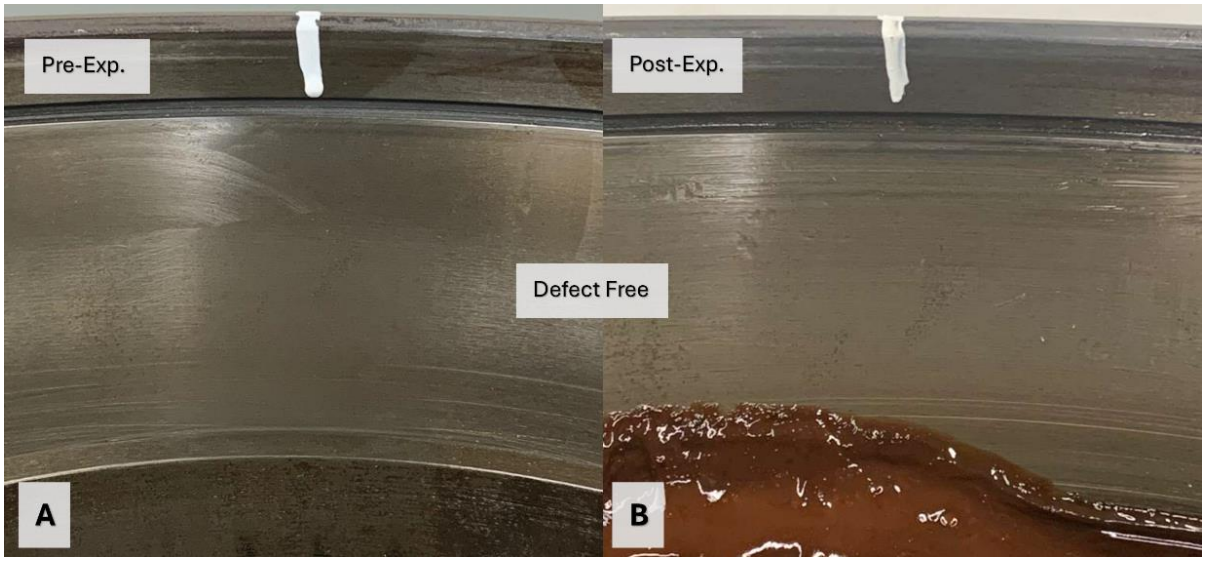

Figure 88: Exp.303A 2MxV14 (A) Pre-test inspection, (B) Post-test inspection

2MxV9 EXPERIMENT 298A INSPECTION

Figure 89: 2MxV11 (A) Pre-test inspection, (B) Post-test inspection

REFERENCES

[1] U.S. Department of Transportation, “Freight Rail Overview | FRA,” *railroads.dot.gov*, Jul. 08, 2020. https://railroads.dot.gov/rail-network-development/freight-rail-overview

[2] J. M. Montalvo, “Defect Detection Algorithm Optimization for use in Freight Railcar Service,” Master’s Thesis, The University of Texas Rio Grande Valley, August 2019.

[3] V. V. Hernandez, “Assessing the Performance of Reconditioned Railroad Tapered-Roller Bearings used in Freight Rail Service,” Master’s Thesis, The University of Texas Rio Grande Valley, December 2020.

[4] Amsted Rail, "Amsted Rail – The global leader in fully integrated freight car systems," [Online]. Available: https://www.amstedrail.com/.

[5] R. H. Cantwell, “Bearings Down on Bearings”, *Railway Age,* Mar. 15, 2024. https://www.railwayage.com/mechanical/freight-cars/bearing-down-on-bearings/#.

[6] J. D. Lima, *Residual Service Life Prognostic Models for Tapered Roller Bearings*, Master’s Thesis, Dept. of Mechanical Engineering, Univ. of Texas Rio Grande Valley, 2020.

[7] M. Stewart, E. Flynn, B. P. Marquis, and Sharma & Associates, Department of Transportation. Federal Railroad Administration. “An Implementation Guide for Wayside Detector Systems,” Washington, DC, United States, May 2019.

[8] C. M. Tarawneh, K. D. Cole, B. M. Wilson, and M. Reed, 2008,” A Metallurgical and Experimental Investigation into Sources of Warm Bearing Trending,” *Proceeding of the 2008 IEEE/ASME Joint Rail Conference,* Wilmington, Delaware, April 22-24.

[9] C. Group, “HOT BOX DETECTORS: WHAT YOU NEED TO KNOW,” *Railwayresource.com*, Dec. 21, 2023. https://www.railresource.com/company/760832/news/3363261/hot-box-detectors-what-you-need-to-know.

[10] H. Wang, T. F. Conry, and C. Cusano, 1996, “Effects of Cone/Axle Rubbing Due to Roller Bearing Seizure on the Thermomechanical Behavior of a Railroad Axle,” *Journal of Tribology*, vol. 118, no. 2, pp. 311-319.

[11] C. M. Tarawneh, L. Soltelo, A. A. Villarreal, N. De Los Santos, R. L. Lechtenberg, and R. Jones, “Temperature Profiles of Railroad Tapered Roller Bearings with Defective Inner and Outer Rings,” ScholarWorks @ UTRGV (University of Texas Rio Grande

Valley), Apr. 2016.

[12] E. V. Zaretsky and E. V. Branzai, “Effect of Rolling Bearing Refurbishment and Restoration on Bearing Life and Reliability,” *Tribology Transactions*, vol. 48, no. 1, pp. 32-44, Jan. 2005.

[13] Induortals Media Publishing, “The benefits of train refurbishment,” *Railway USA*, Sep. 06, 2024. https://railway-usa.com/news/85185-the-benefits-of-train-refurbishment?.

[14] P. Price and G. Kure, 2002, “High-Quality Railway Bearing Service at RBI”, https://evolution.skf.com/high-quality-railway-bearing-service-at-rbi-2/#.

[15] M. Trimm, “An overview of nondestructive evaluation methods,” *Practical Failure Analysis*, vol. 3, no. 3, pp. 17-31, Jun. 2003, https://doi.org/10.1007/bf02715528.

[16] ‘Ultrasonic Testing (UT): A Versatile Method for NDT Inspections,” *Asnt.org*, 2024. https://www.asnt.org/what-is-nondestructive-testing/methods/ultrasonic-testing

[17] T. Menaria and M. Kumar, “Review on Radiographic Imaging Modalities for Non-destructive Testing and Evaluation (NDT & E),” March 20, 2019, Proceedings of International Conference on Sustainable Computing in Science, https://dx.doi.org/10.2139/ssrn.3356362.

[18] *Acoustic emissions applications*. Nondestructive Evaluation Techniques: Acoustic Emission Testing. (n.d.). https://www.ndeed.org/NDETechniques/AcousticEmission/AE_Applications.xhtml

[19] T. K. Adelung, “Ultrasonic nondestructive quantification of case depth in railroad bearing components,” Master’s Thesis, The University of Nebraska-Lincoln, August 2024.

[20] D. Kobayashi, K. Ono, M. Natori, & H. Komata, Non-destructive for rolling bearings by eddy current testing. PHM Society Asia-Pacific Conference, 4(1). (2023), https://doi.org/10.36001/phmap.2023.v4il.3715

[21] Schaeffler Technologies “Repair and Reconditioning of Roller Bearings” (2025, October) https://www.schaeffler.com/remotemedien/media/_shared_media/08_media_library/01_publications/schaeffler_2/tpi/downloads_8/tpi_207_de_en.pdf.

[22] H-II. (2008, October). In 1062201241 809481722 Safety and Operations (Ed.), Manual of Standards and Recommended Practices (pp. H-II-i-H-II [S-756] 102). Washington, D.C.: Association of American Railroads.

[23] The benefits of remanufacturing rolling bearings. Evolution. (2020, April 1). https://evolution.skf.com/the-benefits-of-remanufacturing-rolling-bearings/#

[24] N. Perales and D. Galar, “Inspection and analysis of the functioning of the bearings used on railways a study of the life of a bearing under real operating conditions,” Luleå University of Technology, March 2014

[25] D. Clasby, “Reconditioned bearing performance testing” *Railway Age,* July 11, 2023. https://www.railwayage.com/mechanical/freight-cars/reconditioned-bearing-performance-testing/

[26] J. Hansen, The Eddy Current Inspection Method. Insight - Non-Destructive Testing and Condition Monitoring, 46(5), 279–281. https://doi.org/10.1784/insi.46.5.279.55563 (2004)

[27] J. García-Martín, J. Gómez-Gil, and E. Vázquez-Sánchez, Non-destructive techniques based on eddy current testing. Sensors, 11(3), 2525–2565. https://doi.org/10.3390/s110302525 (2011)

[28] L. A. Rosado, Non-Destructive Testing Based on Eddy Currents. *Instituto Superior Técnico, UTL, Lisbon, Portugal*, 1-10. (2009)

[29] Chapter 4 Eddy Current Inspection Method ... (n.d.-a). https://content.ndtsupply.com/media/Eddy%20Current%20-USAF-Tech-Manual-N-R.pdf

[30] NDT Solutions & Eddy Current Instruments. UniWest. (2025, January 7). https://uniwest.com/

[31] C. M. Tarawneh, A. Martinez, M. Adame, S. Garcia, J. Pams, and C. Pena,” Healthy and Defective Tapered Roller Bearing Temperature Metrics,” *Proceeding of the 2024 IEEE/ASME Joint Rail Conference* (Vol. 87776, p. V001T05A007). American Society of Mechanical Engineers (ASME) 2024

[32] S. Martinez, E. Miranda, C. Tarawneh, N. J. Matz, J. A. Turner, Defect prediction for bearings using ultrasonic and eddy current inspection. International Heavy Haul Association (IHHA) 2025

VITA

Eduardo Miranda attended McAllen High school and graduated in 2020. He attended the University of Texas Rio Grande Valley (UTRGV) and received his Bachelor of Science in Mechanical Engineering in December 2023. Eduardo conducted research in the rail transportation sector at the University of Transportation Center for Railway Safety (UTCRS) from 2023-2025, specializing in utilizing nondestructive evaluation (NDE) methods via eddy current to test the performance of reconditioned freight bearings. He later chose to continue his studies at the UTRGV and obtained his Master of Science in Mechanical Engineering in December 2025. Eduardo may be reached by email at eduardomiranda979@gmail.com.